ABSTRACT

RYAN, JOSEPH ANTHONY. Quantification via Inductively-Coupled Plasma Optical Emission Spectroscopy (ICP-OES) of the Cellular Internalization and Nuclear Localization of Gold Nanoparticles Passivated with BSA-SV40 Large T NLS Conjugates after Incubation with Human Cervical Cancer (HeLa) Cells. (Under the direction of Dr. Stefan Franzen).

Rhodamine-labeled, cysteine-modified SV40 large T NLS peptide sequences were conjugated in varying amounts (~ 3 to 15 molar ratio) with bovine serum albuin (BSA) via the heterobifunctional linker succinimidyl-4-(*N*-maleimidomethyl)cyclohexane-1-carboxylate (SMCC). These conjugates were then used to passivate nanomolar aliquots of citrate-coated gold nanoparticles of varying diameter (5, 10, 15, and 20 nm), and the stability of these nanoparticle complexes were evaluated with respect to: 1) amount of large T-BSA per nanoparticle (found to be stable under the following BSA:nanoparticle ratios: 5 nm diameter = 125:1, 10 nm diameter = 250:1, 15 nm diameter = 250:1, and 20 nm diameter = 500:1), 2) ionic strength of solution (critical coagulation concentration values above 0.85 M), and 3) temperature (found to be stable at 4, 25, and 37 degrees Celsius). A robust method was developed using inductively-coupled plasma optical emission spectroscopy (ICP-OES) as a means to quantify the internalization of nanoparticle complexes after incubation with human cervical cancer cells (HeLa) under many differing conditions. It was determined cellular internalization increased as a function of: 1) increasing amount of large T per nanoparticle complex, 2) longer incubation times, 3) temperature (which is to say incubations at 4 degrees Celsius afforded nearly no internalization), and 4) increasing nanoparticle diameter. Additionally, data from a pulse-chase experiment demonstrated that these nanoparticle complexes tend to remain associated with HeLa cells in similar concentration up to twelve hours after initial exposure. Lastly, a sub-cellular fractionation kit was used to

extract nuclei from HeLa cells post-incubation with 5 nm diameter gold nanoparticle complexes. It was observed that nuclear localization of these nanoparticle complexes increased as a function of large T:nanoparticle ratio, but that resulting cell viability decreased dramatically at the highest large T:nanoparticle ratio.

Quantification via Inductively-Coupled Plasma Optical Emission Spectroscopy (ICP-OES) of the Cellular Internalization and Nuclear Localization of Gold Nanoparticles Passivated with BSA-SV40 Large T NLS Conjugates after Incubation with Human Cervical Cancer (HeLa) Cells

by
Joseph Anthony Ryan

A dissertation submitted to the Graduate Faculty of
North Carolina State University
in partial fulfillment of the
requirements for the degree of
Doctor of Philosophy

Chemistry

Raleigh, North Carolina

2009

APPROVED BY:

_____	_____
Dr. Stefan Franzen Committee Chair	Dr. Edmond Bowden
_____	_____
Dr. Kenneth Hanck	Dr. Wayne Robarge

BIOGRAPHY

Joseph Ryan was born in the Bronx, New York, but his parents saw fit to fix this by moving to New Jersey two-ish years afterwards. Somewhat later, following a period of time of considerable interest to Joseph but of extreme inconsequence to nearly everyone else on the planet, he managed to work his way back to the Bronx and was eventually awarded a Bachelor of Science degree in chemistry from Fordham University. Three years later, after it became painfully obvious (even to our intrepid biographical subject) that he was not, in fact, going to be a multi-millionaire bassist in a heavy metal band despite all his attempts, Joseph left his day-job at the local bank and was fortunately allowed to enroll in the chemistry graduate program at the University of Scranton. It was here that Joseph realized he hugely enjoyed teaching at the undergraduate level, and enjoyed it so much that he decided to try and make a career of it. So, a few years, a thesis, and a Master's degree later, Joseph moved himself to Raleigh, North Carolina, to join the chemistry graduate program at North Carolina State University. During his stay here, he – not unlike many others – has experienced episodes of unbridled optimism and abject despair, times of profound sadness and extreme elation, many "Eureka!" moments and many moments which are better left unprinted. As this dissertation is finally ready to be defended, your humble narrator is reflecting on his life, and while the total experience has been wildly-positive, he is currently contemplating what a long, strange trip it's been…

TABLE OF CONTENTS

LIST OF TABLES

LIST OF FIGURES

Chapter 1

Introduction.

1.1. Introduction and Background.

The main focus of this dissertation is the development of a gold nanoparticle-based cellular delivery vehicle which targets the nuclei of cancerous cells, although it should be noted that the technology described herein can also be used for other applications in drug delivery and contrast agents. The description starts in this Chapter with a brief overview of current cancer research followed by a discussion of existing delivery vectors. This will include a brief review of the inherent cellular processes, of which these vectors are designed to take advantage. The full details of the experiments, used to validate this specific delivery vector and to test the efficacy of nuclear targeting, will be delineated in Chapters 2 – 4. Finally, the last chapter of this dissertation is a summary of all the results from this research and a discussion of future experiments which could be performed in the continuing of this line of scientific inquiry.

1.2. Cancer.

Cancer research is one of the most prolific, intriguing, and vitally important areas of contemporary scientific investigation. Research topics include a study of potential causes of cancer,[1,2,3,4,5] elucidation of new mechanisms by which cancer develops and is sustained,[6,7,8,9,10] and, ultimately, the search for innovative techniques to detect and selectively destroy it.[11,12,13,14,15,16] Despite a massive effort in funding and focus of research regarding cancer in the United States for nearly forty years – since then-President Nixon declared "war" on cancer[17] – refinements in detection and treatment of cancerous conditions have been disappointingly limited.

However, while scientific inquiries may not have yielded a proper cure yet, recent endeavors have not only revealed some of the mechanisms involved in how certain cells become cancerous, but also illuminated how much more complex and comprehensive the disease can be compared to what was initially thought.[18,19] For example, recent research[20,21] has begun to define the dynamic chemical interplay between certain malignant tumors and their host's immune system and has also highlighted the limits of our understanding of immune reactions in general.

1.2.1. Current Cancer Diagnostics.

Whether one is examining an X-ray slide for abnormally dense regions,[22] analyzing blood test results for biochemical byproducts of potential cancerous cells,[23] interpreting anomalous computed tomographic (CT) scan data,[24] physically examining suspect tissue during an endoscopic procedure,[25] or even sifting through data from post-biopsy cytogenetic[26] or immunohistochemistry analyses[27] of potentially cancerous cells – the sooner it is determined that some cells have become cancerous, the greater the chances of a patient's survival. The utility of novel biological probes capable of detecting small changes/accumulations in cancerous (or pre-cancerous) conditions in general can not be understated, and innovative probes useful in harmless, non-toxic cellular analysis would be most helpful.

1.2.2. Current Cancer Treatments.

The most common methods of treating cancer patients typically entail surgery – when practical – to remove as much of a cancerous mass from a patient as possible,[28] combined with subsequent administration of one or more of the following: chemotherapy,[29] radiation therapy,[30] hormonal therapy,[31] and immunotherapy.[32] Additionally, photodynamic therapy has been shown to be quite effective at successfully treating certain types of skin cancers without involving surgery.[33]

Some chemotherapeutic agents, such as cisplatin (*cis*-diamminedichlorido-platinum(II), a square planar molecule), help kill cancer cells by associating with the hereditary material – deoxyribonucleic acid (DNA) – in a cell and cross-linking DNA strands, thereby interfering with DNA replication during cell division and ultimately inducing apoptosis (programmed cell death).[34] Other chemotherapeutic agents interfere with different facets of the mitotic process in a cell: for example, paclitaxel (a tetracyclic molecule with a heptadecane skeleton) binds to tubulin, the "building block" molecule of a cell's cytoskeleton, thus preventing the cytoskeleton from disassembling as/when necessary to aid in cell division.[35] (Moreover, paclitaxel also aids in inducing apoptosis in cancer cells by binding to an apoptosis-stopping protein named Bcl2 (B-cell leukemia 2) present in many cancer cells, subsequently allowing a cell's intrinsic "kill switch" to function.)[36] The administration of both of these particular chemotherapeutic molecules (and many more like them) would benefit greatly from the development of a more efficacious method of delivery to their site of intended activity, which could lessen the negative impact upon otherwise healthy cells in the environment surrounding a cancerous growth.

Radiotherapy is the use of ionizing radiation – potentially a beam of photons,[30] electrons,[37] protons,[38] neutrons,[39] ions[40], or some combination[41] – to damage the DNA of cancerous cells. The DNA of the cells might be damaged directly by the beam, or indirectly attacked by resulting free radicals of other nearby molecules (e.g.: water, O_2) ionized by the beam. However, certain larger tumors can develop a general resistance to radiotherapy when these tumors outgrow their blood supply, thus developing a hypoxic environment (less O_2 in the cell translates to less DNA damage via beam). In these instances, one option is to use a dose of a "radiosensitizing" agent[42] – such as cisplatin[43] – prior to beginning radiotherapy. Once again, any novel method of specifically targeting/transporting these agents to their sites of cellular activity could limit their exposure to uptake by healthy cells surrounding cancerous tissue, potentially lower the necessary doses of both radiotherapy and the transported chemotherapeutic, and directly aid in the destruction of the cancerous cells.

Hormone therapy as a cancer treatment is an attempt to restrict the growth of certain cancerous cells by either administering hormones which cause cells to actively undergo apoptosis[44] or removing a source of hormones which particular cancer cells (e.g. some breast[45] or prostate[46] tumors) need to continue their otherwise unregulated growth. Two drugs of this latter type are tamoxifen,[47] ((*Z*)-2-[4-(1,2-diphenylbut-1-enyl)phenoxy]-*N*,*N*-dimethyl-ethanamine) which competitively inhibits the binding of the hormone estrogen to breast cancer cells, and letrozole,[48] (4-[(4-cyanophenyl)-(1,2,4-triazol-1-yl)methyl]benzonitrile) which blocks the production of estrogen by binding to the heme of the cytochrome P450 subunit of the aromatase enzyme responsible for producing estrogen. Cancer treatment via immunotherapy involves the triggering of a patient's immune system to

attack cancerous cells, either through immunization against certain antigens commonly expressed (or overexpressed) by cancerous cells,[49] or by administering a therapeutic antibody to actively promote an immune response in a given area of the body.[50] Treating cancer through hormonal therapy or immunotherapy could be made more beneficial through the use of any novel delivery vector which could aid in transporting the respective therapeutic moieties to their cellular sites of consequence.

1.3. Brief Review of Relevant Cellular Biology.

1.3.1. Eukaryotic Cell Structure.[51]

All living organisms are comprised of cells, the simplest unit capable of independent existence. Organisms can be classified into two fundamentally different types according to the structure and complexity of their cells. Prokaryotes – kingdom Monera (bacteria and cyanobacteria) – are single-celled organisms which have a plasma membrane confining the contents of that cell to a discrete compartment, but lack distinct internal membrane systems (organelles). The DNA in prokaryotic cells is generally confined to one or more nuclear regions (but these regions are not bounded by a separate membrane), and some prokaryotic cells have a cell wall or outer membrane enveloping the entire cell, including their plasma membrane. Eukaryotic cells contain a membrane-bounded structure called a nucleus, which is where the cell's DNA is localized. Additionally, these cells have many other organelles bounded by distinct membranes, and the structure and function of these organelles can vary greatly among the different types of eukaryotic cells.

When growing cells reach a certain size, they either stop growing or divide. The life cycle of cells – also referred to as the cell cycle – is an attempt to describe the general activities of cells which are actively growing and dividing. This cycle is defined as the period from the start of one division to the onset of the next, and a typical cell cycle diagram is shown in Figure 1.1. The major defining parts of the cell cycle are the S phase ("S" for "synthesis") when DNA is replicated in preparation for division, and the actual cell division itself – termed "mitosis," the M phase. Separating these two events are "gap" phases – G_1 and G_2 – when the cell is manufacturing the mRNAs and proteins necessary to enter the next phase. Cells which do not divide – i.e. mature red blood cells or neurons – are considered perpetually in the G_1 phase, and are therefore not engaged in the cell cycle. During the G_1, S, and G_2 phases (collectively termed "interphase"), a cell will roughly double its mass, and the end result of the M phase is two cells, which are typically (but not always) identical to each other. Lastly, under certain conditions (i.e. starvation), a cell may exit the cell cycle and enter a state of waiting – G_0 phase – for conditions to change before reentering the cycle.

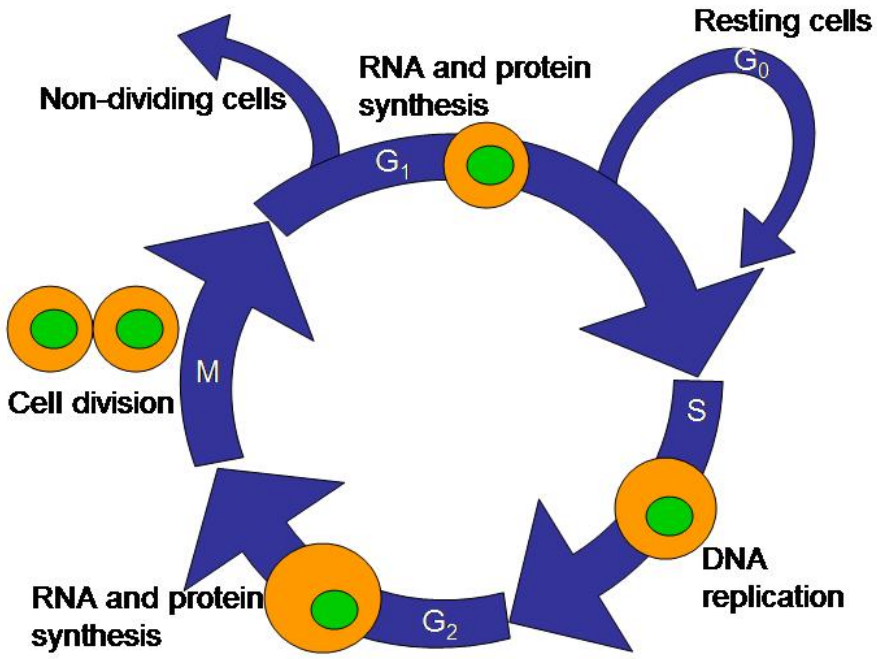

Figure 1.1. Drawing of eukaryotic cell cycle.

1.3.2. Cell Membrane.[51]

Cell membranes are phospholipid bilayers which form an external boundary around a cell. The aqueous environment both inside and outside a cell helps form and maintain the bilayer structure. Diverse proteins are embedded through the cell membrane (Figure 1.4), and these proteins can function as mediators by which a cell can actively and selectively internalize various moieties. It should be noted that while it is energetically unfavorable for the phospholipids comprising the membrane to escape the bilayer formation, nothing prevents individual molecules from moving laterally within the plane of the bilayer. The membrane (including any unanchored trans-membrane proteins), in essence, behaves like a two-dimensional fluid, and this fluidity is critical to membrane function.

1.3.3. Cellular Internalization Mechanisms.[51]

Since the topic of cellular internalization (that is, the ability/process of a cell to take in some external species) is a quite extensive subject area, the main methods by which a cell actively internalizes external moieties will be mentioned here, and only one will be examined in more detail. It should be noted passive diffusion across a eukaryotic cell membrane is possible for very small, uncharged molecules (e.g. water, O_2), but ions and other larger molecules must be actively transported across the membrane via a protein channel of some form. Thus, cellular membranes are semi-permeable.

Phagocytosis is the process by which a cell engulfs a relatively large particle (e.g. cell debris or some microorganism) and ingests these particles in a vesicle called a phagosome (> 250 nm in diameter). Phagocytosis is a specialized function of macrophages and certain white blood cells. Most eukaryotic cells ingest fluid and small molecules by means of relatively small vesicles (< 150 nm in diameter) in a process called pinocytosis. Primarily using a process which involves the proteins clathrin, adaptin, and dynamin, a small portion of the cell membrane is invaginated and pinched off into the cytoplasm, becoming a discrete vesicle. These vesicles are then fused with other vesicles in the cell – endosomes and lysosomes – in order to digest the internalized substance, while the vesicle proteins are then recycled.

While pinocytosis can be a non-specific process, merely capturing any molecules which happen to be in the extracellular environment near a burgeoning clathrin-coated vesicle, this general mechanism can also be used by a cell to internalize specific

macromolecules. A complementary receptor on the surface of the cell may bind to a given macromolecule and then be internalized by the cell via a clathrin-coated vesicle. This process is called receptor-mediated endocytosis (RME), and is the method of cellular internalization of macromolecules important to the homeostasis of cells, such as cholesterol, vitamin B_{12}, and iron, to name a few. However, RME can also be used by viruses attempting to infect cells.[52]

Another way to look at the RME process is to consider the various forces at work at the interface between a particle potentially able to be internalized by a cell via RME (meaning the surface of the particle contains some concentration of a ligand complimentary to a receptor on a cell membrane) and the outer side of a cell membrane.[53] Forces which aid in the internalization process could be: 1) forming new bonds between ligands on the particle and receptors on the cell surface (driven by a reduction in the overall free energy of the system); and 2) potential non-specific attractions between the cell surface and the particle. Forces which hinder the internalization process could be: 1) the cell membrane bending to surround the particle (including thermal fluctuations in the cell membrane potentially opposed to such deformation); 2) the ability of receptor molecules to diffuse laterally along the membrane to get to the site of particle-membrane interaction; 3) the degree to which a ligand-receptor bond is able to stretch as a cell membrane is drawn around a particle; and 4) potential non-specific repulsive forces between the cell surface and the particle. Though there are many factors which would affect the relative contribution of one force over another – for example, the density of receptors on the cell surface, or the density of the ligands on the

particle surface – as long as the attractive forces are greater than the repulsive forces, then the particle will become enveloped by the cell membrane and internalized.

1.3.4. Nuclear Localization.[51]

The DNA in a eukaryotic cell is bounded by two concentric membranes referred to as the nuclear membrane. This membrane is contiguous with the endoplasmic reticulum (ER), and is perforated by nuclear pores. Each pore contains an intricate protein mechanism – a nuclear pore complex – which restricts and regulates the flow of large molecules (i.e. RNAs, proteins), while allowing for the free, non-specific passing of small water-soluble molecules (i.e. ions, small metabolites) to and from the nucleus.

Any protein which is to be taken into a nucleus will necessarily contain a particular amino acid sequence – a nuclear localization sequence – which will initiate a cascade of events involving the binding of this protein with one or more transport molecules, which then facilitate transport through the nuclear pore complex.

1.3.5. General Cellular Internalization Considerations.

In summary, any potential cellular internalization vector or drug delivery vehicle intending to transport a molecular cargo of some sort to a cell's nucleus (for example) will necessarily have a series of issues with which to contend, as shown in Figure 1.2:

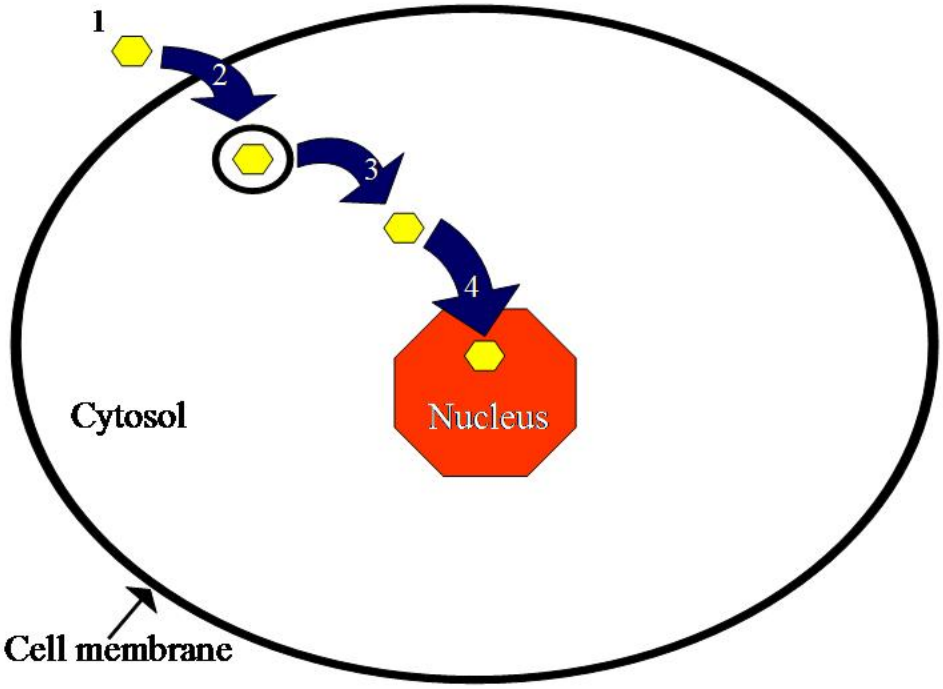

Figure 1.2. General intracellular delivery vehicle considerations. The four major considerations enumerated here are detailed in the text.

First, a potential vector must be both stable with regard to the *in vitro* or *in vivo* salt concentrations surrounding the cells of interest, and with equal regard to the ability to protect that vector's "payload" from premature digestion or from some otherwise inactivating process. Moreover, consideration should be given to the degree of toxicity the presence of this potential vector may cause. Additionally, when working *in vivo*, the vector must be capable of extended circulation and not subject to phagocytosis by other cells. Second, a potential intracellular vector must be capable of getting into the cell of interest, meaning the entire vector should be small enough to gain entry and, ideally, be targeted to increase both likelihood of entry and concentration of delivered moiety upon uptake. Third, once targeted

uptake has occurred, this potential vector needs some method of escaping any endosomal pathway to which it may be subjected, in order to avoid being digested or excreted. Finally, this potential vector should ideally be targeted for localization at the site of intended activity for the "payload." While achieving localization in the nucleus of a cell is not the goal of every cellular delivery vector,[54,55] the active site of many drugs is in the nucleus and any attempts at novel genetic manipulation experiments are likely to need access to cell nuclei. The vector described in this dissertation is intended for use with experiments which require nuclear localization after internalization, and subsequently employs a method for gaining efficient entry to the nucleus via the nuclear pore complex – a nuclear localization sequence (NLS) described in detail in a later section.

1.4. Nanotechnology.

Establishing a greater understanding of nanoscopic materials has permitted their subsequent utilization across many disciplines. In this dissertation, I am interested in potential medical applications. Exciting advances in "gene chip" apparati[56] are spurring the development of innovative diagnostic tools. Nanowires composed of various metals and metal oxides are being used as "nanosensors" for the detection and monitoring of varying biomaterials; most notably antibodies,[57] DNA,[58] viruses,[59] and bacteria.[60] Gold nanowires have even been used as a plasmid DNA delivery vector.[61] Carbon nanotubes are also being explored as potential biosensors,[62] and some research has shown certain nanotubes have been used in cellular uptake experiments,[63] though the toxicity of these nanotubes is problematic.[64]

Nanoparticles comprised of varying polymers[65] have been developed and used to aid in the cellular internalization of a range of materials both *in vitro*[66] and *in vivo*.[67] However, common issues with some such polymeric nanoparticles involve inefficiency of delivery[68,69] or cytotoxicity,[70,71] though very promising research using biodegradable polymers is currently being performed.[72] Many metallic colloids have been put to common use in biological experiments. Quantum dots (nanoparticles commonly comprised of a cadmium-selenide core and a zinc sulfide shell)[73] are used frequently as "tracers" during intracellular experiments.[74,75] Aluminum,[76] iron,[77] platinum,[78] silver,[79] and other metallic colloidal sols[80,81] are also commonly used in many different bioapplications.

Unfortunately, using these materials as cellular delivery vectors can be subject to many issues. They can exhibit low delivery efficiency, expensive and prohibitively time-consuming to make, difficult to modify or fine-tune, can be quite toxic, or perhaps have other inherent properties which make for problematic assays (i.e.: quantum dot "blinking"). Moreover, to get around some of these limitations, many cellular uptake experiments are run under complex/harsh conditions specifically in order to effect internalization of whatever moiety is intended to be delivered; that is, many experiments are dependant upon the use of chemical methods (i.e. digitonin, a chemical used to open pores in cellular membranes *in vitro*),[82] physical manipulation (i.e. microinjection: literally using a syringe to inject materials into cells, thus bypassing the cellular membrane)[83,84] or even electrical shocks (e.g. electroporation, which is the administering an electric shock to cells, causing pores in cellular membranes to open)[85] to permit materials of interest to enter cells.

1.4.1. Colloidal Gold.

Colloidal gold has perhaps the longest history of medicinal use of all metallic sols.[86,87] In the interest of constructing a novel drug delivery vector capable of cellular internalization, gold nanoparticles certainly are a strong candidate for such use: the biocompatibility of gold has been well established,[88] gold nanoparticles are simple to make and easily size-tunable,[89] the surface chemistry of gold nanoparticles permit facile and straight-forward modification with different passivating ligands,[90] many biologically significant moieties have been shown to complex readily and in a stable fashion with gold nanoparticles,[91] and their optical properties – specifically the presence of a strong localized surface plasmon resonance band[92] – make for simple detection schema.

One potential problem[93] involved with using inorganic nanoparticles (or any prospective non-biodegradable delivery vector, for that matter) *in vivo*: the inability of the body to clear/excrete these particles. Since there is no way to easily dissolve metallic nanoparticles in cells, these particles can accumulate in a cell (which may impede cell growth), and the ability of the body to excrete these nanoparticles decreases dramatically when the diameter of the particles is larger than ~ 5 nm.[93] However, while this is a serious consideration in the overall development of any inorganic nanoparticle intracellular delivery vehicle, the research described in this dissertation should be thought of as a preliminary *in vitro* "proof of concept" that the nanoparticle vehicles synthesized will localize in the nuclei of certain cells, and it is recognized that further refinement will be necessary to achieve proper future *in vivo* delivery capability.

1.4.1.1. Synthesis of Gold Nanoparticles.

There have been many published methods of gold nanoparticle preparations in both aqueous and organic solutions since Faraday's groundbreaking work.[86] Generally, tetrachloroauric ($HAuCl_4$) is reduced to form spheres of reasonably uniform diameter in all of these methods, but under widely-varying conditions: choice of reducing agent, differing reagent concentrations or order of addition of these reagents, differing temperatures, and mixing rate. All of these variations have been used to routinely synthesize spherical gold nanoparticles from 1 to 200 nm,[94] and to construct nanoparticles modified with a panoply of functional and/or protective ligands, including carboxylic acids,[95,96] phosphenes,[95] oligonucleotides,[97] amines,[98] proteins,[99] enzymes,[99] and small drug molecules.[100]

The most common method of synthesizing gold nanoparticles in aqueous solution is using sodium citrate as the reducing agent of $HAuCl_4$, first demonstrated by Turkevich et al.[101] Briefly, an aqueous solution of $HAuCl_4$ is heated to 100 ^oC and kept at refluxing conditions. While stirring vigorously, an amount of sodium citrate is added quickly, resulting in the solution changing color from the initial yellow to clear, then to grey, and finally to burgundy, which marks the end of the reaction. The mixture is kept at 100 ^oC for a further 15 minutes and subsequently cooled to room temperature, maintaining vigorous stirring throughout. Varying the initial ratio of sodium citrate to $HAuCl_4$ will determine the ultimate size of the nanoparticles; larger ratios yield smaller particles. The resulting nanoparticles will be approximately spherical, and have an overall negative surface charge, due to adsorption of citrate ions onto the surface. These surface charges, together with

counter ions in solution, form an electric double layer which causes nanoparticles to be repelled from one another in solution, thus preventing the aggregation of the colloids.

1.4.1.2. Stability of Gold Nanoparticles. [102]

A colloidal system is defined as a suspension of solid particles dispersed in a continuous liquid phase. The nature and magnitude of interactions between particles in a suspension greatly affect the stability of the system. These interactions are typically characterized by the extent to which they either behave as a stabilizing or destabilizing force towards the system. For example, van der Waals forces – the collection of universal attractive forces between atoms and molecules – draw colloidal particles together while electrostatic forces – arising from a charged double layer present at each particle's surface – cause particles to be repelled from one another. If the attractive forces between particles in suspension become greater than the repulsive forces (e.g. if the distance between particles is smaller than the sum of their electric double layer distances), the particles will fuse irreversibly (flocculate) and precipitate.

Moreover, the addition of other species to a suspension – for example, a polymer – can induce either stabilization or flocculation of the particles in suspension. If an added polymer is non-adsorbing with respect to the particle surfaces, an attractive force may be created between two particles if a polymer molecule is ejected from between two approaching particle surfaces. Due to an osmotic pressure difference between the relatively high concentration of polymer outside the area between the two surfaces, the surfaces are subject to an attractive depletion force – a phenomenon known as depletion flocculation.

However, at higher polymer concentrations, it is possible that polymer molecules would be unable to be ejected from the area between two approaching surfaces. This could give rise to a repulsive force with respect to the two surfaces as the polymer molecule(s) resist compression; this is known as depletion stabilization. If an added polymer is capable of simultaneously adsorbing to more than one particle in suspension, this polymer will hold the particles together, giving rise to a phenomenon known as bridging flocculation. The degree to which a polymer capable of adsorbing to a particle in suspension can create a thick, dense adsorbed layer completely covering each individual particle will determine the amount of steric stabilization afforded to the system. Using a polyionic polymer in a suspension where the particles are oppositely-charged compared to the polymer will likely result in bridging, and subsequent flocculation. However, adsorption of a polyionic polymer to neutral particles in suspension then effectively adds an electrostatic stabilization mechanism to any steric stabilization effects. This is known as electrosteric stabilization, and is very common in biological systems.

1.5. Existing Intracellular Delivery Vehicles.

Scientists are continually developing and refining the ability to both deliver desired therapeutic molecules to specific areas in the body and to selectively manipulate genetic material in a living cell. Cancer research is just one of the many possible fields of biomedical research which would benefit greatly from advances in targeted drug delivery and tailored gene manipulation. In general, the development of an efficient, non-cytotoxic vector with which to deliver any molecule of choice into desired cells – and specifically into cell

nuclei – would be of great value with regard to typical experiments. A prospective reliable delivery vector could prove invaluable in defining intracellular mechanisms (i.e. transport mechanisms, feedback mechanisms in protein synthesis, etc.), examining known oncogenes and tumor repressor mechanisms, or perhaps aid in the discovery of new dynamics of this nature. To that end, there have been many different methods developed to deliver genetic material or molecules of biological significance to locations within cells, and a brief review of these vectors is in order.

1.5.1. Viral Vectors.

Many different methods of implementing targeted drug delivery and genetic modification are currently being used and refined. For example, mammalian viruses – retroviruses,[103] adenoviruses,[104,105] adeno-associated viruses,[106,107] and even plant viruses[108,109] – are themselves commonly being "re-outfitted" to function as a delivery vehicle for a payload of genetic material. This strategy is an attempt to modify the DNA of a given cell; take an existing vehicle (a virus) which is known both to invade cells and deliver genetic material with high efficiency, and merely replace the intrinsic, otherwise cell-damaging/disease-causing bits with some desired genetic material. A vector of this composition would seem to be ideal with respect to actually delivering some moiety of consequence. Disappointingly, the major obstacles in using these modified viruses *in vivo* are the propensity for the vectors themselves to elicit a strong immune response, and they can also be quite toxic. Furthermore, the modification of these viruses is a non-trivial procedure, and the viruses themselves inherently limit the "payload" for potential delivery only to what

can fit inside a native virus with a typical diameter of 30 – 100 nm. Also, uncontrolled recombination can be a concern in using a viral vector, since each specific function of a given virus' inherent DNA/RNA may not always be clear.[110] It should be mentioned that plant viruses are least limited by these considerations.

1.5.2. Non-Viral Vectors.

Other approaches to targeted genetic manipulation involve delivery methods of a non-viral nature. Liposomes,[111] hydrogels,[112] and dendrimers[113] have been used successfully as carriers for genetic material in cellular uptake experiments. Gene guns[114] have been used to achieve the same effects, although this method is typically more for use with plant cell transfection than with mammalian cells due to the more robust character of the exterior membrane of plant cells. Even "naked" DNA (and cationic-packed DNA)[115,116] has been shown to be taken up by certain cells under specific circumstances. However, all of these methods – especially the latter three – can be inefficient, are often cytotoxic, are prone to inserting DNA non-specifically in cells (increasing likelihood of tumor formation), and will often only yield a transient transfection of the desired DNA instead of a permanent change.[117,118]

1.5.3. Viral/Non-Viral Combination Vectors.

While there is much current research attempting to manipulate entire viruses in such a fashion as to make them plausible cellular delivery vectors, various active regions of the viruses of themselves have been extremely valuable research tools. Scientists have long been

using relevant pieces of viruses as biological probes;[119] one such piece being the NLS sequence of the simian virus 40 (SV40) large tumor ("large T") antigen.

1.5.3.1. SV40 Large T NLS.

SV40, a polyomavirus, was discovered in 1959 as a contaminant in poliovirus vaccines prepared using rhesus monkey renal cell cultures.[120] It was found that this virus could induce large tumors in rodents (hence the "large T" moniker) and immortalize many types of cells in culture (including human cells). The entire SV40 large T antigen is an oncoprotein known to both stimulate cell division and attenuate intrinsic cellular tumor suppression mechanisms, such as the p53 regulatory mechanism.[121] The large T NLS peptide sequence – PKKKRKV – is a very small piece of the entire antigen (708 amino acids),[122] and is itself the most thoroughly-characterized NLS.[123] It has been shown to effectively penetrate cell nuclei using a mediated process via nuclear pore complexes.[83]

Some of the seminal studies examining nuclear penetration involving this peptide sequence were performed using colloidal gold stabilized with a conjugate of large T bound to larger proteins, notably bovine serum albumin (BSA).[84,124] In this early research, these complexes were microinjected into both amoeba and BALB/3T3 cells, and differing parameters (i.e. using different peptides, using point-mutated peptide sequences, varying carrier protein) were manipulated to examine the extent to which nuclear localization would or would not take place. The gold nanoparticle merely functioned as a marker for the complexes' location as determined via transmission electron microscopy (TEM) analyses post-incubation.

1.6. Summary.

There is a distinct need for innovative approaches to intracellular drug delivery and genetic manipulation. Whether one desires to activate/suppress/change a given gene in a particular cell, deliver a therapeutic molecule to a specific organelle within a cell, or even if one merely wants to probe a cellular process of interest, then getting moieties of interest into cells reliably, efficiently, and without generating significant toxicity is of paramount importance.

This dissertation demonstrates that an intracellular delivery vehicle can be developed using large T/BSA-gold nanoparticle complexes. In order to examine the potential interaction of these complexes with cells cultured *in vitro*, human cervical cancer cells (HeLa) were selected for analysis since they are a very widely-used cell line, easy to maintain, and allow for facile transport of external moieties across their cell membrane. Additionally, the degree to which complexes could efficiently localize in cell nuclei even when administered merely by incubating cells in media containing these complexes was demonstrated and quantified. Moreover, various parameters of particle synthesis (i.e. number of large T peptides per BSA, overall stability of large T/BSA-colloidal gold complexes, nanoparticle diameter, temperature, etc.) were tested to optimize the internalization and subsequent nuclear localization of these complexes.

Using colloidal gold as a "scaffold" upon which one can place a stabilizing, non-toxic substance (such as a serum albumin, for example) which itself can be quickly and relatively easily modified with certain peptide sequences that target either specific cells or particular organelles/locations inside cells is the ultimate long-range goal for the line of scientific

inquiry detailed in this dissertation. There is a precedent for this idea – Feldherr et al used such colloidal constructs in their ground-breaking examinations of nuclear uptake mechanisms.[83,84] However, the quantification of cellular internalization of exogenous nanoparticles has not been previously presented.

One other issue involved in intracellular experimentation: imaging methods used when examining cells after incubation with colloidal gold delivery vectors (i.e.: video enhanced color differential interference contrast (VECDIC) microscopic techniques, TEM, confocal microscopy) have considerable limitations concerning potential delivery methods themselves. For example, VECDIC and confocal microscopy are both limited in the size of the discrete particles which can be detected, and TEM employs a random sectioning of cells for examination, potentially leading to inaccurate reporting of internalization. To address this issue, the use of inductively-coupled plasma – optical emission spectroscopy (ICP-OES) as a routine detection method of nanoparticle complex internalization was defined and developed. This technique provided quantitative information otherwise unavailable via other common detection methods.

While the research presented on the following pages does not attempt to address all the issues in designing the ideal delivery method or probe described previously, this research can be seen as a "first step" with regard to both learning about issues associated with cellular uptake of colloidal constructs and eventually addressing potential needs of cancer research in general.

1.7. References.

[1] Hussain, S. P.; Hofseth, L. J.; Harris, C. C. *Nature Reviews*, **2003**, *3*, 276 – 285.

[2] Smith, J. S.; Green, J.; Berrington de Gonzalez, A.; Appleby, P.; Peto, J.; Plummer, M.; Franceschi, S.; Beral, V. *Lancet*, **2003**, *361*, 1159 - 67.

[3] Jones, P. A.; Baylin, S. B. *Nature Reviews: Genetics*, **2002**, *3*, 415 – 428.

[4] Kuper, H.; Adami, H.-O.; Trichopoulos, D. *Journal of Internal Medicine*, **2000**, *248*, 171 – 183.

[5] Clemons, M.; Goss, P. *New England Journal of Medicine*, **2001**, *344(4)*, 276 – 285.

[6] Marks, P. A.; Rifkind, R. A.; Richon, V. M.; Breslow, R.; Miller, T.; Kelly, W. K. *Nature Reviews: Cancer*, **2001**, *1*, 194 – 202.

[7] Calle, E. E.; Rodriguez, C.; Walker-Thurmond, K.; Thun, M. J. *New England Journal of Medicine*, **2003**, *348(17)*, 1625 – 1638.

[8] Ueda, H.; Ullrich, S. J.; Gangemi, J. D.; Kappel, C. A.; Ngo, L.; Feitelson, M. A.; Jay, G. *Nature Genetics*, **1995**, *9*, 41 – 47.

[9] Nigg, E. A. *Nature Reviews: Cancer*, **2002**, *2*, 1 – 11.

[10] Carmeliet, P.; Jain, R. K. *Nature*, **2000**, *407*, 249 – 257.

[11] Bach, P. B.; Kelley, M. J.; Tate, R. C.; McCrory, D. C. *Chest*, **2003**, *123(1)*, 72 – 82.

[12] Ilic, D.; O'Connor, D.; Green, S.; Wilt, T. *Cancer Causes Control*, **2007**, *18*, 279 – 285.

[13] Otto, S. J.; Fracheboud, J.; Looman, C. W. N.; Broeders, M. J. M.; Boer, R.; Hendriks, J. H. C. L.; Verbeek, A. L. M.; de Koning, H. J. *Lancet*, **2003**, *361*, 1411 – 1417.

[14] Walsh, J. M. E.; Terdiman, J. P. *Journal of the American Medical Association*, **2003**, *289(10)*, 1288 – 1296.

[15] Noteborn, M. H. M.; Zhang, Y.-H.; van der Eb, A. J. *Mutation Research*, **1998**, 447 – 455.

[16] Lian, F.; Hu, K.-Q.; Russell, R. M.; Wang, X.-D. *Int. J. Cancer*, **2006**, *119*, 2084 – 2089.

[17] http://dtp.nci.nih.gov/timeline/noflash/milestones/M4_Nixon.htm

[18] Tagscherer, K. E.; Fassil, A.; Campos, B.; Farhardi, M.; Kraemer, A.; Böck, B. C.; Macher-Goeppinger, S.; Radlwimmer, B.; Wiestler, O. D.; Herold-Mende, C.; Roth, W. *Oncogene*, **2008**, 1 – 11.

[19] Henson, J. D.; Neumann, A. A.; Yeager, T. R.; Reddel, R. R. *Oncogene*, **2002**, *21*, 598 – 610.

[20] Mantovani, A.; Allavena, P.; Sica, A.; Balkwill, F. *Nature*, **2008**, *454*, 436- 454.

[21] Mantovani, A.; Romero, P.; Palucka, A. K.; Marincola, F. M. *Lancet*, **2008**, *371*, 771 – 783.

[22] Iwai, K.; Maeda, H.; Konno, T. *Cancer Research*, **1984**, *44*, 2115 – 2121.

[23] Wyld, D. K.; Selby, P.; Perren, T. J.; Jonas, S. K.; Allen-Mersh, T. G.; Wheeldon, J.; Burchill, S. A. *Int. J. Cancer*, **1998**, *79*, 288 – 293.

[24] Gosselin, M. V.; Rubin, G. D.; Leung, A. N.; Huang, J.; Rizk, N. W. *Radiology*, **1998**, *208(1)*, 209 – 215.

[25] Kiesslich, R.; Burg, J.; Vieth, M; Gnaendiger, J.; Enders, M.; Delaney, P; Polgase, A.; McLaren, W.; Janell, D.; Thomas, S.; Nafe, B.; Galle, P. R.; Neurath, M. F. *Gasteroenterology*, **2004**, *127*, 706 – 713.

[26] Pinkel, D.; Straume, T.; Gray, J. W. *Proc. Natl. Acad. Sci. USA*, **1986**, *83*, 2934 – 2938.

[27] Jiao, X.; Eslami, A.; Ioffe, O.; Kwong, K. F.; Henry, M.; Zeng, Q.; Refaely, Y.; Burrows, W.; Gamliel, Z.; Krasna, M. J. *The Annals of Thoracic Surgery*, **2003**, *76(4)*, 996- 1000.

[28] Nelson, H.; Petrelli, N.; Carlin, A.; Couture, J.; Fleshman, J.; Guillem, J.; Miedema, B.; Ota, D.; Sargent, D. *J. Nat. Cancer Inst.*, **2001**, *93(8)*, 583 – 596.

[29] Spano, J.-P.; Chodkiewicz, C.; Maurel, J.; Wong, R.; Wasan, H.; Barone, C.; Létourneau, R.; Bajetta, E.; Pithavala, Y.; Bycott, P.; Trask, P.; Liau, K.; Ricart, A. D.; Kim, S.; Rixe, O. *Lancet*, **2008**, *371*, 2101 – 2108.

[30] Bolla, M.; Gonzalez, D.; Warde, P.; Dubois, J. B.; Mirimanoff, R.-O.; Storme, G.; Bernier, J.; Kuten, A.; Sternbeg, C.; Gil, T.; Collette, L.; Pierart, M. *New England Journal of Medicine*, **1997**, *337(5)*, 295 – 300.

[31] Bubendorf, L.; Kolmer, M.; Kononen, J.; Kovisto, P.; Mousses, S.; Chen, Y.; Mahlamäki, E.; Schraml, P.; Moch, H.; Willi, N.; Elkahloun, A. G.; Pretlow, T. G.; Gasser, T. C.; Mihatsch, M. J.; Sauter, G.; Kallioniemi, O.-P. *J. Nat. Cancer Inst.*, **1999**, *91(20)*, 1758 – 1764.

[32] Parmiani, G.; Castelli, C.; Dalerba, P.; Mortarini, R.; Rivoltini, L.; Marincola, F. M.; Anichini, A. *J. Nat. Cancer Inst.*, **2002**, *94(11)*, 805 – 818.

[33] Lehman, P. *British Journal of Dermatology*, **2007**, *156*, 793 – 801.

[34] Samuel, S. K.; Spencer, V. A.; Bajno, L.; Sun, J.-M.; Holth, L. T.; Oesterreich, S.; Davie, J. R. *Cancer Research*, **1998**, *58*, 3004 – 3008.

[35] Giannakakou, P.; Sackett, D. L.; Kang, Y.-K.; Zhan, Z.; Buters, J. T. M.; Fojo, T.; Poruchynsky, M. S. *J. Biol. Chem.*, **1997**, *272(27)*, 17118 – 17125.

[36] Blagosklonny, M. V.; Fojo, T. *Int. J. Cancer*, **1999**, *83*, 151 – 156.

[37] Gieschen, H. L.; Spiro, I. J.; Suit, H. D.; Ott, M. J.; Rattner, D. W.; Ancukiewicz, M.; Willett, C. G. *Int. J. Radiation Oncology Biol. Phys.*, **2001**, *50 (1)*, 127 – 131.

[38] Bush, D. A.; Hillebrand, D. J.; Slater, J. M.; Slater, J. D. *Gastroenterology*, **2004**, *127 (5)*, S189 – S193.

[39] Schwartz, D. L.; Einck, J.; Bellon, J.; Laramore, G. E. *Int. J. Radiation Oncology Biol. Phys.*, **2001**, *50 (2)*, 449 – 456.

[40] Krämer, M.; Jäkel, O.; Haberer, T.; Kraft, G.; Schardt, D.; Weber, U. *Phys. Med. Biol*, **2000**, *45*, 3299 – 3317.

[41] Huber, P. E.; Debus, J.; Latz, D.; Zierhut, D.; Bischof, M.; Wannenmacher, M.; Engenhart-Cabillic, R. *Radiotherapy and Oncology*, **2001**, *59*, 161 – 167.

[42] Hoskin, P. J.; Saunders, M. I.; Dische, S. *Cancer*, **1999**, *86 (7)*, 1322 – 1328.

[43] Al-Sarraf, M.; Pajak, T. F.; Marcial, V. A.; Mowry, P.; Cooper, J. S.; Stetz, J.; Ensley, J. F.; Velez-Garcia, E. *Cancer*, **1987**, *59*, 259 – 265.

[44] Meresman, G. F.; Bilotas, M.; Buquet, R. A.; Barañao, R. I.; Sueldo, C.; Tesone, M. *Fertility and Sterility*, **2003**, *80 (2)*, 702 – 707.

[45] Schneider, J.; Huh, M. M.; Bradlow, H. L.; Fishman, J. *J. Biol. Chem.*, **1984,** *259 (8)*, 4840 – 4845.

[46] Huggins, C. *Science*, **1967**, *156 (3778)*, 1050 – 1054.

[47] Overgaard, M.; Jensen, M.-B.; Overgaard, J.; Hansen, P. S.; Rose, C.; Andersson, M.; Kamby, C.; Kjær, M.; Gadeberg, C. C.; Rasmussen, B. B.; Blichert-Toft, M.; Mouridsen, H. T. *Lancet*, **1999**, *353*, 1641 – 1648.

[48] Mouridsen, H.; Gershanovich, M.; Sun, Y.; Pérez-Carrión, R.; Boni, C.; Monnier, A.; Apffelstaedt, J.; Smith, R.; Sleeboom, H. P.; Jänicke, F.; Pluzanska, A.; Dank, M.; Becquart, D.; Bapsy, P. P.; Salminen, E.; Snyder, R.; Lassus, M.; Verbeek, J. A.; Staffler, B.; Chaudri-Ross, H. A.; Dugan, M. *J. Clin. Oncol.*, **2001**, *19*, 2596 – 2606.

[49] Pejawar-Gaddy, S.; Finn, O. J. *Crit. Rev. in Oncology/Hematology*, **2008**, *67*, 93 – 102.

[50] von Mehren, M.; Adams, G. P.; Weiner, L. M. *Annu. Rev. Med.*, **2003**, *54*, 343 – 369.

[51] Alberts, B.; Bray, D.; Hopkin, K.; Johnson, A.; Lewis, J.; Raff, M.; Roberts, K.; Walter, P. *Essential Cell Biology, 2nd Edition*, Garland Science, New York, NY, **2004**.

[52] Smith, A. E.; Helenius, A. *Science*, **2004**, *304*, 237 – 242.

[53] Decuzzi, P.; Ferrari, M. *Biomaterials*, **2007**, *28*, 2915 – 2922.

[54] Hoye, A. T.; Davoren, J. E.; Wipf, P.; Fink, M. P.; Kagan, V. E. *Acc. Chem. Res.*, **2008**, *41 (1)*, 87 – 97.

[55] Rosania, G. R. *Current Topics in Medicinal Chemistry*, **2003**, *3*, 659 – 685.

[56] Langer, R.; Tirrell, D. A. *Nature*, **2004**, *428*, 487 – 492.

[57] Zheng, G.; Patolsky, F.; Cui, Y.; Wang, W. U.; Lieber, C. M. *Nature Biotechnology*, **2005**, *23 (10)*, 1294 – 1301.

[58] Hahm, J.; Lieber, C. M. *Nano Letters*, **2004**, *4 (1)*, 51 – 54.

[59] Patolsky, F.; Zheng, G.; Hayden, O.; Lakadamyali, M.; Zhuang, X.; Lieber, C. M. *Proc. Nat. Acad. Sci.*, **2004**, *101 (39)*, 14017 – 14022.

[60] Pal, S.; Alocilja, E. C.; Downes, F. P. *Biosensors and Bioelectronics*, **2007**, *22*, 2329 – 2336.

[61] Kuo, C.-W.; Lai, J.-J.; Wei, K. H.; Chen, P. *Nanotechnology*, **2008**, *19*, 1 – 7.

[62] Li, C.; Curreli, M.; Lin, H.; Lei, B.; Ishikawa, F. N.; Datar, R.; Cote, R. J.; Thompson, M. E.; Zhou, C. *J. Am. Chem. Soc.*, **2005**, *127*, 12484 – 12485.

[63] Kam, N. W. S.; O'Connell, M.; Wisdom, J. A; Dai, H. *Proc. Nat. Acad. Sci.*, **2005**, *102 (33)*, 11600 – 11605.

[64] James, J. T.; McCluskey, R.; Arepalli, S.; Hunter, R. L. *Critical Reviews in Toxicology*, **2006**, *36*, 189 – 217.

[65] Brigger, I.; Dubernet, C.; Couvreur, P. *Adv. Drug Del. Rev.*, **2002**, *54*, 631 – 651.

[66] Hans, M. L.; Lowman, A. M. *Curr. Opin. Sol. State and Mat. Sci.*, **2002**, *6*, 319 – 327.

[67] You, H. S.; Lee, K. H.; Oh, J. E.; Park, T. G. *Journal of Controlled Release*, **2000**, *68*, 419 – 431.

[68] Cherng, J.-Y.; van de Wetering, P.; Talsma, H.; Crommelin, D. J. A.; Hennik, W. E. *Pharm. Res.*, **1996**, *13 (7)*, 1038 – 1042.

[69] Huang, M.; Khor, E.; Lim, L.-Y. *Pharm. Res.*, **2004**, *21 (2)*, 344 – 353.

[70] Fischer, D.; Li, Y.; Ahlmeyer, B.; Krieglstein, J.; Kissel, T. *Biomaterials*, **2003**, *24*, 1121 – 1131.

[71] Kirchner, C.; Javier, A. M.; Susha, A. S.; Rogach, A. L.; Kreft, O.; Sukhorukov, G. B.; Parak, W. J. *Talanta*, **2005**, *67*, 486 – 491.

[72] Shenoy, D.; Little, S.; Langer, R.; Amiji, M. *Mol. Pharm.*, **2005**, *2 (5)*, 357 – 366.

[73] Pinaud, F.; King, D.; Moore, H.-P.; Weiss, S. *J. Am. Chem. Soc.*, **2004**, *126*, 6115 – 6123.

[74] Ballou, B.; Lagerholm, B. C.; Ernst, L. A.; Bruchez, M. P.; Waggoner, A. S. *Bioconj. Chem.*, **2004**, *15*, 79 – 86.

[75] Gao, X.; Cui, Y.; Levenson, R. M.; Chung, L. W.; Nie, S. *Nature Biotechnology*, **2004**, *22 (8)*, 969 – 976.

[76] Jouet, R. J.; Warren, A. D.; Rosenberg, D. M.; Bellitto, V. J.; Park, K.; Zachariah, M. R. *Chem. Mater.*, **2005**, *17 (11)*, 2987 – 2996.

[77] Gupta, A. K.; Gupta, M. *Biomaterials*, **2005**, *26*, 3995 – 4021.

[78] Hrapovic, S.; Liu, Y.; Male, K. B.; Luong, J. H. T. *Anal. Chem.*, **2004**, *76*, 1083 – 1088.

[79] Redmond, P. L.; Wu, X.; Brus, L. *J. Phys. Chem. C*, **2007**, *111*, 8942 – 8947.

[80] Murayama, H.; Narushima, T.; Negishi, Y.; Tsukuda, T. *J. Phys. Chem. B*, **2004**, *108 (11)*, 3496 – 3503.

[81] Mornet, S.; Vasseur, S.; Grasset, F.; Duguet, E. *J. Mater. Chem.*, **2004**, *14*, 2161 – 2175.

[82] Cserpán, I.; Udvardy, A. *J. Cell Sci.*, **1995**, *108*, 1849 – 1861.

[83] Feldherr, C. M.; Akin, D.; Cohen, R. J. *J. Cell Sci.*, **2001**, *114*, 4621 – 4627.

[84] Dworetzky, S. I.; Lanford, R. E; Feldherr, C. M. *J. Cell Biol.*, **1988**, *107*, 1279 – 1287.

[85] Jen, C.-P.; Chen, Y.-H.; Fan, C.-S.; Yeh, C.-S.; Lin, Y.-C.; Shieh, D.-B.; Wu, C.-L.; Chen, D.-H.; Chou, C.-H. *Langmuir*, **2004**, *20*, 1369 – 1374.

[86] Faraday, M. *Philosophical Transactions of the Royal Society of London*, **1857**, *147*, 145 – 181.

[87] Daniel, M.-C.; Astruc, D. *Chem. Rev.*, **2004**, *104*, 293 – 346.

[88] Bhattacharya, R.; Mukherjee, P. *Adv. Drug Del. Rev.*, **2008**, *60*, 1289 – 1306.

[89] Templeton, A. C.; Wuelfing, W. P.; Murray, R. W. *Acc. Chem. Res.*, **2000**, *33*, 27 – 36.

[90] Shenhar, R.; Norsten, T. B.; Rotello, V. M. *Adv. Mater.*, **2005**, *17 (6)*, 657 – 669.

[91] Joshi, H.; Shirude, P. S.; Bansal, V.; Ganesh, K. N.; Sastry, M. *J. Phys. Chem. B*, **2004**, *108*, 11535 – 11540.

[92] Quinten, M. *Appl. Phys. B*, **2001**, *73*, 317 – 326.

[93] Choi, H. S.; Liu, W.; Misra, P; Tnaka, E.; Zimmer, J. P.; Ipe, B. I.; Bawendi, M. G.; Frangioni, J. V. *Nature Biotechnology*, **2007**, *25 (10)*, 1165 – 1170.

[94] Grabar, K. C.; Brown, K. R.; Keating, C. D.; Stranick, S. J.; Tang, S.-L.; Natan, M. J. *Anal. Chem.*, **1997**, *69*, 471 – 477.

[95] Franzen, S.; Folmer, J. C. W.; Glomm, W. R.; O'Neal, R. *J. Phys. Chem. A*, **2002**, *106*, 6533 – 6540.

[96] Simard, J.; Briggs, C.; Boal, A. K.; Rotello, V. M. *Chem. Commun.*, **2000**, 1943 – 1944.

[97] Storhoff, J. J.; Elghanian, R.; Mucic, R. C.; Mirkin, C. A.; Letsinger, R. L. *J. Am. Chem. Soc.*, **1998**, *120*, 1959 – 1964.

[98] Gomez, S.; Philippot, K.; Collière, V.; Chaudret, B.; Senocq, F.; Lecante, P. *Chem. Commun.*, **2000**, 1945 – 1946.

[99] Hayat, M. A. *Colloidal Gold: Principles, Methods and Applications*; Academic Press: New York, **1989**; Vol. 1.

[100] Wang, G.; Zhang, J.; Murray, R. W. *Anal. Chem.*, **2002**, *74 (17)*, 4320 – 4327.

[101] Turkevich, J.; Garton, G.; Stevenson, P. C. *J. Colloid Science*, **1954**, *9*, S26 – S35.

[102] Hiemenz, P. C.; Rajagopalan, R. *Principles of Colloid and Surface Chemistry*; 3rd ed.; Marcel Dekker, Inc.: New York, **1997**.

[103] Zufferey, R.; Dull, T.; Mandel, R. J.; Bukovsky, A.; Quiroz, D.; Naldini, L.; Trono, D. *J. Virol*, **1998**, *72(12)*, 9873 – 9880.

[104] Bouvet, M.; Ellis, L. M.; Nishizaki, M.; Fujiwara, T.; Liu, W.; Bucana, C. D.; Fang, B.; Lee, J. J.; Roth, J. A. *Cancer Research*, **1998**, *58*, 2288 – 2292.

[105] Wan, Y. Y.; Leon, R. P.; Marks, R.; Cham, C. M.; Schaack, J.; Gajewski, T. F.; DeGregori, J. *Proc. Nat. Acad. Sci.*, **2000**, *97(25)*, 13784 – 13789.

[106] Xiao, X.; Li, J.; McCown, T. J.; Samulski, R. J. *Experimental Neurology*, **1997**, *144*, 113 – 124.

[107] Monahan, P. E.; Samulski, R. J. *Mol. Med. Today*, **2000**, *6*, 433 – 440.

[108] Loo, L.; Guenther, R. H.; Lommel, S. A.; Franzen, S. *J. Am. Chem. Soc.*, **2007**, *129*, 11111 – 11117.

[109] Ren, Y.; Wong, S. M.; Lim, L.-Y. *Bioconjugate Chem.*, **2007**, *18*, 836 – 843.

[110] Thomas, C. E.; Ehrhardt, A.; Kay, M. A. *Nature Reviews: Genetics*, **2003**, *4*, 346 – 358.

[111] Liu, Y.; Liggit, D.; Zhong, W.; Tu, G.; Gaensler, K.; Debs, R. *J. Biol. Chem.*, **1995**, *270 (42)*, 24864 – 24870.

[112] Huang, H.; Pierstorff, E.; Osawa, E.; Ho, D. *Nano Letters*, **2007**, *7 (11)*, 3305 – 3314.

[113] Dufes, C.; Keith, W. N.; Bilsland, A.; Proutski, I.; Uchegbu, I. F.; Schätzlein, A. G. *Cancer Researh*, **2005**, *65(18)*, 8079 – 8084.

[114] Rakhmilevich, A. L.; Turner, J.; Ford, M. J.; McCabe, D.; Sun, W. H.; Sondel, P. M.; Grota, K.; Yang, N.-S. *Proc. Nat. Acad. Sci.*, **1996**, *93*, 6291 – 6296.

[115] Dean, D. A.; Strong, D. D.; Zimmer, W. E. *Gene Therapy*, **2005**, *12*, 881 – 890.

[116] Padmanabhan, K.; Smith, T. J. *Pharm. Dev. Tech.*, **2002**, *7 (1)*, 97 – 101.

[117] Niidome, T.; Huang, L. *Gene Therapy*, **2002**, *9*, 1647 – 1652.

[118] Pack, D. W.; Hoffman, A. S.; Pun, S.; Stayton, P. S. *Nature Reviews: Drug Discovery*, **2005**, *4*, 581 – 593.

[119] Lundberg, P. Langel, Ü. *J. Mol. Recognit.*, **2003**, *16*, 227 – 233.

[120] Sullivan, C. S.; Pipas, J. M. *Microbiology and Molecular Biology Reviews*, **2002**, *66 (2)*, 179 – 202.

[121] Carbone, M.; Rizzo, P.; Grimley, P. M.; Procopio, A.; Mew, D. J. Y.; Shridhar, V.; de Bartolomeis, A.; Esposito, V.; Guiliano, M. T.; Steinberg, S. M.; Levine, A. S.; Giordano, A.; Pass, H. I. *Nature Medicine*, **1997**, *3 (8)*, 908 – 912.

[122] DeCaprio, J. A.; Ludlow, J. W.; Figge, J.; Shew, J.-Y.; Huang, C.-H.; Lee, W.-H.; Marsilio, E.; Paucha, E.; Livingston, D. M. *Cell*, **1988**, *54*, 275 – 283.

[123] Robb, J. *J. Virol.*, **1973**, *12 (5)*, 1187 – 1190.

[124] Feldherr, C. M.; Akin, D. *J. Cell Biol.*, **1990**, *111*, 1 – 8.

Chapter 2

Synthesis and Characterization of Large T-SMCC-BSA/Nanoparticle Complexes.

2.1. Introduction.

This dissertation chapter begins with a brief discussion of the constituent pieces of the large T/BSA-gold nanoparticle complexes used in this research and the differences between these complexes and similar constructs used in other research. Then, the processes involved in synthesizing these complexes are described, including results from experiments performed to define certain parameters of the assembly of these nanoparticle complexes. Finally, data are presented concerning the stability of these complexes under varying conditions. Note that all experimental results are shown and discussed first, followed by a section defining materials used and a methodical description of experimental procedures which were performed.

Briefly, the general three-step scheme utilized in this research for construction of the large T/BSA-gold nanoparticle complexes is depicted in the cartoon in Figure 2.1.

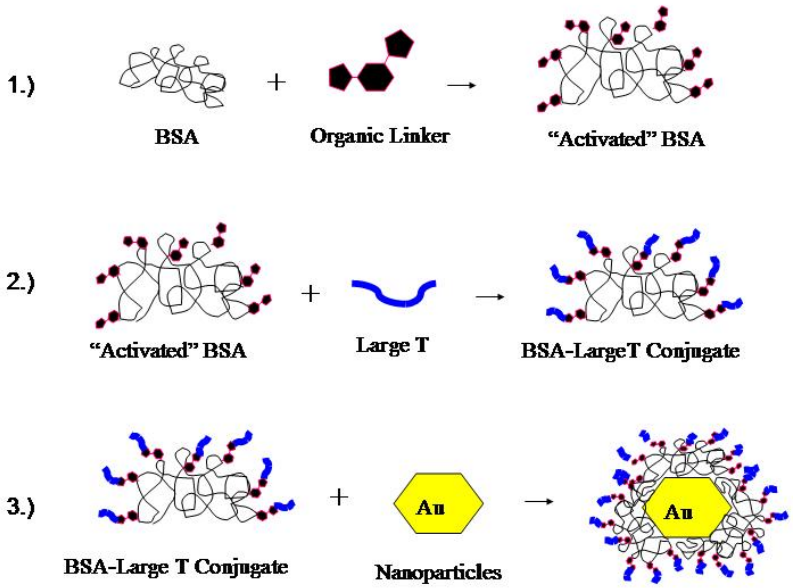

Figure 2.1. Cartoon representing the general construction scheme of large T/BSA-nanoparticle complexes.

While the general idea of having large T NLS peptides conjugated to BSA as a passivating layer for colloidal gold has been previously utilized – most notably by Feldherr, et. al.[1,2]; see Chapter 1 for full discussion – there are differences between the individual parts of this cellular probe used in the original Feldherr research and what was used in the research presented in this dissertation. The most ostensible difference is the organic heterobifunctional linker employed in conjugating the large T peptides to BSA molecules. The principle of using a heterobifunctional reagent is extremely useful for these types of conjugations – one side of this linker preferentially reacts with terminal amines while the other side preferentially binds with thiols. This enables one to use such molecular "preferences" in sequence to give rise to 1) linkage of the heterobifunctional reagent to BSA via its terminal amines, then 2) allow thiol-modified peptides to react with the other side of the bound linkers. Previous research performed by Feldherr et. al.[1,2] using these conjugates utilized m-maleimidobenzoyl-N-hydroxysuccinimide ester (MBS) as the organic linker between large T peptide sequence and BSA. However, it is known[3] that maleimides are subject to hydrolysis over short periods of time, which would potentially lower the amount of peptides one might otherwise be able to attach to BSA. Consequently, the heterobifunctional reagent chosen for use in this dissertation research was succinimidyl-4-(*N*-maleimidomethyl)cyclohexane-1-carboxylate (SMCC), which does not have its maleimide moiety directly connected to an extended π-system as MBS does, thus minimizing opportunity for hydrolysis. The structural differences between the two molecules can be seen in Figure 2.2.

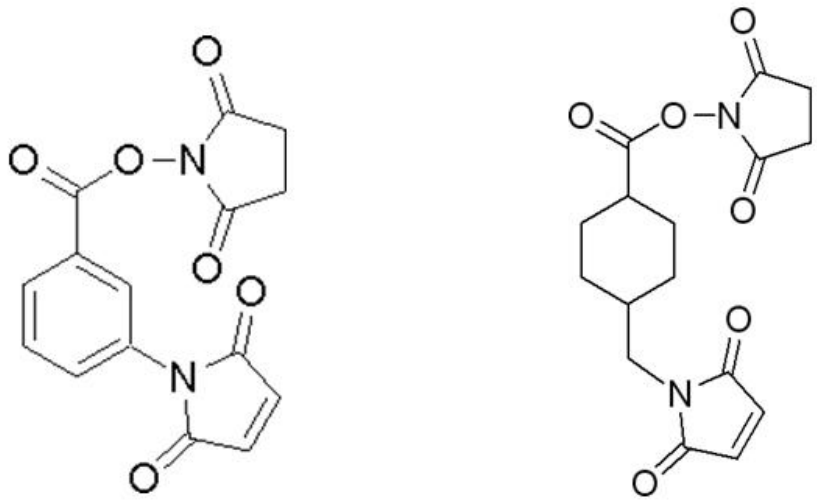

Figure 2.2. Structures of m-maleimidobenzoyl-N-hydroxysuccinimide ester (MBS) and succinimidyl-4-(*N*-maleimidomethyl)cyclohexane-1-carboxylate (SMCC).[4]

The large T NLS peptide sequence itself is a well-studied moiety which is known to penetrate cell nuclei efficiently[5,6,7] and is a fairly short peptide sequence compared to other known nuclear localization sequences; these are both good reasons to use this particular NLS in the assembly of a novel cellular delivery vehicle. BSA is a well-studied protein, biologically inert in its native form,[8] theoretically has many attachment points for SMCC (54 available surface lysines),[9] has many existing protocols for attaching various moieties of interest,[10] and is also commonly used with colloidal gold.[11,12]

15 nm diameter gold nanoparticles were chosen as the nanoparticles to be used in the cellular uptake experiments described in the next chapter. This decision was based upon the following: 1) nuclear pores in human cervical cancer cells (HeLa, described further in Chapter 3) have been reported to have a maximum diameter of 23 – 25 nm,[2,13] thus setting an

upper bound upon the overall nanoparticle complex size in order to allow for potential nuclear localization during an experiment (moreover, dynamic light scattering experiments performed during similar experiments involving BSA-20 nm diameter gold nanoparticle complexes determined the overall complex size was increased by approximately 2 nm,[14] potentially approaching the lower limit of what might pass through a nuclear pore); 2) 15 nm diameter nanoparticles are readily visible using other microscopy methods – such as VECDIC and confocal imaging; and 3) 15 nm particles can be seen as a compromise between potential facile detection using optical microscopy and having a large enough surface area to accommodate several conjugates/polypeptides for possible multifunctionality.[15]

2.2. Results and Discussion

2.2.1. Large T-SMCC-BSA Synthesis.

As mentioned previously, the conjugation of large T to BSA is accomplished via an organic linker, SMCC. An overview of the steps involved can be seen in Figure 2.1. Each of these steps is described in detail below.

2.2.1.1. SMCC-BSA Conjugation.

The first step in the process of synthesizing these conjugates is attaching SMCC (in organic solvent) to aqueous solution of BSA. There are existing protocols for this general process,[16] but it was decided to probe exactly how robust the system would be for our needs and to examine the ability to potentially modify any procedure at any step. To this end, it

was decided to expand and examine the general method of conjugation while we assembled our own conjugation protocol, tailored for our purposes.

In response to an potentially problematic issue observed during certain previous conjugation experiments, a quick study was performed in order to gauge any solubility issues with adding organic solvent (in which SMCC would ultimately be suspended) to aqueous solutions of BSA. Two common organic solvents used in these types of conjugations – dimethyl sulfoxide (DMSO)[17] and dimethyl formamide (DMF)[18] – and tetrahydrofuran (THF)[19] were chosen as the organic solvents of interest for these experiments. After mixing a calculated amount of this organic solvent to a given solution of BSA, many of these mixtures immediately and unexpectedly turned cloudy. Samples which did not immediately turn visibly cloudy were allowed to mix on a rocker for 30 minutes, which would be the time allowed for any SMCC solution to mix with BSA in the future conjugation experiments. It was observed some solutions which hadn't immediately turned cloudy upon addition of organic solvent had, in fact, turned visibly cloudy within 30 minutes. The results of these experiments are summarized in Table 2.1.

Table 2.1. Chart showing solubility of BSA in solutions of varying percentages of three different organic solvents at 25 °C. Diagonally-shaded boxes indicate immediate visual observation of cloudy solution upon addition of organic solvent to aqueous BSA solution in the indicated ratio, vertically-shaded boxes indicate visual cloudiness developed within 30 minutes after mixing, and clear boxes indicated no observable (by eye) evolution of cloudiness in solution.

[BSA]	% DMSO in Solution					% DMF in Solution					% THF in Solution				
(mg/mL)	20.0	10.0	5.0	2.5	2.0	20.0	10.0	5.0	2.5	2.0	20.0	10.0	5.0	2.5	2.0
10.0															
7.5															
5.0															
2.5															
2.0															

Based on the data shown in Table 2.1, all future conjugations of SMCC to BSA were performed: 1) upon BSA samples of 2 mg/mL concentration, 2) using SMCC in either DMSO or DMF based on availability, and 3) care was taken when introducing SMCC to BSA to ensure the overall amount of organic solvent used never exceeded 2 % of the resulting mixture. It should be noted that no effort was made to determine the exact nature of the cloudiness observed in solutions where it evolved; it was considered sufficient to define the experimental parameters necessary to avoid this visually-determined cloudiness for future experiments.

To determine the extent to which SMCC binds to BSA, fluorescamine assays (detailed in Figure 2.6 below) were performed after addition of varying amounts of SMCC to identical aliquots of BSA in sodium phosphate buffer. Fluorescamine is an inherently non-fluorescent molecule which becomes fluorescent when it binds to a primary amine.[20] Since BSA has many external lysine residues – each of which contains a terminal primary amine – fluorescamine was used in this research to determine the mole ratio of free lysines present in

a given BSA sample after mixing with SMCC, and compared to the mole ratio of free lysines when no SMCC was added to a sample of BSA. This difference was taken to be the approximate mole ratio of SMCCs conjugated to a given sample of BSA. The results of these experiments are listed in Table 2.2.

Table 2.2. General evaluation of SMCC binding to BSA. The calculated mole ratio of SMCC per BSA for each sample is the difference between free lysine residues determined for a given sample and the free lysines determined in native BSA (no SMCC added).

$SMCC:BSA_{Added}$ (mole ratio)	# Lys_{Free}:BSA (mole ratio)*	$SMCC:BSA_{Calc}$ (mole ratio)
0 (native BSA)	50 ± 4	0
20	41 ± 4	9 ± 6
40	32 ± 3	18 ± 5
60	19 ± 2	31 ± 5
80	11 ± 1	39 ± 4
100	8 ± 2	42 ± 5
125	6 ± 3	44 ± 4
150	3 ± 2	47 ± 5
175	2.4 ± 2.0	48 ± 5
200	2.0 ± 1.7	48 ± 4

* Uncertainty represents the standard deviation of nine fluorescence measurements; three measurements each from three replicate samples.

At this point, it was decided that the highest molar ratio of large T:BSA synthesized in the next experiments was going to be 30 large T peptides per BSA, so the SMCC:BSA molar ratio would need to be at least 30:1. Consequently, it was determined any molar ratio of SMCC:BSA at least 60:1 or greater would be appropriate in future conjugations.

2.2.1.2. Quantification of Large T Peptides per BSA-SMCC.

Having examined and refined the first part of the protocol for conjugation, the next part involved linking the large T peptide sequence to the BSA-SMCC conjugates. Again, methods for this type of conjugation already exist,[16] but in the interest of defining modifiable parameters for customization purposes, it was also necessary to provide as much quantification in this process as was possible.

Six different molar ratios of large T:BSA were intended to be synthesized, so eighteen separate aliquots of BSA-SMCC were prepared and placed into six groups of three aliquots each. The amount of SMCC per BSA was calculated for each sample created, and these results are shown in Table 2.3.

Table 2.3. Mole ratio of SMCC molecules conjugated with BSA for samples to be used in HeLa delivery experiments; $[Lys]_{Pre}$ refers to the experimentally-determined concentration of lysine in the BSA samples prior to addition of SMCC, while $[Lys]_{Post}$ refers to the detectable concentration of lysine in the BSA samples after samples were mixed with an aliquot of SMCC, filtered to remove excess SMCC, and resuspended in sodium phosphate buffer. Assays were performed immediately prior to conjugation with varying amounts of large T.

BSA Sample	$[Lys]_{Pre}$, μM*	$[Lys]_{Post}$, μM*	SMCC:BSA (mole ratio)
1	410 ± 30	148 ± 10	29 ± 2
2	390 ± 33	125 ± 8	30 ± 2
3	430 ± 41	124 ± 9	34 ± 3
4	420 ± 38	122 ± 8	34 ± 3
5	400 ± 39	150 ± 12	26 ± 3
6	380 ± 32	128 ± 8	27 ± 2
		Average:	***30 ± 2***

* Uncertainty represents the standard deviation of nine fluorescence measurements; three measurements each from three replicate samples.

Experiments were then performed to not only to determine how much of varying amounts of the rhodamine-labeled large T peptide was bound to aliquots of BSA (done via fluorescence measurements after conjugation and filtration, using a rhodamine-labeled large T standard curve), but also to determine how much of the rhodamine-labeled large T peptide sample was available for binding to the SMCC-BSA (done via Ellman's assay). A sample of peptide was dissolved in sodium phosphate buffer and added in varying molar ratios to each of the eighteen resuspended SMCC-BSA solutions, increasing the amount of peptide added per sample group; that is, the three SMCC-BSA samples corresponding to BSA Sample 1 in Table 2.3 each received an amount of peptide in a 5:1 large T:BSA molar ratio, thus ultimately making three stock solutions of large-T/BSA conjugate of this molar ratio. In this fashion, large T was mixed with the SMCC-BSA samples in 5:1, 10:1, 15:1, 20:1, 25:1, and 30:1 large T:BSA molar ratios. While these conjugations were taking place, an Ellman's assay was performed on aliquots of the peptide solution to determine how many free thiols were present, thus examining the "upper limit" of binding affinity for this specific solution. As shown in Table 2.4, approximately 68 % of the large T solution was available for binding with the SMCC-BSA conjugates, and Figure 2.3 shows the number of peptides determined to be bound to BSA (in terms of molar ratio) after conjugation, filtering away excess (unreacted) peptide, and resuspension in buffer versus how many large T peptides were added to the SMCC-BSA conjugates.

Table 2.4. Concentration of active cysteine residues determined via Ellman's reagent assay prior to conjugation to BSA:SMCC. Initial amount of peptide assayed was 100 μM.

Sample	[-SH], μM
1	69.1
2	66.7
3	68.0
Average:	***68 ± 1***

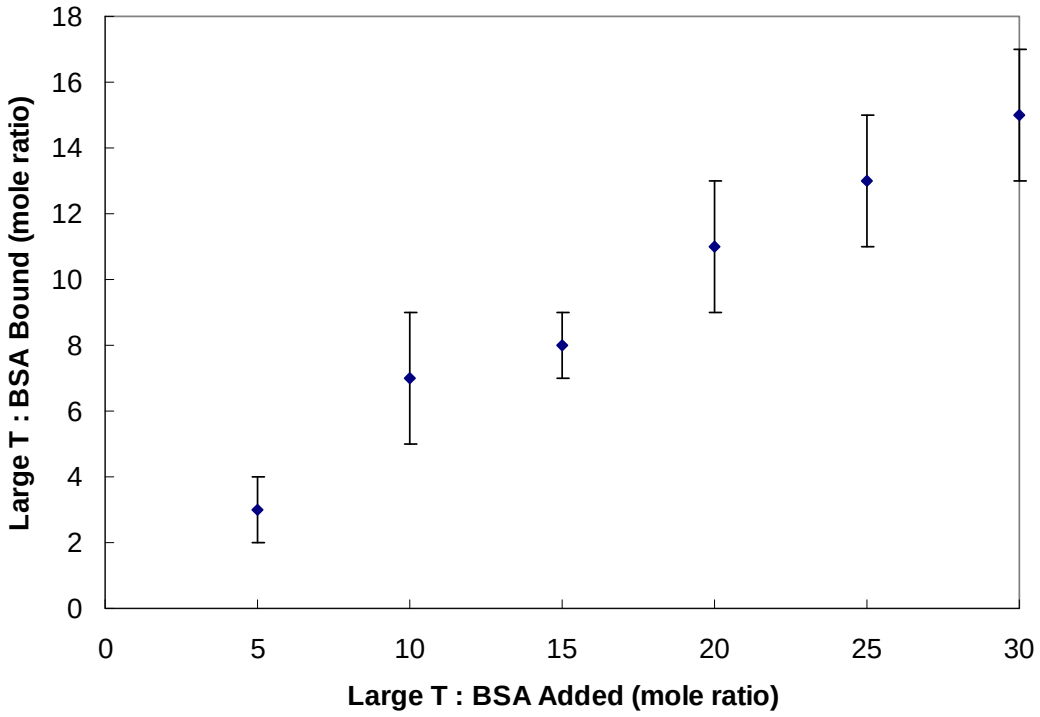

Figure 2.3. Molar ratio of large T peptides bound per BSA versus molar ratio of large T peptides initially added to SMCC-BSA samples. The bound values were determined via fluorescence after mixing, filtering excess unreacted peptide, and resuspension of large T-BSA conjugate. The errors displayed are the standard deviations of nine fluorescence measurements; three each from three replicate samples.

As can be seen in Figure 2.3, the amount of peptide detected post-conjugation was linearly dependent upon the amount of large T added to the SMCC-BSA samples.

2.2.2. Passivation of Gold Nanoparticles with Large T/BSA Conjugates.

The last step in constructing these intracellular vectors was to associate the large T/BSA conjugates with gold nanoparticles, quantify this association as well as possible, and examine the stability of the resulting nanoparticle complexes. The actual association was performed merely by adding the large T-BSA conjugates to aliquots of citrate-passivated gold nanoparticles, and it should be noted here (though it is discussed in greater detail in Chapter 3) that no attempts were made to remove any excess large T/BSA conjugates which were not directly associated with the surface of the nanoparticle aliquots. The fact that these large T/BSA:gold nanoparticle complexes can be made easily and used without a further purification step (see Chapter 3) is considered an advantage in synthetic protocol.

2.2.2.1. Quantification of Large T/BSA Conjugates per Nanoparticle.

Time-correlated single photon counting (TCSPC) was previously used[9] to determine the number of $[Ru(bipy)_2bipy\text{-}C_6H_{12}\text{-}S]^{2+}$-BSA molecules adsorbed to the surface of 20 nm diameter gold nanoparticles. This technique is well-suited for this application because gold-bound $[Ru(bipy)_2bipy\text{-}C_6H_{12}\text{-}S]^{2+}$-BSA moieties exhibit a quenched emission lifetime compared to free $[Ru(bipy)_2bipy\text{-}C_6H_{12}\text{-}S]^{2+}$-BSA in solution. Figure 2.4 shows time-resolved emission of $[Ru(bipy)_2bipy\text{-}C_6H_{12}\text{-}S]^{2+}$-BSA (0.2 μM) and $[Ru(bipy)_2bipy\text{-}C_6H_{12}\text{-}S]^{2+}$-BSA adsorbed to 20 nm diameter gold nanoparticles (concentrations of 0.2 μM and 0.4 nM, respectively, corresponding to a $[Ru(bipy)_2bipy\text{-}C_6H_{12}\text{-}S]^{2+}$-BSA:gold molar ratio of 500:1). $[Ru(bipy)_2bipy\text{-}C_6H_{12}\text{-}S]^{2+}$-BSA decays with single-exponential kinetics and an observed lifetime of 1.5 μs. The mixed protein-gold transient was best fit to a biphasic

model, with observed lifetimes of 1.8 μs and 14 ns, respectively. Table 2.5 shows the observed lifetimes of the systems investigated herein, as well as their relative populations. Based on these observed relative populations, it was determined that 160 ± 8 $[Ru(bipy)_2bipy\text{-}C_6H_{12}\text{-}S]^{2+}$-BSA conjugates were associated with 20 nm diameter gold nanoparticles. Other experiments with fluorescently-labeled BSA[9] confirmed this number.

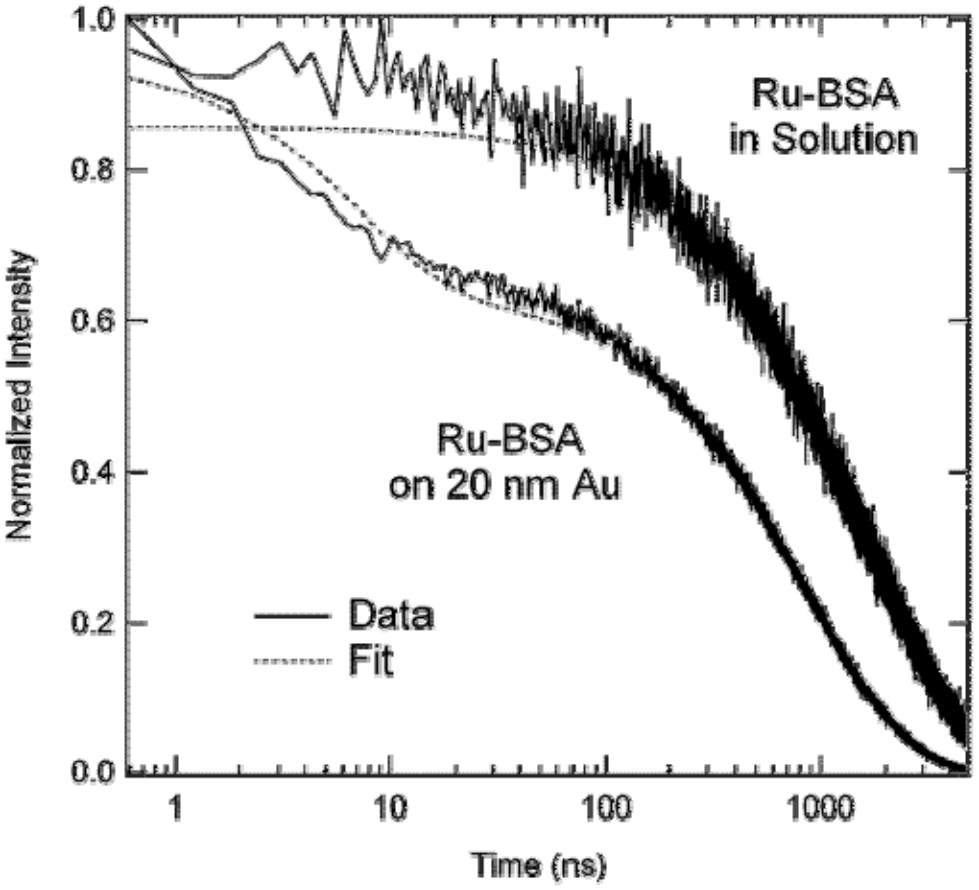

Figure 2.4. Normalized intensity versus time for solutions of $[Ru(bipy)_2bipy\text{-}C_6H_{12}\text{-}S]^{2+}$-BSA in solution and $[Ru(bipy)_2bipy\text{-}C_6H_{12}\text{-}S]^{2+}$-BSA + 20 nm diameter gold colloids. The concentration of $[Ru(bipy)_2bipy\text{-}C_6H_{12}\text{-}S]^{2+}$-BSA was 0.2 μM in solution, and the 20 nm diameter gold colloid concentration was 0.4 nM. The data are shown as solid lines and the fits as dashed lines.

Table 2.5. Lifetimes and calculated populations.*

system	lifetime τ_{obs}, ns	relative population	lifetime designation*
$[Ru(bipy)_2bipy\text{-}C_6H_{12}\text{-}SH]^{2+}$	1366.6	0.95	solution
$[Ru(bipy)_2bipy\text{-}C_6H_{12}\text{-}S]^{2+}$-BSA	1496.4	0.92	solution
$[Ru(bipy)_2bipy\text{-}C_6H_{12}\text{-}S]^{2+}$-BSA +	14.4	0.31	surface
20 nm citrate gold	1785.8	0.63	solution

* Refers to the classification of an adsorbate and its relative population as either surface-confined or free in solution.

It was presumed for the purposes of this research that: 1) large T/BSA conjugates and $[Ru(bipy)_2bipy\text{-}C_6H_{12}\text{-}S]^{2+}$-BSA conjugates associate with gold nanoparticle surfaces in a similar fashion, and 2) large T-BSA conjugates will associate with a gold nanoparticle with a constant surface density irrespective of nanoparticle diameter, and should thus scale directly with the total nanoparticle surface area; that is, the amount of large T/BSA conjugates associated with a given gold nanoparticle should be directly proportional to the surface area of that nanoparticle. Table 2.6 is a listing of calculated estimations of how many large T peptides are associated with 15 nm and 5 nm diameter nanoparticles for each molar ratio of large T:BSA conjugate previously synthesized, correcting the number of large T/BSA conjugates associated with a given nanoparticle for nanoparticle surface area compared to that of 20 nm diameter nanoparticles.

Table 2.6. Large T peptides per BSA and per nanoparticle complex.

Large T:BSA Mole Ratio in Reaction Mixture	Large T:BSA Mole Ratio Determined Experimentally*	Estimated Large T per 15 nm Diameter Nanoparticle Complex†	Estimated Large T per 5 nm Diameter Nanoparticle Complex†
5.0	3 ± 1	300 ± 100	30 ± 10
10.0	7 ± 2	600 ± 100	70 ± 20
15.0	8 ± 1	700 ± 100	80 ± 10
20.0	11 ± 2	1000 ± 200	110 ± 20
25.0	13 ± 2	1200 ± 200	130 ± 20
30.0	15 ± 2	1300 ± 200	150 ± 20

* Uncertainty represents the standard deviation of nine fluorescence measurements; three measurements each from three replicate samples.
† Estimate was based on the number of BSA molecules per 20 nm diameter gold nanoparticle determined using both fluorescence labeling and time-correlated single-photon counting (TCSPC) and adjusting for surface area. The standard deviation provided for each estimate was calculated from the % error in the corresponding entry in column 2 and is not a propagated error.

2.2.2.2. Critical Coagulation Concentration (CCC) Tests.

The stability of colloidal sols is due to a balance of forces including electrostatic repulsion, van der Waals attraction, and free energy of mixing.[21] The former two forces have been condensed into the well-known DLVO theory (Derjaguin, Landau, Verway, Overbeek), which explains the stability of charged particles. In DLVO theory, the attraction between two spheres due to their polarizability (van der Waals attraction) is compensated by repulsive forces acting between the electrical double layers of the two spheres. Specifically, the electrostatic repulsion varies as r^{-1} while the van der Waals attraction has an r^{-3} dependence, where r is separation distance. Thus, the electrical double layer normally prevents charged particles from approaching each other to within distances where their van der Waals attraction can pull them together. This phenomenon is described graphically in Figure 2.5.

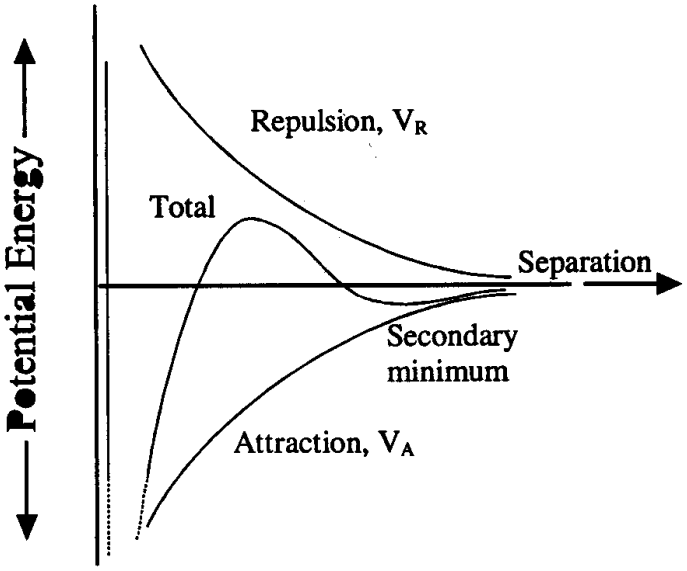

Figure 2.5. Potential energy versus nuclear separation; general description of DLVO theory.[21]

Under certain conditions, however, the length of electrical double layer surrounding a particle (the Debye length) can be reduced. When this occurs, the particles may approach one another to within distances that enable the van der Waals attraction to dominate the total interaction energy. Provided a secondary minimum does not exist, irreversible particle flocculation (fusion of a small number of particles) will then occur followed by precipitation. The conditions which cause flocculation of charged particles are predicted by the equation governing Debye length (ζ):

$$\zeta = \left(\varepsilon T / 8\pi n e^2 \nu^2\right)^{1/2} \qquad (1)$$

where ε is solution dielectric constant, T is temperature, n is salt concentration, and ν is salt valence. Therefore, lower temperatures, higher salt concentrations, and higher salt valences

all lead to decreasing the Debye length between colloidal particles and thus increase the likelihood of particle flocculation.

The following experiments describe the probing of the stability of the large T/BSA-gold nanoparticle complexes by varying the ionic strength of the solution around the nanoparticle complexes – a measure of the dielectric constant of this solution. The ionic strength of the growth media – Eagle's minimum essential media (EMEM) – to be used in experiments described later is approximately 0.149 M, so it was necessary to examine whether the large T/BSA-gold nanoparticle conjugates would be stable in just such an ionic environment. To this end, small aliquots of 1.7 M sodium chloride were successively added to nanoparticle complexes of many different formulations to determine the concentration at which flocculation of the nanoparticles themselves was observed – the critical coagulation concentrations (CCC) for each of these variations.

2.2.2.2.1. Varying BSA:Nanoparticle Ratio.

These first experiments were performed to get a quick idea of what general trends could be seen in BSA associating with gold nanoparticles. Consequently, a rigorous analysis (UV-Vis) was not performed for all combinations of BSA and gold nanoparticles but was performed on samples with the lowest amount of BSA added which visually appeared to remain stable for an appreciable amount of time. Moreover, while it was determined that each diameter nanoparticle had a threshold amount of BSA above which flocculation was not observed, it was considered sufficient to have such a value be a minimum value of BSA necessary to stabilize the colloids rather than 1) definitively determine the exact amount of

BSA per nanoparticle necessary to avoid flocculation or 2) further refine the experimentally-determined CCC region than was convenient (meaning there was no compelling reason to use smaller aliquots of salt solution). This is why certain CCC values are listed as "less than" certain amounts. Also, any potential CCC value above 0.85 M was not precisely ascertained as it was thought the demonstration of BSA-nanoparticle complex stability up to this point was adequate for the purposes of this research. All results from these first experiments can be seen in Table 2.7.

Table 2.7. CCC values of 15 nm diameter citrate- passivated gold nanoparticles after mixing with varying amounts of BSA. All CCC values listed – with noted exceptions – were determined visually using three independent samples per listing.

	Critical Coagulation Concentrations (M)					
BSA:Au	20 nm	20 nm	15 nm	15 nm	10 nm	5 nm
(molar ratio)	Uncentrifuged	Centrifuged	Uncentrifuged	Centrifuged	Uncentrifuged	Uncentrifuged
0 (citrate)	< 0.03	< 0.03	< 0.03	< 0.03	< 0.07	< 0.15
50:1	< 0.03	< 0.03	< 0.03	< 0.03	< 0.13	< 0.21
125:1	< 0.03	< 0.03	< 0.13	< 0.03	< 0.21	> 0.85*
250:1	< 0.07	< 0.03	> 0.85*	< 0.03	> 0.85*	> 0.85
500:1	> 0.85*	< 0.03	> 0.85	< 0.03	> 0.85	> 0.85
1000:1	> 0.85	< 0.03	> 0.85	< 0.03	> 0.85	> 0.85
2000:1	> 0.85	< 0.03	> 0.85	< 0.03	> 0.85	> 0.85

* Stability confirmed via UV-Vis analysis.

The first round of examination of stability via CCC testing was performed using BSA and citrate-passivated nanoparticle of 4 different diameters, and in certain cases samples were centrifuged to remove excess BSA prior to CCC testing. No effort was made to centrifuge 10 nm and 5 nm diameter nanoparticle samples. Additionally, since all 20 nm and

15 nm diameter nanoparticle experiments appeared to flocculate upon first addition of sodium chloride solution post-centrifugation and resuspension, it was decided that future cellular deliveries would not involve any centrifugation on nanoparticle complexes during construction and prior to actual incubation with cells. Instead, extra experiments were planned to evaluate any potential effect of excess conjugate upon ultimate cellular uptake (Chapter 3).

2.2.2.2.2. Varying Large T/BSA:Nanoparticle Ratio.

The next logical parameter explored using CCC testing was the stability of large-T/BSA conjugates with citrate-passivated 15 nm gold nanoparticles. The large T/BSA conjugate of the highest molar ratio (15:1 large T:BSA, experimentally determined) was used in the following experiments rather than testing all possible large T/BSA conjugates since it was reasoned that all lower amounts of large T present on BSA would progressively approach the behavior of native BSA, and the conjugate containing the largest amount of large T per BSA would clearly demonstrate the maximum possible difference from data already obtained for native BSA (Table 2.7). All samples were analyzed using UV-Vis spectroscopy, and the results are tabulated in Table 2.8.

Table 2.8. CCC values of 15 nm diameter citrate-passivated gold nanoparticles after mixing with varying amounts of large T-BSA conjugates. The large T-BSA conjugate of 15:1 (experimentally-determined) molar ratio of large T:BSA was used in all experiments listed in this table. All CCC values listed were determined via UV-Vis spectroscopy, using three independent samples per listing.

Large T/BSA:Au (molar ratio; $[\text{Large T}]_{\text{Constant}}$)	CCC (M)
0	< 0.03
67.5:1	< 0.03
125:1	< 0.35
250:1	> 0.85
500:1	> 0.85

Less large T/BSA conjugate was necessary to stabilize the 15 nm diameter gold nanoparticles than native BSA. While the 125:1 molar ratio of large T/BSA:15 nm diameter gold nanoparticle exhibited stability at over twice the minimum threshold necessary for later cellular incubations (recall the ionic strength of cellular growth media is 0.149 M), it was thought that using the lowest ratio of large T/BSA per 15 nm gold nanoparticle which exhibited the maximum CCC value over the ranges assayed would be most prudent. Consequently, the 250:1 molar ratio of large T/BSA:15 nm diameter gold nanoparticle was heretofore adopted into the evolving protocol for constructing these potential intracellular vectors.

2.2.2.2.3. Varying Large T:BSA Ratio.

Having determined a minimum value for large T/BSA-15 nm diameter gold nanoparticle complex stability (Table 2.8), the next parameter under scrutiny was the effect amount of large T peptide per BSA upon resulting nanoparticle complex stability. All 6

molar ratios of large T:BSA (and one native BSA) were mixed with 15 nm diameter gold nanoparticles in a 250:1 large T/BSA:nanoparticle ratio, and CCC values were generated as shown in Table 2.9.

Table 2.9. CCC values of 15 nm diameter citrate- passivated gold nanoparticles after mixing with large T-BSA conjugates of varying large T concentration. The molar ratio of large T-BSA conjugates per gold nanoparticle was 250:1 for all experiments listed in this table. All CCC values listed were determined via UV-Vis spectroscopy, using three independent samples per listing.

Large T:BSA (molar ratio; $[BSA]_{Constant}$)	CCC (M)
0	> 0.85
5:1	> 0.85
10:1	> 0.85
15:1	> 0.85
20:1	> 0.85
25:1	> 0.85
30:1	> 0.85

Not surprisingly, the amount of large T per BSA did not alter the perceived stability of resulting nanoparticle complexes at the 250:1 large T/BSA conjugate:15 nm diameter gold nanoparticle molar ratio. However, it was useful to have assayed this to definitively claim variations in large T per BSA did not adversely affect nanoparticle complex stability.

2.2.2.2.4. Varying Temperature.

Finally, the last parameter potentially affecting nanoparticle complex stability was temperature: cellular uptake experiments are typically performed at 37 ^{o}C, and certain

additional experiments were planned to be run at 4 ^{o}C. It was useful to check the stability of the nanoparticle complexes at these temperatures using UV-Vis equipped with a temperature control unit. Again, the large T/BSA conjugate with the highest molar ratio of large T per BSA (15:1, experimentally determined) was used in all samples, and was added to all aliquots of 15 nm diameter nanoparticle in a 250:1 large T/BSA:nanoparticle molar ratio. These results are shown in Table 2.10.

Table 2.10. CCC values of 15 nm diameter large T-BSA-passivated gold nanoparticles determined after conjugation at room temperature (approximately 25 ^{o}C), then storage at varying temperatures for 12 hours. Large T-BSA conjugates of 15:1 experimentally-determined molar ratio of large T:BSA were used in all experiments listed in this table, and the molar ratio of large T-BSA conjugates per 15 nm diameter gold nanoparticle was 250:1. All CCC values listed were determined via UV-Vis spectroscopy, using three independent samples per listing.

Temperature (^{o}C) ([Large T]$_{Constant}$; [BSA]$_{Constant}$)	CCC (M)
37	> 0.85
25	> 0.85
4	> 0.85

It should be noted that all nanoparticle complexes were found to be sufficiently stable at all three temperatures of interest.

2.3. Conclusions.

A general protocol for the conjugation of large T peptides to BSA and association of these conjugates to 15 nm diameter gold nanoparticles was refined and quantified. The number of organic linkers (in this case, SMCC) per BSA was found to be capable of

modifying with relative ease, and the large T itself was subsequently observed to bind to SMCC-BSA conjugates at a reasonably favorable rate. Nanoparticle complexes constructed with a 250:1 molar ratio of large T/BSA conjugate:15 nm diameter gold nanoparticle were found to be stable 1) irrespective of how much large T was present in the large T/BSA conjugates and 2) at three different temperatures.

2.4. Experimental.

2.4.1. Materials.

All gold nanoparticles were purchased from Ted Pella, Inc. (Redding, CA). The modified large T peptide sequence (rhodamine-Cys-Gly-Gly-Gly-Pro-Lys-Lys-Lys-Arg-Lys-Val-Gly-Gly-OH) was synthesized at the University of North Carolina Microprotein Sequencing and Peptide Synthesis Facility (Chapel Hill, NC). Bovine serum albumin (BSA) was purchased from Pierce Co. (Rockford IL). Dulbecco's phosphate-buffered saline (DPBS), Sephadex G-50, and 64-well cell culture plates were purchased from Bio-Whittaker, Inc. (Walkersville, MD). Dimethylformamide (DMF), dimethylsulfoxide (DMSO) tetrahydrofuran (THF), 4-(*N*-maleimidomethyl)-cyclohexane-1-carboxylic acid *N*-hydroxysuccinimide ester (SMCC), 5, 5'-dithio-bis-(2-nitrobenzoic acid) (DTNB; Ellman's reagent), Tris, ethylenediaminetetraacetic acid (EDTA), sodium acetate, glutathione, fluorescamine, lyinse, cysteine, sodium chloride, monobasic sodium phosphate (NaH_2PO_3), dibasic sodium phosphate (Na_2HPO_3), and Centricons (MWCO: 30,000), were all purchased from Fisher Scientific. Ruthenium-(II) tris(2,2'-bipyridine)monohexanethiol ($[Ru(bipy)_2bipy\text{-}C_6H_{12}\text{-}SH]^{2+}$) was synthesized as described previously.[22]

All UV-vis absorption measurements were acquired using a Hewlett-Packard 8453 Chemstation photodiode array spectrophotometer with attached Chemstation software and, in certain experiments, a temperature control unit. Quantification of $[Ru(bipy)_2bipy\text{-}C_6H_{12}\text{-}S]^{2+}$-labeled BSA on gold nanoparticles was performed by time-correlated single photon counting (TCSPC) using instrumentation at the University of North Carolina at Chapel Hill. Fluorescence spectra were acquired using a BioTek FL-600 plate reader with 1) 550 ± 40 nm (excitation) and 590 ± 40 nm (emission) filters for rhodamine detection, 2) 365 ± 40 nm (excitation) and 470 ± 40 nm (emission) filters for fluorescamine assays.

2.4.2. Methods.

2.4.2.1. SMCC-BSA Conjugation.

A fluorescamine assay was used to determine the amount of free lysine residues on many aliquots of aqueous BSA solutions obtained both before and after mixing with SMCC (described in Section 2.2.1.1. above). Fluorescamine itself is a non-fluorescent molecule, but upon reaction with a primary amine becomes fluorescent, and this reaction is depicted in Figure 2.6.

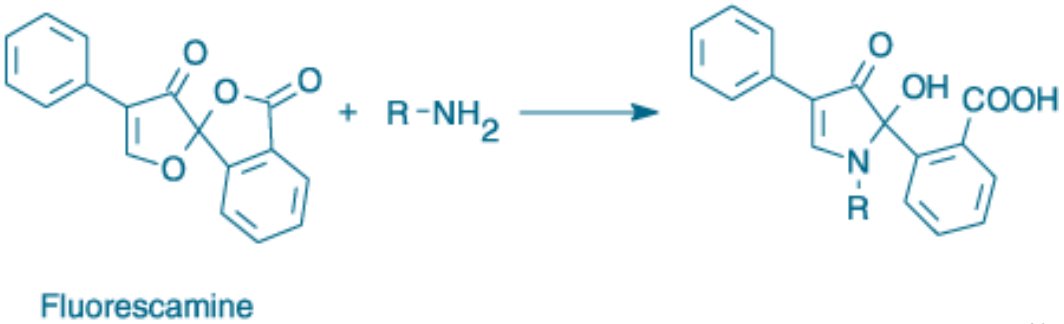

Figure 2.6. Fluorescamine structure before and after conjugation with primary amines.[20]

All determinations of free lysine residues before and after SMCC addition to BSA samples were performed using a standard curve of the difference between samples containing various concentrations of lysine and independent samples containing identical concentrations of cysteine.

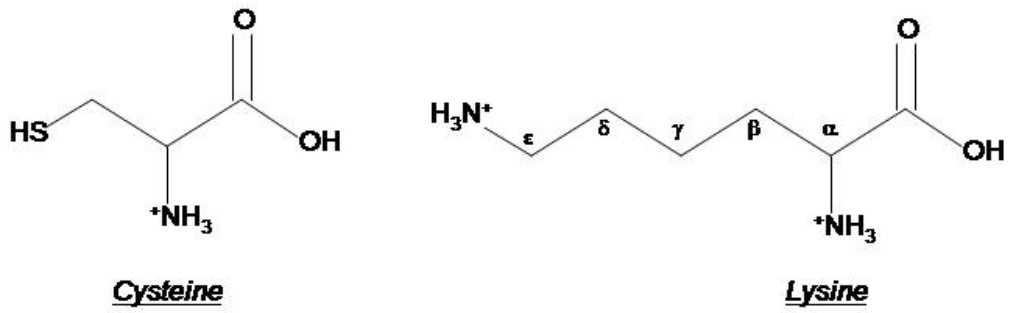

Figure 2.7. Molecular structures of cysteine and lysine.

As can be seen in the structures shown in Figure 2.7, merely using native lysine as a standard curve in this assay would present a problem; native lysine has two potential amines capable of binding with fluorescamine – one on its α-carbon and one on its ε-carbon – but the lysine residues contained in BSA would only have one available amine for binding with fluorescamine – the ε-carbon amine. Native cysteine, however, only has one available amine for reaction with fluorescamine, and it is analogous to the α-carbon amine of native lysine. Subsequently, subtracting the fluorescence readings of cysteine standards after reaction with fluorescamine from fluorescence readings obtained from identical standards of lysine post-reaction with fluorescamine would yield a fluorescence standard curve of ε-carbon amines which have reacted with fluorescamine, which is a much more accurate model of the lysine residues under scrutiny on BSA.

A 64-well plate was prepared for use in these assays by placing 135 μL of DPBS in 20 of the 64 wells, and 150 μL of DPBS in 4 of the wells (blanks). Ten 0.5 mL samples of BSA (1 mg/mL; in sodium phosphate buffer, pH = 7.8) were prepared, and a 15 μL aliquot of each sample was individually placed in a well on the 64-well plate, in the interest of ultimately determining how many lysine residues were present before reaction with SMCC ($[Lys]_{Pre}$). Aliquots of a SMCC solution (20 mg/mL, in DMF) were added in increasing SMCC:BSA molar ratios – 20:1, 40:1, 60:1, 80:1, 100:1, 125:1, 150:1, 175:1, and 200:1 – to the BSA samples, and one BSA sample received an aliquot of DMF (0:1 molar ratio of SMCC:BSA). All samples were allowed to mix at room temperature on a rocker for 60 minutes. Excess unreacted SMCC was removed via centrifugation (Centricon; MWCO = 30,000) and each sample was resuspended in 0.5 mL of sodium phosphate buffer (pH = 7.8). 15 μL of each resuspended sample was now added to ten other individual wells on the 64-well plate ($[Lys]_{Post}$). 50 μL of a freshly-prepared fluorescamine solution (3 mg/mL, in DMSO), was added to each well containing samples, blanks, or lysine/cysteine standards (ranging from 1.89 to 15.15 μM). The well was allowed to rock at room temperature for 15 minutes, after which fluorescence readings were obtained ($\lambda_{Emission}$ = 470 nm). This entire procedure was repeated three times. It should be noted that it was presumed 5% of BSA samples were considered lost due to the Centricon. This loss was factored into calculations.

2.4.2.2. Quantification of Large T Peptides per BSA/SMCC.

Eighteen 1.0 mL samples of BSA (1 mg/mL, NaPi; pH = 7.8) were prepared and divided into six groups of three samples per group. All BSA samples had 15 μL aliquots taken from each of them for use in a fluorescamine assay as described in the previous section (determining $[Lys]_{Pre}$). All BSA samples were then treated with an aliquot from an SMCC solution (20 mg/mL, in DMF) in a 60:1 SMCC:BSA molar ratio and allowed to mix on a rocker at room temperature for 60 minutes. However, the addition of the SMCC aliquots was performed in a staggered fashion, meaning two groups of BSA samples received an aliquot of SMCC and were allowed to mix for 60 minutes, then 20 minutes later the next two groups of BSA samples received their aliquots of SMCC, then finally 40 minutes after the initial addition, the remaining two groups of BSA samples received their aliquots of SMCC. (This was done to streamline the large amount of samples needing to be centrifuged post-mixing.) When the 60 minute mixing period had elapsed for a given bunch of samples, excess unreacted SMCC was removed via centrifugation (Centricon; MWCO = 30,000) and samples were resuspended in 1.0 mL of sodium phosphate buffer (pH = 7.0). Another 15 μL aliquot was taken from each sample for use in a fluorescamine assay as described in the previous section (determining $[Lys]_{Post}$). It should be noted that it was presumed 5% of BSA samples were considered lost due to the Centricon; this loss was factored into calculations.

Varying volumes (49.5, 99.1, 148.6, 198.1, 247.6, and 297.2 μL) of rhodamine-labeled modified large T peptide (rhodamine-CGGGPKKKRKVGG; 3 mg/mL in sodium phosphate buffer; pH = 7.0) were subsequently added to each SMCC-BSA sample to achieve six groups (each group consisting of triplicate samples) of large T:SMCC-BSA molar ratios

(5:1, 10:1, 15:1, 20:1, 25:1, and 30:1, respectively), and all samples were allowed to mix at room temperature for 24 h. Excess unreacted peptide was removed via centrifugation (Centricon; MWCO = 30,000). All samples were then diluted to 1.0 mL with sodium phosphate buffer (pH = 7.0). Following dilution, the degree of peptide conjugation was then determined via examination of rhodamine 6G fluorescence at 595 nm for each sample, utilizing a standard curve of rhodamine 6G-labeled peptide solution. It should be noted that it was again presumed 5% of BSA samples were considered lost due to the Centricon; this loss was factored into calculations appropriately.

While large T was mixing with SMCC-BSA solutions, an Ellman's assay was performed on aliquots taken from the large T solution in the interest of determining how many free thiols were present, and, therefore, what percentage of peptide was actually available for binding to the SMCC-BSA conjugate samples. 5, 5'-dithio-bis-(2-nitrobenzoic acid) (DTNB; Ellman's reagent) is a molecule which, when acted upon by a free thiol, gives rise to a product with a strong absorbance at 421 nm. This general reaction is depicted in Figure 2.8.

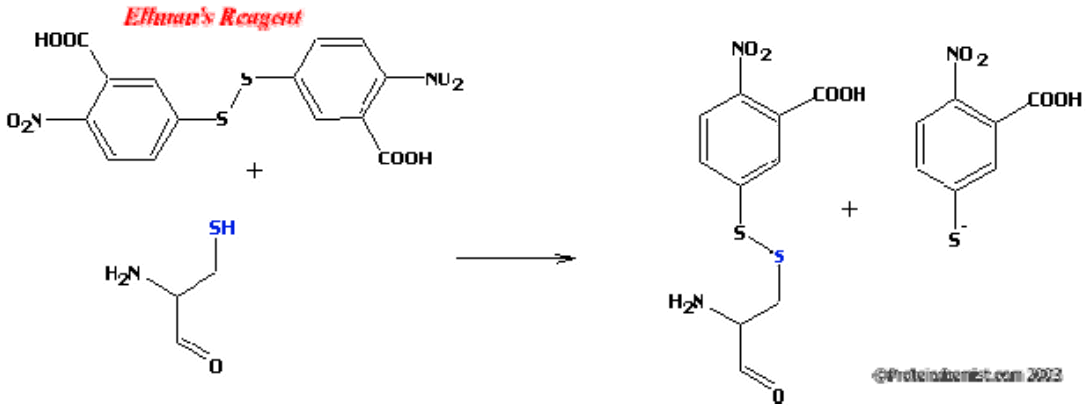

Figure 2.8. Structure of DTNB (Ellman's Reagent) and general mechanism.[23]

Since each large T peptide contains exactly one cysteine residue and each cysteine residue contains exactly one terminal thiol (see structure in Figure 2.7), this Ellman's assay was a quick way of measuring how many large T peptides in our sample were free to bind to the SMCC-BSA conjugates. An aliquot of the large T solution was taken and diluted to 100 μM for use in this assay, and varying concentrations (10 to 150 μM) of glutathione were used to generate a standard curve. All assays were performed in disposable UV cuvettes.

Two solutions were prepared for use in the Ellman's assay: 10.0 mL of a DTNB stock solution (50 mM sodium acetate, 2mM DTNB in H_2O; kept refrigerated) and 100.0 mL of a Tris dilution buffer (1 M Tris, pH = 8.0; kept refrigerated). 50 μL of DTNB stock solution, 100 μL of Tris dilution buffer, and 840 μL of water were then placed in every cuvette and mixed rapidly via pipette. 10 μL of analyte – either blank, standard, or sample – was added to a given cuvette, covered with a small piece of parafilm, then vortexed for approximately 30 seconds. The cuvette was then allowed to sit at room temperature for 5 minutes, after which an absorbance reading at 412 nm was taken. Thiol concentration was calculated using an extinction coefficient of 13,600 $M^{-1}cm^{-1}$ and a dilution factor of 100.

2.4.2.3. Quantification of Large T/BSA Conjugates per Nanoparticle.

2.4.2.3.1. Preparation of BSA-MBS-$[Ru(bipy)_2bipy\text{-}C_6H_{12}\text{-}SH]^{2+}$ Conjugates.

MBS was dissolved in dimethylformamide (10 mg/mL) and added to aqueous solutions containing BSA (10 mg/mL, in pH 7.2 PBS buffer) to produce a molar ratio of MBS to BSA of 40:1. The reaction was allowed to proceed for 30 min at room temperature. Sephadex G-50 was employed to remove unreacted MBS.

A solution of $[Ru(bipy)_2bipy\text{-}C_6H_{12}\text{-}SH]^{2+}$ (1 mM) was added to 1 mL aliquots of BSA/MBS (1 mg/mL) to yield an initial molar ratio of 15:1 $[Ru(bipy)_2bipy\text{-}C_6H_{12}SH]^{2+}$ per BSA-MBS and allowed to mix at room temperature for 60 min. All samples were then separated from excess $[Ru(bipy)_2bipy\text{-}C_6H_{12}\text{-}SH]^{2+}$ by centrifugal filtration (Centricon,YM-30). Steady-state emission spectra were recorded on a PTI Quantamaster luminescence spectrometer (MD-5020) using 450-nm excitation while monitoring emission intensity from 530 to 700 nm. The emission quantum yield of the C_6H_{12}-SH-modified $[Ru(bpy)_3]^{2+}$ was determined using a luminescent compound with a known quantum yield; $[Ru(bpy)_3]^{2+}$ (QY = 0.042 ± 0.002 at 25 °C).[24] Absorbance (UV-visible) and steady-state emission spectra were collected for aqueous solutions containing either modified or unmodified $[Ru(bpy)_3]^{2+}$. By comparing the steady-state emission peak areas for solutions containing identical concentrations of modified and unmodified $[Ru(bpy)_3]^{2+}$, the ratio of the quantum yields was found. The quantum yield of $[Ru(bpy)_2bpy\text{-}C_6H_{12}\text{-}SH]^{2+}$ was calculated to be 0.026 ± 0.003 at 25 °C.

The number of $[Ru(bipy)_2bipy\text{-}C_6H_{12}\text{-}SH]^{2+}$ labels attached to BSA was determined by comparing the emission of the BSA-$[Ru\text{-}(bipy)_2bipy\text{-}C_6H_{12}\text{-}SH]^{2+}$ conjugate to that of a free $[Ru(bipy)_2bipy\text{-}C_6H_{12}\text{-}SH]^{2+}$ standard curve. After comparison of sample emissions to the standard curve, it was determined that there were 8 ± 1 $[Ru(bipy)_2bipy\text{-}C_6H_{12}\text{-}SH]^{2+}$ molecules/BSA under conditions where ~20 MBS molecules were conjugated to BSA. The yield for reaction of $[Ru(bipy)_2bipy\text{-}C_6H_{12}\text{-}SH]^{2+}$ with MBS was ~0.5 under the conditions studied here.

2.4.2.3.2. Time-Resolved Emission Methods.

Time-resolved emission spectra were acquired with an argon ion laser whose continuous output was used to pump a mode-locked Ti:sapphire oscillator. The Ti:sapphire laser output was frequency doubled to 423 nm using a BBO crystal to produce ~1 ps pulses with a pulse energy of ~0.26 nJ/pulse. This pulse train was pulse picked and the repetition rate selected to be roughly 5 times the natural lifetime of the sample. Luminescence lifetime data were collected using the time-correlated single photon counting technique published earlier.[25] Samples were sparged with argon for ~45 minutes prior to use.

The method for analysis of the fraction of luminescent molecules on the surface of a nanoparticle and in solution has been also published previously.[25] Relaxation from the radiative excited states was modeled using the following exponential decays:

$$Y(t) = \sum_{i=1}^{N} A_i e^{-k_i t} \qquad (2)$$

where N is the total number of phosphorescent components and A_i and k_i represent the amplitude is rate constant for each component, respectively. The final fit was approached using an iterative process where exponentials were added until no significant improvements in the correlation coefficient of the fit could be seen. The calculated populations associated with each observed lifetime were then compared to the initial added concentration of emitter (free in solution) in order to determine the number of emitters associated with the gold colloids. For example, if there are two populations, there will be two observed lifetimes. The radiative rate constant for unquenched $Ru(bipy)_3^{2+}$ in solution is:

$$1/\tau_{obs} = 1/\tau_{phos} + 1/\tau_{non-rad} \qquad (3)$$

where $k_{obs} = 1/\tau_{obs}$, $k_{phos} = 1/\tau_{phos}$, etc. The phosphorescence lifetime is τ_{obs}, and the nonradiative lifetime is $\tau_{non\text{-}rad}$. Quenching can occur by electron or energy transfer from $[Ru(bipy)_2bipy\text{-}C_6H_{12}\text{-}S]^{2+}$ to the gold nanoparticle with rate constant, k_{et} to give an observed lifetime of:

$$1/\tau_{obs} = 1/\tau_{phos} + 1/\tau_{non-rad} + 1/\tau_{et} \qquad (4)$$

The phosphorescence quantum yield is:

$$\phi = k_{phos} / \left(k_{phos} + k_{non-rad} + k_{et}\right) \qquad (5)$$

where $k_{et} = 0$ for the solution fraction. It turns out that the ratio of the amplitudes, A_i/A_j in the fit correspond exactly to the ratio of the amounts of $[Ru(bipy)_2bipy\text{-}C_6H_{12}\text{-}S]^{2+}$ in phases *i* and *j*, respectively.

2.4.2.4. Critical Coagulation Constant (CCC) Tests.

2.4.2.4.1. Varying BSA:Nanoparticle Ratio.

Beginning with a stock solution of 20 nm diameter citrate-passivated nanoparticles (1.2 nM), seven 500 μL aliquots of this stock solution were placed into disposable centrifuge tubes. Each sample received an aliquot of a BSA stock solution (2mg/mL in dH_2O) to achieve one of the following molar ratios of BSA per nanoparticle: 0:1 (nanoparticle samples received only dH_2O), 50:1, 125:1, 250:1, 500:1, 1000:1, or 2000:1. After mixing via vortex for approximately 15 seconds, the samples were allowed to sit at room temperature for 5 minutes. 10 μL of a 1.7 M sodium chloride solution was added to one sample, mixed via vortex for approximately 15 seconds, then visually inspected to see if any observable

coagulation of particles had occurred – if not, then another 10 μL of 1.7 M NaCl was added and the sample vortexed again and rechecked for flocculation. This process was repeated until either flocculation was observed (at which point the approximate CCC value was calculated) or until 500 μL of 1.7 M NaCl had been added with no observable aggregation of particles. In this latter case, the sample was vortexed a final time and allowed to sit at room temperature for 30 minutes, after which the sample was transferred to a disposable UV cuvette and an absorbance scan on the sample was performed to confirm there was no evidence of particle coagulation. This entire procedure was repeated three times for 1.2 nM solutions of four particle diameters (20, 15, 10, and 5 nm), and repeated again in triplicate for separate samples of 20 nm and 15 nm diameter BSA-nanoparticle complexes which had been centrifuged to a pellet and resuspended in fresh dH_2O.

2.4.2.4.2. Varying Large T/BSA:Nanoparticle Ratio.

Aliquots of the previously-described 15:1 large T:BSA conjugate (experimentally-determined molar ratio) were added to five different 500 μL samples of 15 nm diameter citrate-passivated gold nanoparticles (2.3 nM) in disposable UV cuvettes to achieve the following large T/BSA per nanoparticle molar ratio: 0:1 (an aliquot of NaPi @ pH = 7.0 was added), 67.5:1, 125:1, 250:1, and 500:1. After covering each cuvette with parafilm and mixing via vortex for approximately 15 seconds, the samples were allowed to sit at room temperature for 5 minutes. 10 μL of a 1.7 M sodium chloride solution was added to one sample, mixed via vortex for approximately 15 seconds, then an absorbance scan was performed on the sample to see if any detectable coagulation of particles had occurred – if

not, then another 10 μL of 1.7 M NaCl was added and the sample vortexed again and rechecked via UV for flocculation. This process was repeated until either flocculation was observed (at which point the approximate CCC value was calculated) or until 500 μL of 1.7 M NaCl had been added with no detectable aggregation of particles. In this latter case, the sample was vortexed a final time and allowed to sit at room temperature for 30 minutes, after which an absorbance scan on the sample was performed to confirm there was no evidence of particle coagulation. This entire procedure was then repeated twice, yielding triplicate sets of data.

2.4.2.4.3. Varying Large T : BSA Ratio.

Aliquots of each of the previously-described large T:BSA conjugates were added to six different 500 μL samples of 15 nm diameter citrate-passivated gold nanoparticles (2.3 nM) in disposable UV cuvettes to achieve a 250:1 large T/BSA per nanoparticle molar ratio. After covering each cuvette with parafilm and mixing via vortex for approximately 15 seconds, the samples were allowed to sit at room temperature for 5 minutes. 10 μL of a 1.7 M sodium chloride solution was added to one sample, mixed via vortex for approximately 15 seconds, then an absorbance scan was performed on the sample to see if any detectable coagulation of particles had occurred – if not, then another 10 μL of 1.7 M NaCl was added and the sample vortexed again and rechecked via UV for flocculation. This process was repeated until either flocculation was observed (at which point the approximate CCC value was calculated) or until 500 μL of 1.7 M NaCl had been added with no detectable aggregation of particles. In this latter case, the sample was vortexed a final time and allowed

to sit at room temperature for 30 minutes, after which an absorbance scan on the sample was performed to confirm there was no evidence of particle coagulation. This entire procedure was then repeated twice, yielding triplicate sets of data.

2.4.2.4.4. The Effect of Temperature Variation.

Nine 0.5 mL samples of 15 nm diameter citrate-passivated gold nanoparticles (2.3 nM) in disposable UV cuvettes were allowed to equilibrate overnight at one of three separate temperatures: three samples at 4 ^{o}C (in a refrigerator), three samples at 25 ^{o}C (on notebook in lab), and three samples at 37 ^{o}C (temperature-controlled incubator; carefully sterilized). Additionally, aliquots of the previously-described 15:1 large T:BSA conjugate (experimentally-determined molar ratio) and stock solutions of 1.7 M NaCl were allowed to equilibrate overnight at the three temperatures.

For the experiments performed at 25 ^{o}C, identical aliquots of the large T:BSA conjugate were added to three different 500 μL samples of the 15 nm diameter citrate-passivated gold nanoparticles to achieve a 250:1 large T/BSA per nanoparticle molar ratio. After covering each cuvette with parafilm and mixing via vortex for approximately 15 seconds, the samples were allowed to sit at room temperature for 5 minutes. 50 μL of a 1.7 M sodium chloride solution was added to one sample, mixed via vortex for approximately 15 seconds, then an absorbance scan was performed on the sample to see if any detectable coagulation of particles had occurred – if not, then another 50 μL of 1.7 M NaCl was added and the sample vortexed again and rechecked via UV for flocculation. This process was repeated until either flocculation was observed (at which point the approximate CCC value

was calculated) or until 500 μL of 1.7 M NaCl had been added with no detectable aggregation of particles. In this latter case, the sample was vortexed a final time and allowed to sit at room temperature for 30 minutes, after which an absorbance scan on the sample was performed to confirm there was no evidence of particle coagulation.

For the experiments performed at 4 ^{o}C, the UV-Vis spectrophotometer (and accompanying computer) were wheeled into a nearby 4 ^{o}C cold room, allowed to sit in the cold room for 2 hours prior to experimentation, and the entire procedure utilized for the 25 ^{o}C experiments was repeated exactly (aside from temperature references) using the materials which had been equilibrated at 4 ^{o}C overnight.

For the experiments performed at 37 ^{o}C, a temperature control unit was used to keep samples at 37 ^{o}C during the experiment. After allowing this element to heat to 37 ^{o}C, materials for the experiment (one cuvette of nanoparticles, the large T/BSA aliquot, and the stock solution of 1.7 M NaCl) were removed from the incubator and the experiment was performed as quickly as possible. Considering the cuvette in undergoing analysis was largely kept at temperature when not being vortexed (and the cuvette, in fact, was allowed to remain in the temperature control unit for three extra minutes after each NaCl addition), the additions of small amounts of slowly-cooling NaCl solution to the sample was considered to have negligible effect upon the system temperature. The entire procedure utilized for the 25 ^{o}C experiments was repeated otherwise exactly as described previously (aside from temperature references).

2.5. References.

[1] Dworetzky, S. I.; Lanford, R. E.; Feldherr, C. M. *J. Cell Biol.*, **1988**, *107*, 1279 – 1287.

[2] Feldherr, C. M.; Akin, D. *J. Cell Biol.*, **1990**, *111*, 1 – 8.

[3] Ishikawa, E.; Imagawa, M.; Hashida, S.; Yoshitake, S.; Hamaguchi, Y.; Ueno, T. *Journal of Immunoassay*, **1983**, *4 (3)*, 209 – 327.

[4] Structures obtained from: http://www.piercenet.com.

[5] Feldherr, C. M.; Akin, D.; Cohen, R. J. *J. Cell Sci.*, **2001**, *114 (24)*, 4621 – 4627.

[6] Fontes, M. R. M.; Teh, T.; Toth, G.; John, A.; Pavo, I.; Jans, D. A.; Kobe, B. *Biochem. J.*, **2003**, *375*, 339 – 349.

[7] Lange, A.; Mills, R. E.; Lange, C. J.; Stewart, M.; Devine, S. E.; Corbett, A. H. *J. Biol. Chem.*, **2007**, *282 (8)*, 5101 – 5105.

[8] Berg, J. M.; Tymoczko, J. L.; Stryer, L. *Biochemistry, 5th Edition*; W. H. Freeman and Company; New York, **2002**.

[9] Xie, H.; Tkachenko, A. G.; Glomm, W. R.; Ryan, J. A.; Brennaman, M. K.; Papanikolas, J. M.; Franzen, S.; Feldheim, D. L. *Anal. Chem.*, **2003**, *75*, 5797 – 5805.

[10] Depalo, N.; Mallardi, A.; Comparelli, R.; Striccoli, M.; Agostiano, A.; Curri, M. L. *J. Colloid and Interface Science*, **2008**, *325*, 558 – 566.

[11] Neutra, M. R.; Phillips, T. L.; Mayer, E. L.; Fishkind, D. J. *Cell and Tissue Research*, **1987**, *247*, 537 – 546.

[12] Xu, W.; Xu, S.; Ji, X.; Song, B.; Yuan, H.; Ma, L.; Bai, Y. *Colloids and Surfaces B: Biointerfaces*, **2005**, *40*, 169 – 172.

[13] Feldherr, C. M.; Akin, D. *J. Cell Sci.*, **1997**, *110*, 3065 – 3070.

[14] Tkachenko, A. G.; Xie, H.; Coleman, D.; Glomm, W.; Ryan, J.; Anderson, M. F.; Franzen, S.; Feldheim, D. L. *J. Am. Chem. Soc.*, **2003**, *125*, 4700 – 4701.

[15] Engel, M. F. M.; van Mierlo, C. P. M.; Visser, A. J. W. G. *J. Biol. Chem.*, **2002**, *277 (13)*, 10922 – 10930.

[16] Lanford, R. E.; Kanda, P.; Kennedy, R. C. *Cell*, **1986**, *46*, 575 – 582.

[17] Parker, K. C.; Bednarek, M. A.; Hull, L. K.; Utz, U.; Cunningham, B.; Zweerink, H. J.; Biddison, W. E.; Coligan, J. E. *J. Immunology*, **1992**, *149 (11)*, 3580 – 3587.

[18] Cruz, L. J.; Iglesias, E.; Aguilar, J. C.; Quintana, D.; Garay, H. E.; Duarte, C.; Reyes, O. *J. Peptide Sci.*, **2001**, *7*, 511 – 518.

[19] Kitagawa, T.; Aikawa, T. *J. Biochem.*, **1976**, *79*, 233 – 236.

[20] Structures obtained from: http://probes.invitrogen.com/handbook/figures/0840.html.

[21] Glomm, W. R. *Journal of Dispersion Science and Technology*, **2005**, *26*, 389 – 414.

[22] Sato, Y.; Uosaki, K. *Journal of Electroanalytical Chemisty*, **1995**, *384*, 57 – 66.

[23] http://www.proteinchemist.com/chemistry/ellmans.html.

[24] Van Houten, J.; Watts, R. J. *J. Am. Chem. Soc.*, **1976**, *98 (16)*, 4853 – 4858.

[25] Brennaman, M. K.; Alstrum-Acevedo, J. H.; Fleming, C. N.; Jang, P.; Meyer, T. J.; Papanikolas, J. M. *J. Am. Chem. Soc.*, **2002**, *124 (50)*, 15094 – 15098.

Chapter 3

Incubations of BSA-SMCC-Large T/Nanoparticle Complexes with Human Cervical Cancer Cells.

3.1. Introduction.

With stable, well-characterized nanoparticle complexes in hand, the focus of this research shifted to cellular delivery. Primarily, the initial experiments detailed in this chapter were performed to gauge the utility of ICP-OES in measuring nanoparticle complexes internalized by human cervical cancer cells *in vitro*. It was found that while analysis of gold nanoparticles using this method had been performed previously,[1] this detection method was typically used merely as a quick analysis of colloidal concentration, and none of the existing protocols were listed in detail (nor were attempts to optimize such measurements readily available). Consequently, the research detailed in the first part of this chapter sought to define a repeatable and reliable protocol to utilize ICP-OES as an integral part of cellular internalization experiments involving gold nanoparticle complexes. After this analytical technique was shown to be extremely valuable to these experiments, examination of the consequences of nanoparticle complex composition (and various other experimental conditions) upon resulting cellular internalization for this particular cell line were assayed in detail. Once again, note that all experimental results are shown and discussed first, followed by a section defining materials used and a methodical description of experimental procedures which were performed.

3.1.1. The HeLa Cell Line.

Human cervical adenocarcinoma epithelial cells – HeLa; from Henrietta Lacks, a 31-year-old African-American female at the time of initial harvesting – were chosen for this research. They were the first human cells discovered to thrive and multiply outside the

body,[2] and are currently a widely-used cell line, easy to maintain, and useful in that they are known to allow easy transport of moieties across the outer cell membrane. In considering the ultimate delivery of a potential vector to a cell's nucleus – experiments concerning which will be shown in Chapter 4 – this potential ease of entering a cell from the surrounding microenvironment is of no small consequence. It should therefore be noted that this is a model system for these types of experiments; truly optimized delivery for these nanoparticle complexes would certainly need to be accomplished on a per cell line basis, tailored to a given target cell line.

3.1.2. Discussion of ICP-OES Method Development.

ICP-OES is very useful for detecting trace amounts of metals in heterogenous samples. For example, ICP-OES has been used to detect free cadmium ions released from quantum dots,[3] measure manganese in blood levels,[4] and specifically determine amounts of gold present in ore samples.[5]

The immediate focus of this section of research was determining the optimal parameters involved in detecting trace amounts of gold nanoparticle complexes incubated with HeLa cells. The first experiments detailed below were designed to address the fundamental question in developing this novel approach to analysis: can ICP-OES precisely and accurately measure the low concentrations of gold which are to be used in experiments involving cellular delivery? Upon answering this question in the affirmative, a protocol was constructed with the ultimate goal of maximizing potential signal of any particular sample. Generally, it was found: 1) replicate cellular samples could be combined to augment resulting

gold emission signals in a linear fashion, 2) these samples could be dissolved completely in aqua regia with no apparent ill effects on resulting emission intensities (very important for later cellular incubations), and 3) the dilution of all samples approximately ten-fold with ultrapure water prior to analysis for ease of use in the instrument resulted in very stable and strong emission intensities. It should be noted that the resulting gold emission intensities from the experiments listed below were compared to a standard curve generated from coincident analyses of gold standard solutions, and then these correlated concentrations were back-calculated into numbers of nanoparticles of a given diameter.

3.1.3. General Cellular Incubation Considerations.

All experiments involving HeLa cells were performed at 37 ^{o}C & 5 % CO_2 unless otherwise noted. The HeLa cells themselves were grown in T-75 cell culture flasks to approximately 85 % confluency using Eagle's minimal essential medium (EMEM) containing 10 % fetal bovine serum (FBS). Cells were plated into 12-well plates containing sterilized glass cover slips and allowed to reach 85 % confluency prior to experimentation.

3.2. Results and Discussion

3.2.1. ICP-OES Calibration Experiments

Table 3.1. ICP-OES intensities and calculated number of citrate-stabilized 20 nm diameter nanoparticles for standards prepared with and without acid digestion.*

Analyte	Intensity ($x10^5$)	Number of Nanoparticles ($x10^{10}$)
Au Nanoparticles	1.537 ± 0.005	6.220 ± 0.002
Au Nanoparticles (aqua regia)	1.550 ± 0.009	6.264 ± 0.004

*The uncertainty is the standard deviation of six replicate samples.

The standards used in these first calibration experiments contained 7.0 x 10^{10} gold nanoparticles. It can be seen in the results in Table 3.1 that approximately 10 % of the nanoparticles were not recovered at some point during the experiments.

The intensity values from the two sets of samples were compared using Student's *t* test and were observed to be statistically different from each other at the 95% confidence limit (t_{calc} = 2.99). While there is a small statistical difference between the observed signals obtained from samples with and without aqua regia treatment, it is likely that the acidic dissolution of the nanoparticle complexes prior to ICP-OES analysis enhanced the resulting signal slightly because: 1.) more gold was able to be recovered from the evaporated samples in the well plate compared with those samples which weren't subjected to aqua regia, or 2.) the acid-dissolved samples offer a mildly-enhanced presentation of the gold samples to the ICP itself, or 3.) both. Moreover, the data listed in Table 3.1 imply that if there are any matrix effects associated with the dissolution of nanoparticles, these effects are quite small; in any event, treatment of samples with aqua regia did not hinder the resulting signal obtained via ICP-OES. Since it was desirable to use aqua regia treatment of all future nanoparticle complex delivery studies involving cells (which would streamline the process greatly), these results about the nature of using aqua regia with ICP-OES analysis allowed this acid-dissolution step to be incorporated into the developing protocol.

Table 3.2. ICP-OES intensities of 15 nm diameter nanoparticle complexes constructed with varying passivating layers and incubated on glass coverslips for 6 h at 37 °C and in 5 % CO_2 in the absence of HeLa cells.*

Nanoparticle Passivating Layer	Intensity ($x10^3$)
18 MΩ H_2O (no Au)	0.05 ± 0.03
Citrate	0.18 ± 0.08
Native BSA	1.2 ± 0.1
Large T:BSA Conjugate (15:1)	4.0 ± 0.1

*The uncertainty is the standard deviation of six replicate samples.

Table 3.3. ICP-OES intensities of HeLa cell samples incubated for 6 h at 37 °C and in 5 % CO_2 with and without 15 nm-diameter gold nanoparticle complexes constructed using a 15:1 Large T/BSA (experimentally-determined ratio) conjugate.*

Analyte	Intensity ($x10^4$)
HeLa Cells (no Au)	0.010 ± 0.005
1 Cover Slip	1.051 ± 0.064
2 Cover Slips	2.247 ± 0.105
2 Cover Slips (Heparin Wash)	2.099 ± 0.112

*The uncertainty is the standard deviation of six replicate samples.

The results listed in Table 3.2 indicate nanoparticles passivated with large T/BSA appear to associate with empty glass cover slips in more than three times the amount of BSA-passivated nanoparticles, which, in turn, are nearly an order of magnitude more likely to associate with an empty glass cover slip than citrate-stabilized nanoparticles. It should be noted that the blank sample (18 MΩ H_2O) is included in this Table 3.2 for demonstration – this value was subtracted from all results listed in Table 3.2. Moreover, it should also be noted that all samples were diluted to 1.5 mL with cellular growth media; while there is FBS present in the growth media, it is likely the citrate-stabilized nanoparticles flocculated upon

addition of the cellular growth media, but this potential aggregation of nanoparticles was not assayed in this experiment.

While the ICP-OES signal for the BSA- and large T/BSA-passivated nanoparticles may seem large, comparison of these results with those listed in Table 3.3 reveal that the signals are significantly lower than those from samples of incubations with HeLa cells. HeLa cells were grown to approximately 85 % confluency prior to the introduction of nanoparticle complexes, so the results in Table 3.2 should be seen as a maximum possible adhesion of nanoparticle complexes to the glass cover slip in a given well, and the presence of so many HeLa cells prior to introduction of nanoparticle complexes should strongly mitigate (if not nearly eliminate) the possibility of any meaningful contribution of glass-adhered nanoparticle complexes to the resulting signals seen in Table 3.3. In other words: the resulting signals seen from incubations of nanoparticle complexes with HeLa cells (Table 3.3) are not likely to have a significant contribution from nanoparticle complexes which had solely adhered to the cover slip and not otherwise associated with a HeLa cell (Table 3.2).

In order to optimize ICP-OES signals, the effects of combining two identically treated coverslips into one ICP-OES sample were examined. It was expected that coverslips containing identical cell coverage and incubated with an identical concentration of nanoparticle complexes could be combined to approximately double the resulting ICP-OES signal without introducing nonlinearity in the measured signal. ICP-OES analysis of HeLa cells not exposed to gold nanoparticles gave only a slightly larger signal than pure water (Table 3.3). HeLa cells incubated with large T-BSA/gold nanoparticle complexes yielded signals that were proportional to the number of coverslips combined prior to sample

digestion. Thus, by combining coverslips the ICP-OES signal was increased without introducing artifacts from matrix effects or variability in cell coverage. The practice of combining two cover slips together post-incubation but before preparing the samples for ICP-OES analysis was henceforth incorporated into the developing protocol.

A Student's *t* test examining the variance in analyzing one coverslip versus two yielded no statistical difference at the 95 % confidence limit (t_{calc} = 2.15), and an analysis of the intensity of two coverslips with and without a heparin wash demonstrated a small but statistically significant difference at the 95 % confidence limit (t_{calc} = 2.36). Considering the average ICP-OES intensity values of the samples analyzed with and without a heparin wash, nonspecific binding of nanoparticles to the outer cell membrane contributes a maximum of 7% to the apparent observed internalization of these nanoparticle complexes.

3.2.2. Probing Optimal Time of Incubation

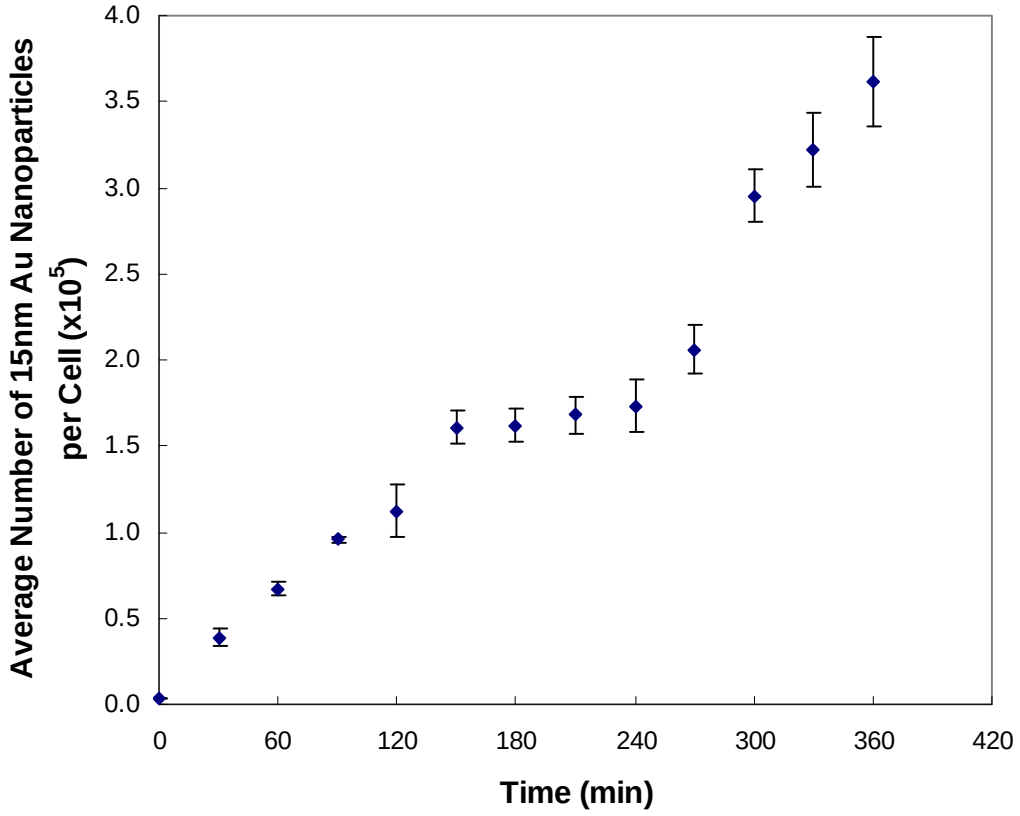

Figure 3.1. Average number of 15 nm diameter gold nanoparticle complexes (determined via ICP-OES analysis) per HeLa cell (determined via cell counting) vs incubation time. The nanoparticles were modified with large T-BSA conjugates of a single, experimentally determined molar ratio, 15:1 large T/BSA. (Error bars not immediately visible are smaller than the data point.)

The first examination of cellular internalization performed was designed to quantitatively examine the relationship between gold nanoparticle complex internalization and incubation time. While the internalization of gold nanoparticle complexes was observed to generally increase as incubation time increased (Figure 3.1), the amount of gold

nanoparticle complexes detected appeared to reach a plateau around 150 min and resumed an increasing trend after 240 min. Other work[6] has shown that certain cell lines under particular incubation conditions can enter a "lag phase" in their growth cycles, meaning the growth cycle of the cells may slow down for a period of time as the cells adjust to the ambient presence of a foreign agent (i.e., experimental probe or delivery vector) but resume normal (or even increased) growth rate after this adjustment period. This may help explain why the internalization of gold nanoparticle complexes by HeLa cells in Figure 3.1 appeared to plateau, but this phenomenon was not further probed in this study. It should be noted these data from this experiment are "nanoparticles per cell" because aliquots of each sample were analyzed via FACS to determine number of cells per well. All subsequent experiments listed in this chapter are "nanoparticles per well." An average number of cells per well from these experiments was deliberately not used to determine "nanoparticles per cell" in the subsequent experiments because of the wide variability in experimental conditions; that is, it would not necessarily be a "true" average number of cells per well because the experimental conditions were too widely disparate among all the experiments.

3.2.3. Probing Optimal Number of Large T Peptides Per Nanoparticle Complex and the Effect of Temperature on Uptake Efficiency

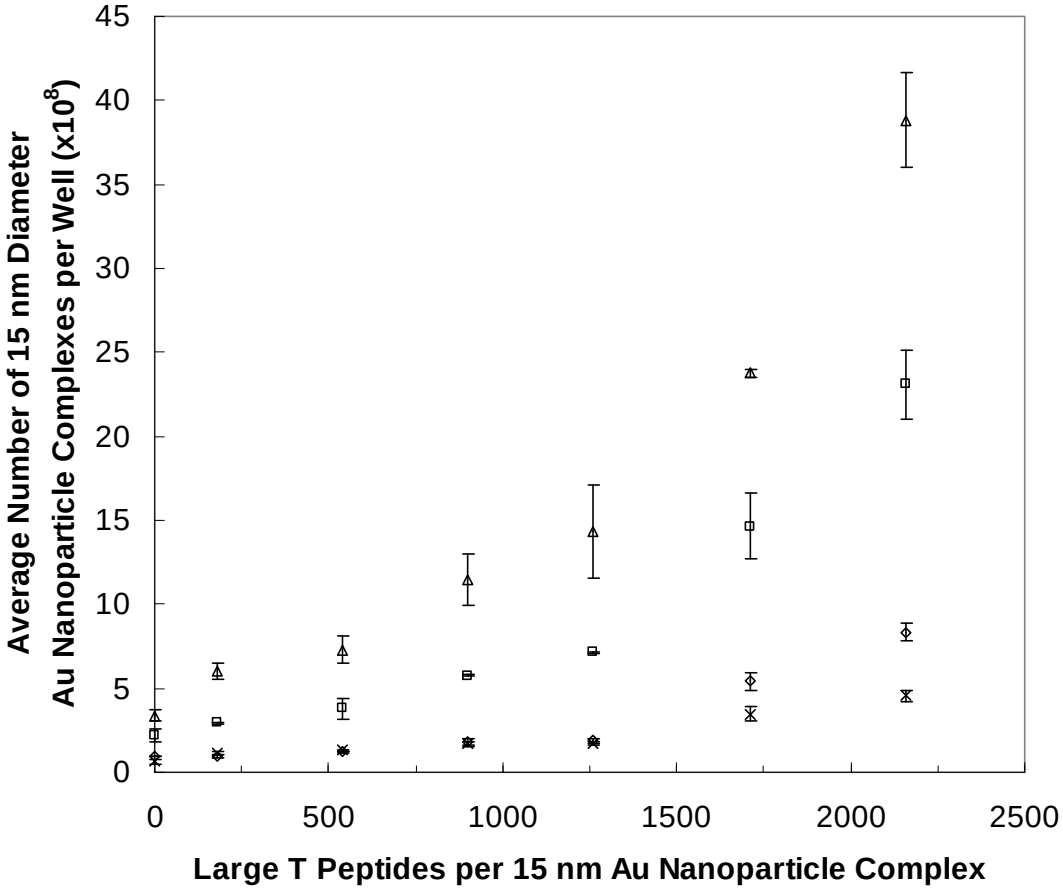

Figure 3.2. Plot of the average number of 15 nm diameter nanoparticle complexes per well as determined via ICP-OES analysis vs number of large T peptides per gold nanoparticle complex. All incubations were performed in 5 % CO_2 and under one of the following additional conditions: 1 h, 37 °C (diamond), 3 h, 37 °C (square), 6 h, 37 °C (triangle), and 6 h, 4 °C (x). (Error bars not immediately visible are smaller than the data point.)

Once a direct relationship between gold nanoparticle complex internalization by HeLa cells and incubation time was established (Figure 3.1), nanoparticle internalization

over time as a function of the number of large T peptides per nanoparticle was probed. Moreover, it was of interest to examine whether this internalization proceeds via an energy-dependent mechanism. To this end, several concurrent experiments were performed on cells incubated with nanoparticle complexes modified with varying amounts of large T (Figure 3.2).

It was observed that increasing the amount of large T peptides per gold nanoparticle complex resulted in more cellular internalization irrespective of incubation time (Figure 3.2). Moreover, larger amounts of gold nanoparticle complexes were internalized at 37 than at 4 °C, and this disparity became greatly pronounced as the number of large T peptides per gold nanoparticle complex increased. It is unclear whether nanoparticle complexes are merely adhering to the outside of the cells at 4 °C or if they are being internalized at a much slower rate. The former option implies this internalization process proceeds through an energy-dependent mechanism, whereas the latter allows for the possibility that at least some of the gold nanoparticle complexes are able to be internalized via an energy-independent pathway. Although it is possible that cellular internalization utilizes an energy-independent pathway, the much higher uptake seen at 37 °C appears to indicate energy dependence for this process. The gold nanoparticle complexes detected at 4 °C may therefore represent complexes bound to their receptors but not internalized due to the energy constraint.

3.2.4. Probing Effect of Particle Size and Excess Passivating Agent on Uptake Efficiency.

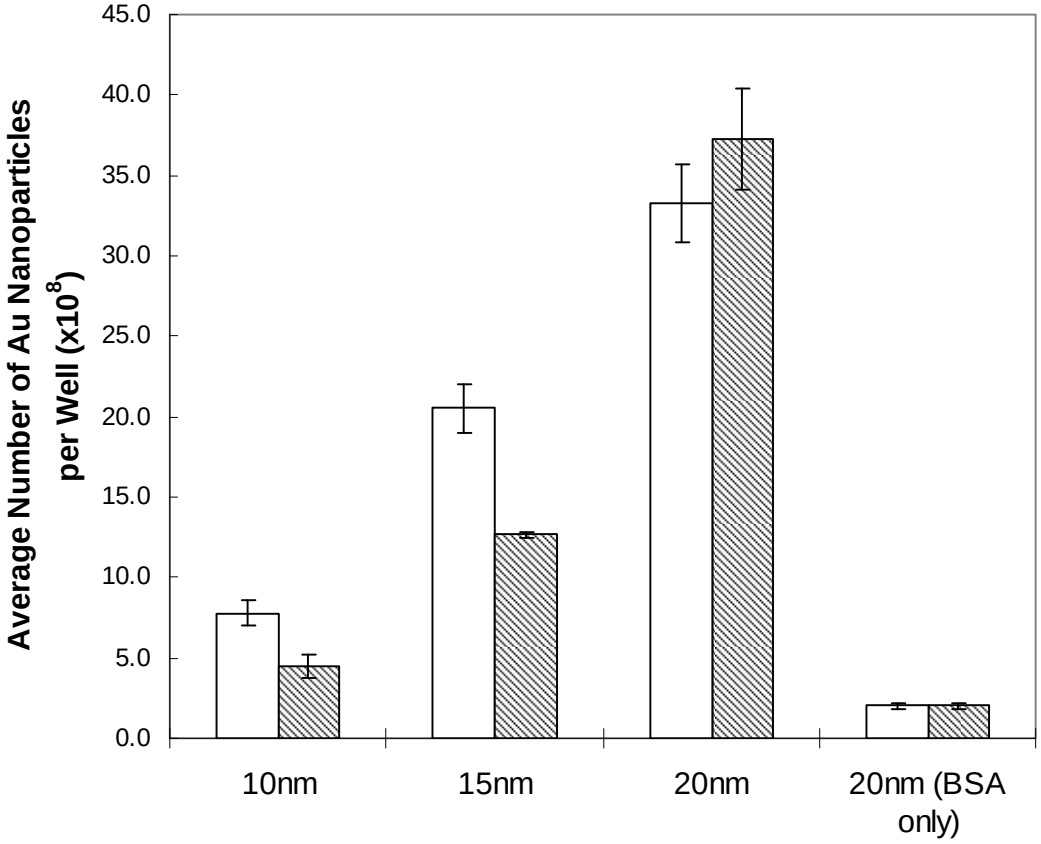

Figure 3.3. Results of ICP-OES analyses of 6 h HeLa incubations with large T-BSA/nanoparticle complexes of varying size. The unshaded data set above corresponds to 6 h HeLa incubations with large T-BSA/nanoparticle complexes of varying size but constant large T-BSA conjugate concentration. The shaded data set corresponds to 6 h HeLa incubations with large T-BSA/nanoparticle complexes of varying size and varying large T-BSA conjugate concentration in an attempt to maintain constant surface coverage of the nanoparticles in accordance with size.

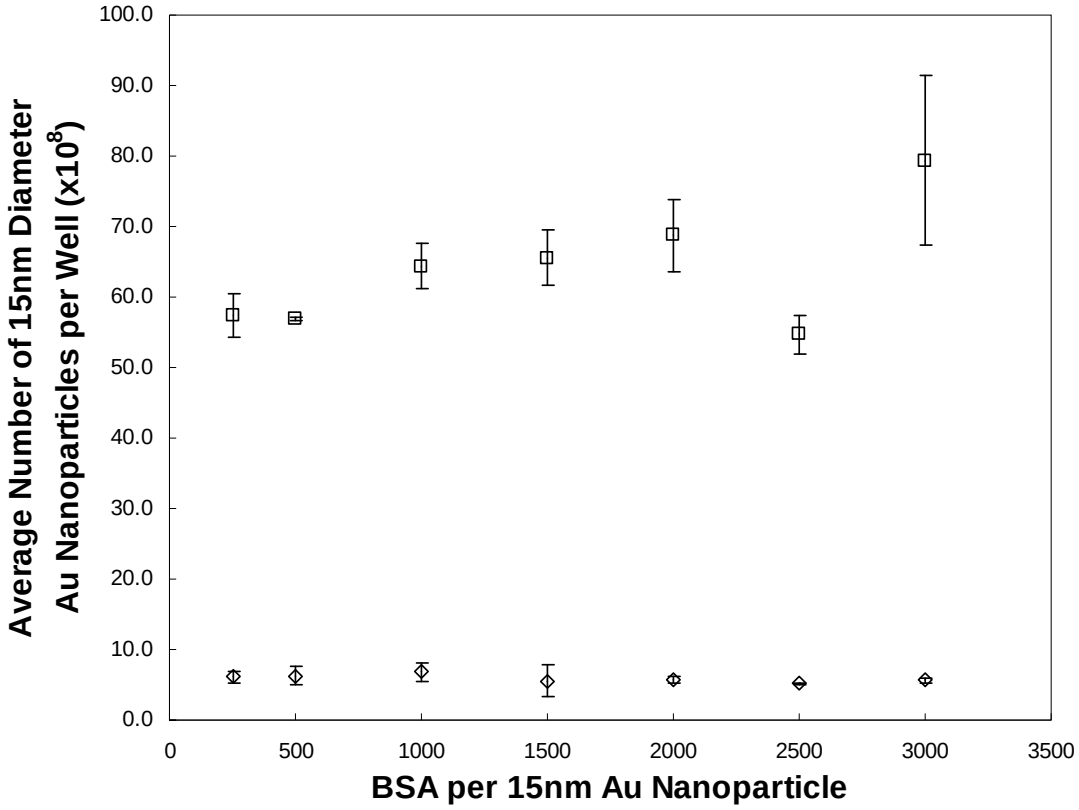

Figure 3.4. Plot of the average number of 15 nm diameter nanoparticle complexes per well as determined via ICP-OES analysis vs number of BSA (diamonds) or large T-BSA (squares) per 15 nm diameter gold nanoparticle complex. (Error bars not immediately visible are smaller than the data point.)

Results from experiments involving complexes of varying nanoparticle size are summarized in Figure 3.3. Although both sets of experiments involve incubations of HeLa cells with a single concentration of gold nanoparticles irrespective of nanoparticle size, the unshaded bars correspond to experiments in which a single concentration of large T-BSA conjugate was used, thus leading to a potentially dramatic excess of large T-BSA conjugate with the large T-BSA/gold nanoparticle complexes of smaller diameter. The shaded bars

correspond to experiments performed with a varying concentration of large T-BSA conjugate such that the concentration of this conjugate is scaled according to available surface area on the gold nanoparticles of a given diameter; that is, the surface areas of the 10 and 15 nm diameter nanoparticles are smaller than that of the 20 nm diameter nanoparticles by a factor of 4 and 1.78, respectively, so a proportionally decreased amount of large T-BSA conjugate was used in synthesizing these particular large T-BSA/gold nanoparticle complexes.

It can been seen in the data in Figure 3.3 that larger-diameter nanoparticle complexes were internalized more readily by HeLa cells than smaller-diameter nanoparticle complexes and the excess large T-BSA conjugate present in certain 10 and 15 nm diameter gold nanoparticle complex samples (unshaded bars) appears to have marginally increased cellular internalization. It should be noted that the cellular internalization of BSA/gold nanoparticle complexes lacking the large T peptide seen in this data is not a novel phenomenon. Other research[7,8,9] has demonstrated the ability of similar complexes (5 nm diameter) to be internalized by other cell lines using specific cell membrane-associated proteins (gp30 and gp18) while native, unassociated BSA in solution was found to internalize via a different moiety (gp60 - albondin). However, the research described in this dissertation did not make any attempt to determine the mechanism of entry of the BSA/gold nanoparticle complexes. Instead, the focus was on the quantity of these BSA/gold nanoparticle complexes internalized relative to the quantity of those complexes containing large T: the data shown in Figure 3.3 demonstrate a decrease over one order of magnitude in cellular internalization of the BSA/gold nanoparticle complexes as compared to analogous nanoparticle complexes containing large T.

Since internalization of 15 nm diameter gold nanoparticle complexes in the previous experiment appeared to increase in the presence of excess large T-BSA conjugate, a further examination of this phenomenon was warranted. It can be concluded from the data in Figure 3.4 that having excess native BSA or large T-BSA present during cellular incubation with nanoparticle complexes did not inhibit cellular uptake of these complexes, even when that excess was increased over 10-fold. Additionally, nanoparticle complexes using large T-BSA once again exhibited greatly enhanced cellular uptake compared to the nanoparticles passivated with native BSA.

These experiments demonstrate a direct relationship between nanoparticle uptake and nanoparticle size. Moreover, although it might have been expected that having excess large T-BSA conjugate in the growth media may have competitively inhibited cellular uptake of the nanoparticle constructs, this was not observed (Figure 3.4). This implies either that under these conditions the size and/or polyvalency of the large T-BSA/gold nanoparticle complexes allows for more efficient internalization versus the large T-BSA conjugates alone or that an excess of cellular receptors are present. As the observation of the internalization of the large T SV40 NLS peptide sequence from the pericellular environment is a new result, any cellular receptor it may be accessing and/or the number of those receptors is currently unknown.

3.2.5. Pulse-Chase Experiments

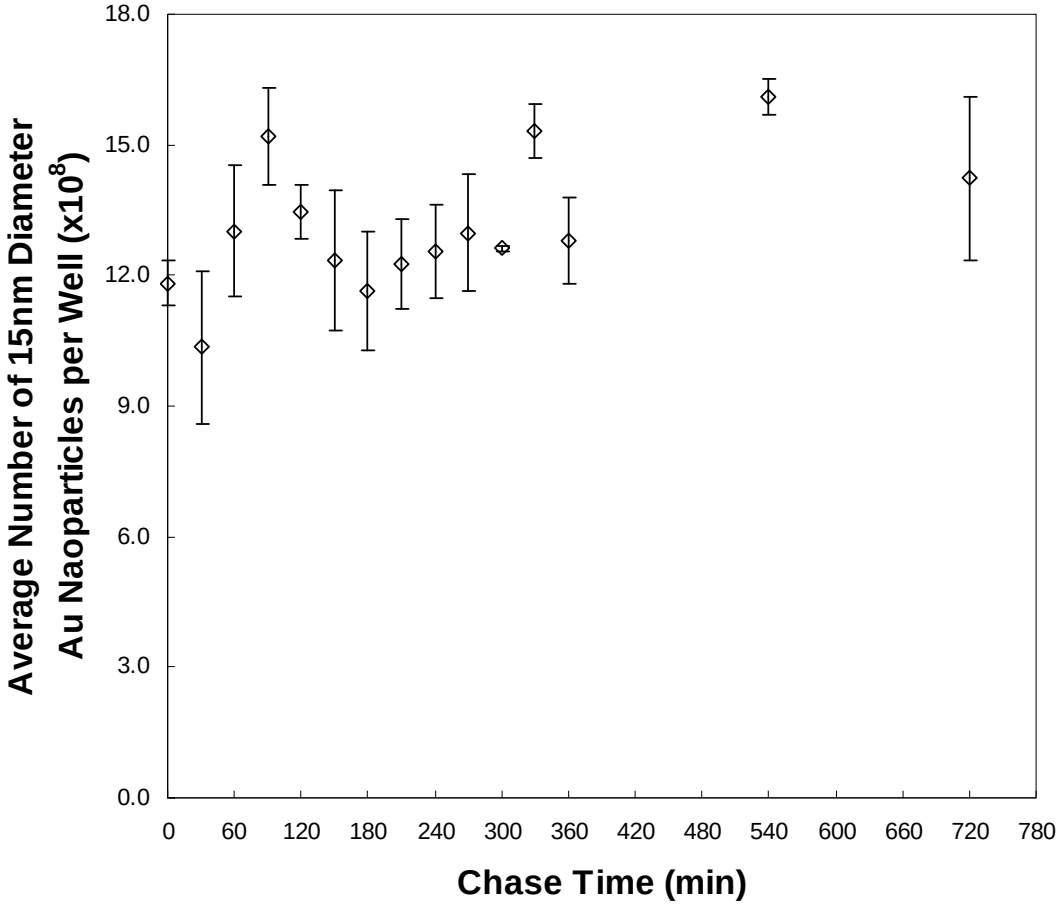

Figure 3.5. Plot of the average number of 15 nm diameter gold nanoparticle complexes per well as determined via ICP-OES analysis versus chase time. The pulse was a 3 h incubation with large T-BSA/gold nanoparticle complexes. (Error bars not immediately visible are smaller than the data point.)

Another dimension to the phenomena under scrutiny in this research is the ultimate fate of a given nanoparticle complex which has been internalized by a HeLa cell. A pulse-chase experiment was performed to determine if the amount of time that internalized gold nanoparticle complexes were in HeLa cells was short (perhaps quickly shunted out of the cell

via some exocytotic pathway) or if these gold nanoparticle complexes associated with a cell for an appreciable amount of time. The gold nanoparticle complexes did, in fact, remain associated with the HeLa cells in similar concentration up to 12 h after the cells were no longer exposed to the complexes (Figure 3.5).

3.3. Conclusions

ICP-OES has demonstrated its efficacy as a valuable analytical tool for quantifying cellular internalization of gold nanoparticles. With regard to the ICP-OES control experiments, it was concluded: (1) there was a small but statistically significant increase within the 95% confidence limit in ICP-OES intensity when gold nanoparticles were prepared by digestion in aqua regia compared to undigested samples (Table 3.1), (2) any residual nanoparticle complexes adhered to the coverslips did not significantly alter the resulting ICP-OES signal (values from Table 3.2 compared to those in Table 3.3), (3) doubling the number of coverslips per sample was an effective way to double the resulting ICP-OES signal without introducing nonlinear matrix effects in the signal (Table 3.3), and (4) although using a post-incubation heparin wash afforded a very small yet statistically significant difference in the resulting ICP-OES signal (Table 3.3), the vast preponderance of complexes detected after incubation with HeLa cells were most likely internalized as opposed to merely associated with the exterior of the cells. This last conclusion is based upon the hypothesis that heparin would remove large T/BSA-gold nanoparticle complexes bound to receptors on the exterior of the cell membrane but not internalized as has been reported for other bound molecules.[10]

In general, it can be concluded that allowing larger nanoparticle complexes containing higher concentrations of large T to incubate with HeLa cells for longer periods of time at 37 ^{o}C afforded the maximum amount of cellular internalization of these complexes. The presence of excess large T/BSA conjugate did not decrease the amount of complexes ultimately detected in the cells post-incubation, and the complexes were detected in the cells in very similar concentration up to 12 hours after the media containing these nanoparticle complexes was removed.

3.4 Experimental.

3.4.1. Materials.

HeLa (human cervical cancer cells) cell line was purchased from the American Type Culture Collection (Rockville, MD). Minimal essential medium Eagle's (EMEM), fetal bovine serum (FBS), Dulbecco's phosphate-buffered saline (DPBS), T-75 cell culture flasks, 12-well cell culture plates, and trypsin were purchased from Bio-Whittaker, Inc. (Walkersville, MD). All gold nanoparticles were purchased from Ted Pella, Inc. (Redding, CA). The modified large T peptide sequence (rhodamine-Cys-Gly-Gly-Gly-Pro-Lys-Lys-Lys-Arg-Lys-Val-Gly-Gly-OH) was synthesized at the University of North Carolina Microprotein Sequencing and Peptide Synthesis Facility (Chapel Hill, NC). Bovine serum albumin (BSA) was purchased from Pierce Co. (Rockford IL). Heparin sulfate, 4-(*N*-maleimidomethyl)-cyclohexane-1-carboxylic acid *N*-hydroxysuccinimide ester (SMCC), sodium chloride, monobasic sodium phosphate (NaH_2PO_3), dibasic sodium phosphate (Na_2HPO_3), Optima-grade HCl, Optima-grade HNO_3, Centricons (MWCO: 30 000), and

glass coverslips (18 mm) were all purchased from Fisher Scientific. All ICP experiments were performed with a Perkin-Elmer Optima 2100DV optical emission spectrometer equipped with a Meinhard type C glass nebulizer, unbaffled cyclonic chamber, and an alumina injection tube (2 mm opening). Other instrument settings include the following: 18 L/min plasma flow, 0.2 L/min auxiliary flow, 0.62 L/min nebulizer flow, 1.00 L/min pump rate, and 1500 W rf power. All ICP standards were made from 100 mg/mL SpexCertiPrep stock solution (lot no. CL3-19AU), and all ICP samples were analyzed at 242.795 nm with a read delay of 80 s and an integration time from 2 to 5 s.

HeLa cells were maintained in T-75 cell culture flasks using EMEM growth media containing 10% FBS at 37 °C and at 5 % CO_2. Prior to experimentation, cells were plated on sterile glass coverslips in 12-well plates. Cells were grown to approximately 75% confluency before beginning experiments. It should be noted that 6 h was chosen as a maximum incubation time of cells with nanoparticle complexes for all experiments in this research to avoid potential effects on any cellular internalization due to overconfluency of the HeLa cells. Cell counting was performed using a fluorescent-activated cell sorting (FACS) instrument (NC State Veterinary College).

3.4.2. Methods.

3.4.2.1. Without Cells (ICP-OES Calibration Experiments).

Four sets of control experiments were performed to probe the utility of ICP-OES as an analytical technique for use in subsequent determinations of nanoparticles internalized by HeLa cells. The first set of experiments was done to ensure that ICP-OES could accurately

determine the concentration of gold nanoparticles in solution and that no matrix effects were introduced by the use of aqua regia in sample preparation. This was accomplished by placing 100 μL of 1 nM citrate-stabilized 20 nm diameter gold nanoparticles in each well of a 12-well cell culture plate and allowing the solutions to evaporate to dryness at room temperature. Six of the wells were then further treated with 0.5 mL of aqua regia while the remaining six wells received 0.5 mL of ultrapure water. The well plate was allowed to remain at room temperature for 2 h, after which 0.4 mL of each sample was placed in a 15 mL centrifuge tube, diluted to 3.9 mL with ultrapure water, and analyzed via ICP-OES.

A second set of experiments was conducted to examine the relative degree to which nanoparticle complexes might associate with the glass coverslips in the absence of HeLa cells. Sterile glass coverslips were individually placed in each well of two 12-well cell culture plates. Six of these wells then received 150 μL of ultrapure water and were diluted to 1.5 mL with EMEM growth media, six wells received 150 μL of citrate-stabilized 15 nm diameter gold nanoparticles and were then diluted to 1.5 mL with growth media (0.23 nM final concentration), six wells received 1.5 mL of growth media containing 10 % 15 nm diameter nanoparticle complexes stabilized with native BSA (0.23 nM final complex concentration), and the remaining six wells received 1.5 mL of EMEM growth media containing 10 % 15 nm diameter nanoparticle complexes stabilized with a large T-BSA conjugate (15:1 large T/BSA experimentally determined molar ratio; 0.23 nM final complex concentration). Both well plates were then incubated at 37 °C and 5 % CO_2 for 6 h thus simulating the conditions used in later incubations with HeLa cells. After incubation, each well was rinsed with 1 mL of DPBS three times, and the coverslips were removed from their

wells and allowed to air-dry in a sterile cell culture hood. These dried coverslips were then placed in a new well plate, treated with 0.5 mL of aqua regia for 2 h, after which 0.4 mL of each sample was placed in a 15 mL centrifuge tube, diluted to 3.9 mL with ultrapure water, and analyzed via ICP-OES.

The third set of ICP-OES control experiments was performed to determine both if the HeLa cells themselves would interfere with the resulting observed ICP-OES signal and if the ICP-OES signal detected from combining HeLa cell samples prior to treatment with aqua regia was linear. The 15 nm gold nanoparticles were passivated with large T-BSA conjugate (15:1 large T/BSA experimentally determined molar ratio) using a large T-BSA/nanoparticle molar ratio of 250:1, and the final concentration of gold nanoparticles in the solution was approximately 2.3 nM. HeLa cells which had been previously cultured on sterilized coverslips placed in two 12-well plates were then allowed to incubate with either 1.5 mL of pure growth media (6 wells) or 1.5 mL of growth media containing 10% large T-BSA/gold nanoparticle complexes (18 wells; 0.23 nM nanoparticle concentration) per well for 6 h. Each well was then rinsed with 1 mL of DPBS three times, and the coverslips were removed from their wells and allowed to air-dry in a sterile cell culture hood. These dried coverslips were then placed in a new well plate; each of the 6 the coverslips containing HeLa cells which had not been incubated with the nanoparticle complexes was placed in its own well, 6 of the remaining coverslips were similarly placed in their own well, while the remaining 12 coverslips were placed in wells in pairs. Each well was then treated with 0.5 mL of aqua regia for 2 h, after which 0.4 mL of each sample was placed in a 15 mL centrifuge tube, diluted to 3.9 mL with ultrapure water, and analyzed via ICP-OES.

A final set of experiments was performed to evaluate binding of nanoparticles to the exterior of the outer cell membrane. Gold nanoparticles, 15 nm in diameter, were passivated with large T-BSA conjugate (15:1 large T/BSA experimentally determined molar ratio) using a large T-BSA/nanoparticle molar ratio of 250:1 and a final concentration of gold nanoparticles of 2.3 nM. HeLa cells, which had been previously cultured on sterilized coverslips and placed in one 12-well plate, were allowed to incubate with 1.5 mL of growth media containing 10 % large T-BSA/gold nanoparticle complexes (0.2 nM nanoparticle concentration) per well for 6 h. After incubation, each well was rinsed three times with 1 mL of DPBS, once with 1 mL of DPBS containing heparin sulfate (5 U/mL), and one final time with 1 mL of DPBS. Heparin sulfate is commonly used to desorb structures (e.g., molecules, biomolecules, particles) adhered to cell outer membranes.[10] The samples were then treated with aqua regia and analyzed by ICP-OES as described above.

3.4.2.2. Probing Optimal Time of Incubation.

Gold nanoparticles 15 nm in diameter were passivated with large T-BSA conjugate (15:1 large T/BSA experimentally determined molar ratio) using a large T-BSA/nanoparticle molar ratio of 250:1, and the final concentration of gold nanoparticles in the solution was approximately 2.3 nM. HeLa cells which had been previously cultured on sterilized coverslips placed in 12-well plates were then allowed to incubate with 1.5 mL of growth media containing 10 % large T-BSA/gold nanoparticle complexes (0.23 nM nanoparticle concentration) per well for varying amounts of time from 0 to 6 h. Six wells of HeLa cells were used for every time period under scrutiny. After the desired incubation time had

elapsed, each well was rinsed with 1 mL of DPBS three times, and the coverslips were removed from their wells and allowed to air-dry in a sterile cell culture hood. These dried coverslips were then placed in a new well plate, combining two coverslips of identical samples per well. Each well was then treated with 0.5 mL of aqua regia for 2 h, and the resulting solution was prepared for ICP-OES analysis.

3.4.2.3. Probing Optimal Number of Large T Peptides Per Nanoparticle Complex and the Effect of Temperature on Uptake Efficiency.

Separate 15 nm diameter gold nanoparticle samples were passivated with one of six large T-BSA conjugates, each one containing a different molar ratio of large T per BSA. The molar ratio of large T-BSA conjugates/gold nanoparticles was 250:1, and the final concentration of gold nanoparticles in the solution was 2.3 nM. HeLa cells which had been previously cultured on sterilized coverslips and placed in 12-well plates were then allowed to incubate with 1.5 mL of growth media containing 10 % large T-BSA/gold nanoparticle complexes (0.23 nM nanoparticle concentration) per well for 1, 3, or 6 h. Additional well plates of HeLa cells which had been previously cultured on sterilized coverslips and placed in 12-well plates were removed from the incubator and cultured at 4 °C for 3 h prior to experimentation (along with the corresponding aliquots of DPBS and growth media containing nanoparticle complexes) in order to allow one replicate set of incubations to take place for 6 h at this temperature. Six wells of HeLa cells were used for every time period under scrutiny. After the desired incubation time had elapsed, each well was rinsed with 1 mL of DPBS three times, and then the coverslips were removed from their wells and allowed

to air-dry in a sterile cell culture hood. These dried coverslips were then placed in a new well plate, combining two coverslips of identical samples per well. Each well was then treated with 0.5 mL of aqua regia for 2 h, and the resulting solution was prepared for ICP-OES analysis. Additional experiments under identical conditions were performed on separate samples of cells for the purposes of obtaining cell count and toxicity data.

3.4.2.4. Probing Effect of Particle Size and Excess Passivating Agent on Uptake Efficiency.

Experiments designed to probe the effect of nanoparticle size on cellular internalization were performed under two different experimental conditions. In both sets of conditions, separate samples of gold nanoparticles of varying diameter (10, 15, and 20 nm) but identical concentration (1.2 nM) were passivated with a large T-BSA conjugate (15:1 peptide/BSA experimentally determined molar ratio) prepared in the same fashion as described earlier. However, in one set of experiments, the large T-BSA conjugate was added to each nanoparticle sample in a large T-BSA/nanoparticle molar ratio of 500:1 irrespective of nanoparticle size, while in the other set of experiments, conjugate was added to the samples of nanoparticles in a large T-BSA/nanoparticle molar ratio commensurate with nanoparticle surface area; that is, 20 nm diameter colloids were exposed to large T-BSA conjugates in a large T-BSA/nanoparticle molar ratio of 500:1, while the molar ratio used for 15 and 10 nm diameter colloids was 250:1 and 125:1, respectively. An additional sample of 20 nm diameter gold nanoparticles was prepared using native BSA in a BSA/nanoparticle molar ratio of 500:1. HeLa cells, which had been previously cultured on sterilized coverslips

and placed in 12-well plates, were allowed to incubate with 1.5 mL of growth media containing 10 % large T-BSA/gold nanoparticle complexes (0.12 nM nanoparticle concentration) per well for 6 h. Six wells of HeLa cells were used for every nanoparticle size under scrutiny. After the desired incubation time had elapsed, each well was rinsed with 1 mL of DPBS three times, and then the coverslips were removed from their wells and allowed to air-dry in a sterile cell culture hood. These dried coverslips were then placed in a new well plate, combining two coverslips of identical samples per well. Each well was then treated with 0.5 mL of aqua regia for 2 h, and the resulting solution was prepared for ICP-OES analysis.

In the experiments examining the potential effects of excess passivating conjugate upon cellular internalization of the nanoparticle complexes, separate samples of 15 nm gold nanoparticles were passivated with a peptide-BSA conjugate (15:1 peptide/BSA experimentally determined molar ratio) in varying large T-BSA/nanoparticle molar ratios (250:1 to 3000:1), and the final concentration of gold nanoparticles in the solution was 2.3 nM. Additional nanoparticle complexes were prepared using native BSA instead of large T-BSA conjugates. HeLa cells, which had been previously cultured on sterilized coverslips and placed in 12-well plates, were allowed to incubate with 1.5 mL of growth media containing 10 % large T-BSA/gold nanoparticle complexes (0.23 nM nanoparticle concentration) per well for 6 h. Six wells of HeLa cells were used for every time period under scrutiny. After the desired incubation time had elapsed, each well was rinsed with 1 mL of DPBS three times, and then the coverslips were removed from their wells and allowed to air-dry in a sterile cell culture hood. These dried coverslips were then placed in a new well plate,

combining two coverslips of identical samples per well. Each well was then treated with 0.5 mL of aqua regia for 2 h, and the resulting solution was prepared for ICP-OES analysis.

3.4.2.5. Pulse-Chase Experiments.

Gold nanoparticles 15 nm in diameter were passivated with a large T-BSA conjugate (15:1 peptide/BSA experimentally determined molar ratio) in a large T-BSA/nanoparticle molar ratio of 250:1, and the final concentration of gold nanoparticles in the solution was 2.3 nM. HeLa cells, which had been previously cultured on sterilized coverslips and placed in 12-well plates, were allowed to incubate with 1.5 mL of growth media containing 10 % large T-BSA/gold nanoparticle complexes (0.23 nM nanoparticle concentration) per well for 3 h. After this "pulse," each well was rinsed with 1 mL of DPBS three times, 1.5 mL of fresh growth media without nanoparticles was applied to each well, and the cells were allowed to further incubate for varying amounts of time ("chase" times) over a period of 12 h. Six wells of HeLa cells were used for every time period under scrutiny. After the desired chase time had elapsed, each well was again rinsed with 1 mL of DPBS three times, and then the coverslips were removed from their wells and allowed to air-dry in a sterile cell culture hood. These dried coverslips were then placed in a new well plate, combining two coverslips of identical samples per well. Each well was then treated with 0.5 mL of aqua regia for 2 h, and the resulting solution was prepared for ICP-OES analysis.

3.5 References.

[1] Bhumkar, D. R.; Joshi, H. M.; Sastry, M.; Pokharkar, V. B. *Pharmaceutical Research*, **2007**, *24 (8)*, 1415 – 1426.

[2] Lodish, H.; Berk, A.; Matsudaira, P.; Kaiser, C. A.; Krieger, M.; Scott, M. P.; Zipursky, S. L.; Darnell, J. *Molecular Cell Biology, 5th Edition*; W. H. Freeman and Company; New York, **2003**.

[3] Derfus, A. M.; Chan, W. C.; Bhatia, S. N. *Nano Letters*, **2004**, *4 (1)*, 11 – 18.

[4] Elder, A.; Gelein, R.; Silva, V.; Feikert, T.; Opanashuk, L.; Carter, J.; Potter, R.; Maynard, A.; Ito, Y.; Finkelstein, J.; Oberdörster, G. *Environmental Health Perspectives*, **2006**, *114 (8)*, 1172 – 1178.

[5] Wemyss, R. B.; Scott, R. H. *Anal. Chem.*, **1978**, *50 (12)*, 1694 – 1697.

[6] Takara, K.; Sakaeda, T.; Yagami, T.; Kobayashi, H.; Ohmoto, N.; Horinouchi, M.; Nishiguchi, K.; Okumura, K. *Biol. Pharm. Bull.*, **2002**, *25 (6)*, 771 – 778.

[7] Schnitzer, J. E.; Sung, A.; Horvat, R.; Bravo, J. *J. Biol. Chem.*, **1992**, *267 (34)*, 24544 – 24553.

[8] Schnitzer, J. E.; Bravo, J. *J. Biol. Chem.*, **1993**, *268 (10)*, 7562 – 7570.

[9] Schnitzer, J. E.; Oh, P. *J. Biol. Chem.*, **1994**, *269 (8)*, 6072 – 6082.

[10] Veldhoen, S.; Laufer, S. D.; Trampe, A.; Restle, T. *Nucleic Acids Research*, **2006**, *34 (22)*, 6561 – 6573.

Chapter 4

Sub-Cellular Fractionation Analysis of Incubations of BSA-SMCC-Large-T/Nanoparticle Constructs with Human Cervical Cancer Cells.

4.1. Introduction.

This dissertation chapter focuses on two critical aspects of any potential intracellular vector: (1) the targeted intracellular location at which these nanoparticle complexes are designed to reside/accumulate, and (2) cytotoxicity. Since large T is known to localize in the cell nucleus when injected directly into the cytoplasm,[1] experiments were designed to quantify nuclear localization of large T/BSA-gold nanoparticle complexes. The use of a cellular fractionation kit and smaller-diameter gold nanoparticles for these nuclear localization analyses are discussed, and experimental results shown. Moreover, data are tabulated from control experiments probing the extent to which a high-speed centrifugation step used in the process of fractionating cells affects the overall amount of nanoparticle complexes associated with the resulting nuclear fraction of cell lysates. Finally, toxicity of these large T/BSA-gold nanoparticle complexes is evaluated and discussed. As in previous chapters, all experimental results are shown and discussed first, followed by a section defining materials used and a methodical description of experimental procedures which were performed.

4.1.1. Development of a Method for Nuclear Extraction From HeLa.

While cellular imaging techniques can be useful in qualitatively determining whether or not any nuclear localization of a given construct occurred, these techniques do not provide quantitative results. In fact, the use of certain types of imaging (such as VECDIC or confocal microscopy) restrict the type of vector which can be used; that is, nanoparticles with diameters less than ~20 nm would need to form aggregates of some threshold size to be

detected (thus potentially eliminating the detection of non-aggregated localizations). Using larger-sized nanoparticles in an experiment to compensate for eventual imaging restrictions is likely to greatly reduce the possibility of having the modified nanoparticle complex enter a cell nucleus via its nuclear pores (~ 25 nm maximum dilation reported for HeLa).[2] Moreover, other imaging techniques (such as atomic force microscopy (AFM), scanning electron microscopy (SEM) and TEM) which are able to resolve structures at the nanometer level, are prone to yielding inconclusive results due to the process by which samples are analyzed (random thin cell slices), and are prohibitively time-consuming and/or expensive to use as a routine analytical methodology. Rather than using a combination of imaging techniques, a method involving the extraction of nuclei from cells and examining resulting cell fractions via ICP-OES the amount of nanoparticle constructs associated with those nuclei was developed and codified to present a considerably faster and strictly quantitative assay for these types of experiments.

There exist many cellular fractionation kits designed to facilitate the process of extracting nuclei from other cellular material. Unfortunately for the goals of this research, most of these fractionation kits utilize high-speed centrifugation as the primary method of separation of nuclei from remaining cellular organelles/debris. This centrifugation would certainly induce accumulation of larger-sized gold nanoparticle aggregates, resulting in an artificially large amount of gold detected in the nuclear fraction. In the interest of minimizing the effects of this centrifugation, the use of a much smaller-sized nanoparticle (5 nm diameter) was chosen, and experiments were designed to examine how much this

centrifugation might affect the observed amount of gold ultimately appearing to associate with nuclear fractions of cells.

4.2. Results and Discussion

4.2.1. Probing the Efficacy of Nuclear Association of Large T.

Table 4.1. The number of 5 nm gold nanoparticle complexes (of varying large T concentration) per HeLa cell detected via ICP-OES, including data from fractionation experiments.*

# Large T per 5 nm Nanoparticle Complex	Nanoparticles per Cell; Unfractionated	Nanoparticles per Cytosolic Fraction	Nanoparticles per Nuclear Fraction	% Nuclear
0 (native BSA)	3.48×10^4	1.33×10^4	8.18×10^3	37.5
30	3.52×10^4	5.22×10^3	9.29×10^3	62.5
70	1.21×10^5	1.54×10^4	7.04×10^3	82.4
80	4.97×10^5	3.21×10^4	1.73×10^5	84.4
110	1.16×10^6	4.74×10^4	9.61×10^5	95.3
130	1.80×10^6	8.97×10^4	1.47×10^6	94.2
150	5.44×10^6	1.20×10^5	3.11×10^6	96.3

*All incubations were performed for 6 hours under standard conditions (37 ^oC, 5 % CO_2). The standard deviations of all listed values are all within +/- 10 %.

As shown in Table 4.1, nanoparticles were detected in the nuclear fractions, and the general trend of increased nuclear targeting with increased large T/BSA coverage was observed. Note from Table 4.1 that the number of nanoparticles detected per unfractionated cell does not equal the sum of nanoparticles detected in the nuclear and cytosolic fractions. This most likely indicates that the fractionation process itself leads to a loss of nanoparticles, a loss that cannot be assigned definitively to the cytosolic or nuclear fraction.

4.2.2. Examination of Centrifugation Effects on Resulting ICP-OES Signal.

Table 4.2. The percentages of 5 nm gold nanoparticle complexes detected via ICP-OES in cytosolic and nuclear fractions after "spiking" HeLa cells during the fractionation process.*

# Large T per 5 nm Nanoparticle Complex	% Cytosolic	% Nuclear	% Nuclear (corrected)
0 (Citrate)	77.7	22.3	N/A
0 (native BSA)	80.9	19.1	18.4
70	77.6	22.4	60.0
110	61.2	38.8	56.5
150	59.1	40.9	55.4

*All incubations were performed for 6 hours under standard conditions (37 ^{o}C, 5 % CO_2), and did not involve delivery of nanoparticle complexes during incubation. The standard deviations of all listed values are all within +/- 10 %.

The number of nanoparticle complexes in both the cytosolic and nuclear fractions was analyzed by ICP-OES (Table 4.2). Note that in these experiments the sums of the nanoparticles determined in each of the two fractions were virtually identical to the total number of nanoparticles originally injected into the fractionated sample. Furthermore, a different concentration of nanoparticle complexes was used in spiking these samples than was used in the previous internalization samples, so the results in Table 4.2 are listed in percentages both to avoid confusion and to allow for direct comparison to those results listed in Table 4.1. The largest recoveries of nanoparticles in this control experiment were found for the highest large T coverage (38.8 % and 40.9 %, before correction; Table 4.2). The column of "% Nuclear (corrected)" values represents the difference between the relevant "% Nuclear" values listed in Tables 4.1 and 4.2. It should be noted that the aliquots of citrate-passivated nanoparticles were likely to have flocculated upon their addition to fractionated cell solutions (solutions were observed to have a tinge of deep purple immediately after the addition of the nanoparticles, but no assays confirming flocculation were performed), so

these specific assays were intended to examine how largely aggregated colloids might potentially behave under these experimental conditions.

Increasing the number of large T peptides per gold nanoparticle complex did increase the percentage of said complexes which ultimately associated with the nuclear pellet solely due to centrifugation (Table 4.2). This could be due to a stronger association between large T-BSA/gold nanoparticle complexes and the outer nuclear membrane as the number of large T peptides per particle is increased. However, when this percentage was used to correct for the number of gold nanoparticles detected per nuclear fraction - undoubtedly an overcorrection - it was clear that centrifugation effects could not completely explain the large percentage of nanoparticles complexes observed to be associated with the nuclei.

The ability of large T to function as a nuclear localization signal when attached to gold nanoparticles can be highlighted by comparing the data for BSA/gold nanoparticle complexes (no large T) and complexes carrying 150 large T peptides per nanoparticle. When corrected for centrifugation effects, 55 % of the nanoparticles modified with large T were detected in the nuclear fraction, compared to 18 % of the BSA-modified complexes. This result clearly demonstrates the efficacy of large T as a nuclear localization agent, even when introduced in the pericellular environment.

As the percentages of nanoparticle complexes detected in the nuclear fractions in the standard deliveries for these same complexes were substantially higher (95.3 % and 96.3 %; Table 4.1) than the corresponding “spiked” samples (38.81 % and 40.86 %; Table 4.2), it is unlikely that the results of nuclear targeting reported in Table 4.1 are mere artifacts of centrifugation. These controls thus mark a lower limit on the number of large T-BSA/gold

nanoparticle complexes that are determined to have reached the nucleus from the extracellular environment.

4.2.3. Examination of Toxicity of Constructs.

Table 4.3. Cell counts per flask as determined via FACS.[*]

# Large T per 5 nm Nanoparticle	Cell Count per Flask ($x10^4$)	% Viable[†]
Control (no gold)	98.6 +/- 4.9	100.0
0 (native BSA)	96.7 +/- 4.4	98.1
30	96.3 +/- 5.1	97.7
70	94.7 +/- 5.5	96.0
80	87.0 +/- 9.8	88.2
110	80.4 +/- 7.0	81.5
130	68.5 +/- 7.3	69.5
150	65.0 +/- 10.1	65.9

[*] All incubations were performed for 6 hours under standard conditions (37 ^oC, 5 % CO_2).
[†] % viability was referenced to the cell count of the control sample.

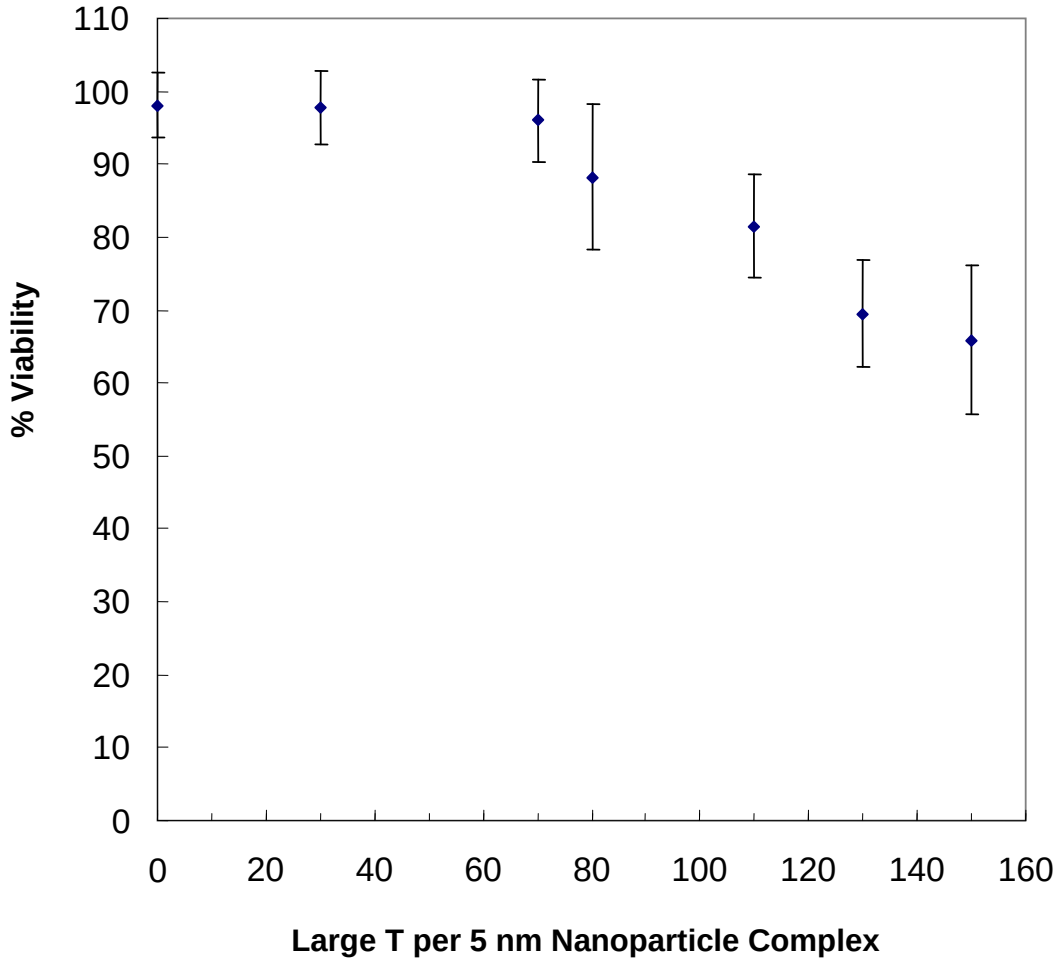

Figure 4.1. Percent viability (as determined via FACS; compared to cell samples with no nanoparticle complexes delivered) versus large T per 5 nm nanoparticle complex.

As the amount of large T per nanoparticle complex is increased, the viability of these cells decreases (Table 4.3 and Figure 4.1). Though strong conclusions cannot be drawn without a more rigorous study, it is interesting to note that the 70 large T per nanoparticle complex samples appear to have been a "best" value of number of large T peptides per 5 nm

nanoparticle in that there was nearly no toxicity associated with these samples (Table 4.3), but these samples exhibited significant cellular internalization (Table 4.2).

4.3. Conclusions

The gold nanoparticle complexes that had the largest concentrations of large T used in this research enhanced cellular internalization in general (and nuclear localization specifically) compared to the gold nanoparticle complexes assembled using the smallest amounts of large T. Additionally, the overall toxicity of the gold nanoparticle complexes increased proportionally with increasing number of large T peptides in the gold nanoparticle complexes. However, the data also demonstrated that using gold nanoparticle complexes of comparatively low large T coverage (~ 70 large T peptides per nanoparticle complex) enhanced cellular uptake and greatly improved the amount of gold nanoparticle complexes which were associated with the nuclei of the cells without introducing significant toxicity.

There is a maximum efficiency for nuclear targeting evident from the data in this study. Tables 4.1 and 4.2 show that although an increase in the number of large T peptides per nanoparticle results in an increase in the number of nanoparticles internalized, the percentage of those nanoparticles that reached the nucleus appears to have decreased slightly. Whether this is related to the increase in cytotoxicity with an increase in large T coverage, an increase in nanoparticle complex size that compromises its ability to pass through the nuclear pore complex, or some other factor is unknown.

Irrespective of the origin of the trends in nuclear targeting discussed above, it is interesting to compare nuclear targeting as judged by ICP-OES with that of VEC-DIC. Using

VEC-DIC, large T-BSA/gold nanoparticle complexes were previously detected in the cytoplasm of HeLa cells after 3 h but not inside the nucleus.[3] It was hypothesized at the time that the apparent failure of these nanoparticle complexes to traverse the nuclear membrane was a result of the inability of these complexes to escape endosomes intact. ICP-OES, in contrast, was able to detect the presence of these complexes inside fractionated HeLa cell nuclei. The only differences in the two experiments were particle size (5 nm diameter gold in ICP vs 20 nm diameter in VEC-DIC) and incubation time (6 h in ICP-OES vs 3 h in VEC-DIC). These disparate results may be justified by considering (i) that ICP-OES is a "ensemble average" technique and is thus less susceptible to sample heterogeneity compared to VEC-DIC, which analyzes a random (and relatively low) population of individual cells, (ii) VEC-DIC may be less sensitive than ICP-OES (particularly with regard to non-aggregated nanoparticle complexes) and thus failed to image nanoparticles in the nucleus that ICP-OES was able to detect, and/or (iii) the larger diameter of the nanoparticles investigated by VEC-DIC slowed their transport through the nuclear pore complex.

4.4. Experimental Section

4.4.1. Materials.

HeLa (human cervical cancer cells) cell line was purchased from the American Type Culture Collection (Rockville, MD). Minimal essential medium Eagle's (EMEM), fetal bovine serum (FBS), Dulbecco's phosphate-buffered saline (DPBS), T-25 cell culture flasks, 12-well cell culture plates, and trypsin were purchased from Bio-Whittaker, Inc. (Walkersville, MD). All gold nanoparticles were purchased from Ted Pella, Inc. (Redding,

CA). The modified large T peptide sequence (rhodamine-Cys-Gly-Gly-Gly-Pro-Lys-Lys-Lys-Arg-Lys-Val-Gly-Gly-OH) was synthesized at the University of North Carolina Microprotein Sequencing and Peptide Synthesis Facility (Chapel Hill, NC). Bovine serum albumin (BSA) and subcellular fractionation kit were purchased from Pierce Co. (Rockford IL). 4-(*N*-maleimidomethyl)-cyclohexane-1-carboxylic acid *N*-hydroxysuccinimide ester (SMCC), sodium chloride, mono basic sodium phosphate (NaH_2PO_3), dibasic sodium phosphate (Na_2HPO_3), Optima-grade HCl, Optima-grade HNO_3, Centricons (MWCO: 30,000), and glass coverslips (18 mm) were all purchased from Fisher Scientific. All ICP experiments were performed with a Perkin-Elmer Optima 2100DV optical emission spectrometer equipped with a Meinhard type C glass nebulizer, unbaffled cyclonic chamber, and an alumina injection tube (2 mm opening). Other instrument settings include the following: 18 L/min plasma flow, 0.2 L/min auxiliary flow, 0.62 L/min nebulizer flow, 1.00 L/min pump rate, and 1500 W rf power. All ICP standards were made from 100 mg/mL SpexCertiPrep stock solution (lot no. CL3-19AU), and all ICP samples were analyzed at 242.795 nm with a read delay of 80 s and an integration time from 2 to 5 s.

HeLa cells were maintained in T-75 cell culture flasks using EMEM growth media containing 10 % FBS at 37 °C and at 5 % CO_2. Prior to experimentation, cells were seeded into T-25 cell culture flasks. Cells were grown to approximately 75% confluency before beginning experiments. It should be noted that 6 h was chosen as a maximum incubation time for all experiments in this research to avoid potential effects on any cellular internalization due to overconfluency of the HeLa cells. Cell counting was performed using a fluorescent-activated cell sorting (FACS) instrument (NC State Veterinary College).

4.4.2. Methods

Separate 5 nm diameter gold nanoparticle samples were passivated with one of the six previously prepared large T-BSA conjugates containing varying amounts of large T per BSA in a peptide-BSA/nanoparticle molar ratio of 10:1, and the final concentration of gold nanoparticles in the solution was 16.6 nM. HeLa cells, which had been previously cultured in T-25 cell culture flasks, were allowed to incubate with 5 mL of growth media containing 10 % large T-BSA/gold nanoparticle complexes (1.6 nM nanoparticle concentration) per well for 6 h. Nanoparticles 5 nm in diameter were chosen for these experiments to minimize the potential accumulation of nanoparticles in nuclear fractions due solely to high-speed centrifugation (used in the cell fractionation protocol). T-25 flasks were chosen for use in these experiments in the interest of increasing the number of cells per experiment and thereby increasing the resulting gold emission signal detect- able via ICP-OES. Consequently, six T-25 flasks of cells were used for each large T-BSA/nanoparticle complex under scrutiny. After the desired incubation time had elapsed, the cells in each flask were rinsed with 1 mL of DPBS three times and then trypsinized. Small aliquots (100 μL) of cells were removed from each flask for cell counting and toxicity assays using FACS, and the remaining cells were concentrated via centrifugation. Three of the six resulting samples per construct were then air-dried in a sterile cell culture hood, treated with 1.0 mL of aqua regia for 2 h, and each subsequent solution was prepared for ICP-OES analysis. The remaining three samples were subjected to fractionation using the Pierce Co. subcellular fractionation kit to obtain nuclear and cytosolic fractions of each sample. Each individual fraction was then air-dried in a sterile cell culture hood, treated with 1.0 mL of aqua regia for 2 h, and each resulting solution was

prepared for ICP-OES analysis. Last, 12 additional T-25 flasks of HeLa cells, which had been incubated for 6 h with standard growth media (not containing colloidal constructs), were trypsinized and concentrated via centrifugation. These 12 flasks were divided into four groups containing three flasks each. All three of the flasks in a particular group had one of four different 5 nm nanoparticle complexes (passivation layers: native BSA, 7:1, 11:1, or 15:1 large T/BSA experimentally determined molar ratios) introduced to the fractionated cells prior to the final separation (via centrifugation) of nuclei from nonnuclear material. The samples created in such fashion are referred to as "spiked" samples. All of these fractions were then allowed to air-dry in a sterile cell culture hood, treated with 1.0 mL of aqua regia for 2 h, and each resulting solution was prepared for ICP-OES analysis.

4.5. References.

[1] Dworetzky, S. I.; Landford, R. E.; Feldherr, C. M. *J. Cell Biol.*, **1988**, *107*, 1279 – 1287.

[2] Feldherr, C. M.; Akin, D. *J. Cell Biol.*, **1990**, *111*, 1 – 8.

[3] Tkachenko, A.G.; Xie, H.; Coleman, D.; Glomm, W.; Ryan, J.; Anderson, M. F.; Franzen, S.; Feldheim, D. L. *J. Am. Chem. Soc.*, **2003**, *125*, 4700 – 4701.

Chapter 5

Conclusions.

5.1. Summary.

A complete line of research has now been presented which has demonstrated the successful accumulation of large T/BSA-gold nanoparticle complexes in nuclei of HeLa cells. The steps involved in the construction of the nanoparticle complexes themselves have been quantified, shown to be quite modifiable, and the stability of these nanoparticle complexes with respect to: 1) molar ratio of large T/BSA conjugate per nanoparticle, 2) molar ratio of large T per BSA (and ultimately, per nanoparticle), and 3) common temperatures used in typical cellular uptake experiments have all been demonstrated. The ability of HeLa cells to take up these nanoparticle complexes has been exhaustively characterized, and the use of ICP-OES as a critical analysis method for polypeptide-gold nanoparticle constructs has been delineated. It was observed that HeLa cells not only internalized these nanoparticle constructs, but this uptake of nanoparticle complexes was found to be modifiable according to different parameters, for example: nanoparticle size, amount of large T present per nanoparticle complex, and time of cellular incubation with the nanoparticle complexes present. Nanoparticle complexes were found to be able to localize in the nuclei of HeLa cells from the extracellular environment, and toxicity levels of these nanoparticle complexes were reported.

Based on these findings these large T/BSA-gold nanoparticle studies can be a baseline for future studies addressing many different questions of interest. Each section of this research can be further optimized, and the results of this investigation also raised more questions, many of which are listed in the section that follows.

5.2. Questions for Further Study.

In order to define which ideas presented earlier in this thesis warrant further exploration, it made sense to break these questions for potential future examination into the broad categories previously detailed in this thesis.

5.2.1. Regarding Construction and Quantification of Large T/BSA-Gold Nanoparticle Complexes.

Perhaps the biggest and most obvious assumptions made in this line of scientific questioning concerned the number of large T/BSA conjugates presumed to be associated with 15 nm diameter gold nanoparticles (and 5 nm diameter gold nanoparticles, for that matter). Specifically, it was assumed: 1) the large T/BSA conjugate would both behave similarly to $[Ru(bipy)_2bipy\text{-}C_6H_{12}\text{-}S]^{2+}$-BSA conjugates with respect to gold nanoparticle surfaces, and 2) the large T/BSA conjugates would maintain a constant surface density on nanoparticles irrespective of number of large T peptides present per BSA (scaling only as a function of nanoparticle surface area). While neither of these assumptions is egregious (in fact, other independent fluorescence experiments demonstrated the same number of BSAs were associated with 20 nm diameter gold nanoparticle surfaces),[1] future studies might choose to run TCSPC analyses on the exact materials for use in cellular uptake experiments, including a rigorous analysis of BSA conjugates of varying peptide concentrations. Not only would this be a better way to develop a quantitative method of peptide/BSA construction (a direct measurement of how many peptide/BSA conjugates are actually associated with surfaces on a given sample of nanoparticles, as opposed to an approximation of how many are likely to

be present), it also would be interesting to see if the percentage of associated peptide/BSA conjugates associated with nanoparticle surfaces was related to the number of peptides attached per BSA.

Moreover, a closer examination of peptide/BSA conjugate interactions at gold nanoparticle surfaces might be useful for future studies of this nature. While studies have been performed concerning the adsorption characteristics of native BSA to gold nanoparticles and gold surfaces using quartz crystal microbalance (QCM) and ζ-potential measurements,[2,3] identical investigations using peptide/BSA conjugates would yield interesting information, particularly as a function of peptide per BSA. Perhaps even a dynamic light scattering (DLS) experiments run in conjunction with these other experiments would give rise to data which could afford very strong conclusions about how the peptide/BSA conjugates were associating with the gold nanoparticle surfaces.

It would also be interesting to determine if minimizing or maximizing the number of SMCC linkers per BSA had any overall effect upon peptide binding, association of peptide/BSA conjugates with gold nanoparticles, and ultimate cellular uptake of the resulting nanoparticle complexes. For example, if a 5:1 peptide:BSA molar ratio were desired, how would the creation of a 5:1 SMCC:BSA conjugate affect ultimate nanoparticle complex stability? (Combined with data from directly measuring the number of peptide/BSA conjugates associated with nanoparticle surfaces via TCSPC, this could be quite telling about surface interactions at the peptide/BSA conjugate-nanoparticle interface.) Would this be substantively different if the initial SMCC:BSA ratio had been 40:1? Examining the subsequent potential effects on cellular uptake – especially the level of toxicity of these

nanoparticle complexes to cells – would be valuable information. Ostensibly, it should be pointed out that gratuitous experimentation with peptide sequences can get very expensive very quickly, but perhaps there are a few small, elegant experiments of this nature which could be performed to give a broad sense of what is likely to be occurring at each step in this system.

Additionally, it would be useful to discern whether peptide/BSA conjugates would retain function if lyophilized and stored for long periods of time.

Using combinations of the analytical techniques previously mentioned, it should be possible to synthesize and quantify nanoparticle complexes with multiple peptide/BSA conjugates (that is, $peptide_1$/BSA conjugates mixed with $peptide_2$/BSA conjugates), and comparison of the stability/performance of each combination would be extremely promising. Perhaps even using combinations of large T/BSA conjugates and a DNA/BSA or RNA/BSA conjugate could yield a nanoparticle delivery vector of extreme consequence.

5.2.2. Regarding Delivery of Large T/BSA-Gold Nanoparticle Complexes to Cells.

Now that a baseline study of general parameters concerning HeLa uptake of large T/BSA-gold nanoparticle complexes has been performed, repeating selected experiments detailed herein with 1) other cell lines and 2) other peptide sequences would be a fascinating line of inquiry. In addition, a few other parameters of this research presented in this thesis warrant further exploration, including (but certainly not limited to) the following ideas.

It would be extremely helpful to incorporate FACS into the standard protocol for every future delivery experiment. This analytical technique not only allows for the ability to

describe detected nanoparticles taken up in a "per cell" fashion, but also simultaneously yields a specific cell count useful in determining toxicity of each sample. For that matter, people studying future cellular uptake experiments might choose to incorporate occasional replicate experiments for use in VECDIC, TEM, and/or confocal imaging. While none of these imaging techniques necessarily lends itself readily to nanoparticle complex quantification post-incubation, these imaging techniques can be useful to examine any discernable qualitative differences where appropriate.

A quantitative comparison of cellular uptake using peptide/BSA-gold nanoparticle complexes versus cellular uptake via liposomes or versus cellular uptake experiments which utilize a "cellular pore-opening" moiety (i.e. digitonin) could be a useful way to compare the utility of the peptide/BSA-nanoparticle complexes to existing cellular delivery vectors, particularly with regard to cytotoxicity.

A more rigorous exploration of cellular incubation times with nanoparticle complexes – particularly rather short times of incubation – would be a good starting point for future research. It would be very interesting to know how fast an appreciable amount of nanoparticle complexes are taken up by a given cell line, including a comparison to a "nanoparticle complex wash" (incubation time of zero) to get an idea how many nanoparticle complexes might be adsorbed to the outside of a sample of cells, and/or if this "pulse" of nanoparticle complexes would ultimately be taken up by the cells over time. A general "rate of uptake" of the nanoparticle complexes would be extremely interesting and valuable data for future experiments, especially as a function of peptide per nanoparticle complex. Moreover, in continuing the line of inquiry seen in the pulse/chase experiments, it would be

very useful to learn at what point the nanoparticle complexes _do_ become expelled/cycled out of the cells, if ever.

It should be noted with regard to the experiments concerning the potential effects of nanoparticle size upon observed cellular uptake (Figure 3.3) that analogous experiments were performed on HeLa cells incubated with 5 nm diameter nanoparticle complexes. The experiments were carried out in the same fashion as the experiments run with the larger diameter nanoparticles – which is to say, cells for the experiment were cultured on glass coverslips in 12-well plates, and two coverslips per sample were combined prior to acid dissolution after the experimental incubation time had elapsed – but the ICP-OES results for the 5 nm diameter nanoparticle complex deliveries were not completely distinguishable from instrument noise. For this reason, the data and references to these experiments with the 5 nm diameter nanoparticle complexes were not listed in the chapter. In future work, it would be useful to perform this experiment again, but quadrupling (instead of merely doubling) the number of coverslips per sample should augment the resulting ICP-OES signal sufficiently for 5 nm diameter nanoparticle complex uptake data to be compared to that of the larger-diameter nanoparticle complexes.

5.2.3. Regarding Sub-Cellular Fractionation of Cells Incubated with Large T/BSA-Gold Nanoparticle Complexes.

There are a few direct questions answerable by future studies involving examination of nuclear fractions of cells post-incubation with nanoparticle complexes. For example, it would be very interesting to know how quickly nanoparticle complexes could be found

inside nuclei. While previous research[4] using microinjection of similar nanoparticle complexes into cells examined how quickly these nanoparticle complexes could migrate into cell nuclei, it would be of interest to know how these rates of localization compare with nanoparticle complexes administered via active cellular uptake from the extracellular environment. Furthermore, it would be very interesting to know exactly what/how these particular nanoparticle complexes are associated with once in the nuclei – perhaps associated with genetic material inside the nuclei or stuck to the nuclear membrane – and if this potential localization can be advantageous to future uses/probe involving these nanoparticle complexes.

One question involving future cellular fractionation experiments: is full cellular fractionation possible when using these nanoparticle complexes? It would be interesting to know where particular nanoparticle complexes ultimately localize post-uptake, and could even lead to some very interesting further experiments involving mixed-moiety nanoparticle complexes. However, certain stages of typical cellular fractionation protocols might not allow for complete fractionation, but perhaps there are other protocols to be investigated which could be more amenable for use with this colloidal cellular vector in future experimentation. Moreover, well-characterized nanoparticle complexes consisting of nanoparticles under 5 nm in diameter would not only be an interesting comparative study to the 5 nm diameter nanoparticles used in this study, they might also be extremely helpful in designing a protocol for complete fractionation analysis of cellular uptake experiments. Problematically, however, as the nanoparticle radius decreases under that of the BSA itself,

the average number of peptide/BSA conjugates per nanoparticle is more likely to become a ratio less than unity.

5.3. Epilogue.

This research is only the beginning of a potentially long line of investigation. However, the questions to be answered in the full pursuit of this line of scientific inquiry should yield many answers not just about this particular system, but also could answer broad questions concerning drug delivery vehicle assembly, and even perhaps address cellular uptake and intracellular translocation mechanisms in general.

One needs to consider as many mechanistic theories as possible to ensure one is examining intended phenomena, particularly when performing cellular uptake experiments. For example, while the internalizations and subsequent nuclear localizations of nanoparticle complexes described in this dissertation were definitely not artifacts of fixation as seen in other research[5] (since no samples were treated with fixative prior to analysis), it is conceivable that cellular uptake increased proportionally due to an increase in toxicity. That is, a cell which is severely stressed by its environment may ingest exogenous material non-specifically, which in the case of this research might have lead in turn to an increased number of observed internalized nanoparticle complexes. This possibility means the cause of the directly-proportional relationship between nanoparticle complex internalization and large T concentration per nanoparticle complex seen in Figure 3.2 (for example) may merely be due certain cells being severely stressed by increased cytotoxic environment (increasing

cytotoxicity being proportional to increasing large T concentration per nanoparticle complex, as seen in Figure 4.1) rather than being due to any other factor (i.e. increase in polyvalency). Perhaps future research done concerning the internalization of these types of delivery vectors would benefit from performing concurrent live cell imaging replicate samples (for example) to attempt to qualify increases in cellular internalization observed via other methods. Moreover, while the pulse-chase experiments data shown in Figure 3.5 imply that once a quantity of nanoparticle complexes enter a given number of cells, they remain there in similar concentration for at least 12 hours, a repeat of these experiments with an accompanying cell count for each sample (thus demonstrating toxicity levels per sample) may help address this issue as well.

5.4. References.

[1] Xie, H.; Tkachenko, A. G.; Glomm, W. R.; Ryan, J. A.; Brennaman, M. K.; Papnikolas, J. M.; Franzen, S.; Feldheim, D. L. *Anal. Chem.*, **2003**, *75*, 5797 – 5805.

[2] Brewer, S. H.; Glomm, W. R.; Johnson, M. C.; Knag, M K.; Franzen, S. *Langmuir*, **2005**, *21*, 9303 – 9307.

[3] Kaufman, E. D.; Belyea, J.; Johnson, M. C.; Nicholson, Z. M.; Ricks, J. L.; Shah, P. K.; Bayless, M.; Pettersson, T.; Feldotö, Z.; Blomberg, E.; Claesson, P.; Franzen, S. *Langmuir*, **2007**, *23*, 6053 – 6062.

[4] Feldherr, C. M.; Akin, D. *J. Cell Biol.*, **1990**, *111*, 1 – 8.

[5] Lundberg, M. Johansson, M. *Biochemical and Biophysical Research Communications*, **2002**, *291(2)*, 367 – 371.